NON-SYMMETRIC FLOW IN LAVAL TYPE NOZZLES

By A. G. WALTERS
R.A.R.D.E., Fort Halstead, Sevenoaks, Kent

(*Communicated by Sir James Lighthill, F.R.S. – Received* 20 *December* 1971)

[Plates 1 to 3]

CONTENTS

The equations of the steady state, compressible inviscid gaseous flow are linearized in a form suitable for application to nozzles of the Laval type. The procedure in the supersonic phase is verified by comparing solutions so obtained with those derived by the method of characteristics in two and three dimensions. Likewise, the solutions in the transonic phase are compared with those obtained by other investigators. The linearized equation is then used to investigate the nature of non-symmetric flow in rocket nozzles. It is found that if the flow from the combustion chamber into the nozzle is non-symmetric, the magnitude and direction of the turning couple produced by the emergent jet is dependent on the profile of the nozzle and it is possible to design profiles such that the turning couples or lateral forces are zero. The optimum nozzle so designed is independent of the pressure and also of the magnitude of the non-symmetry of the entry flow. The formulae by which they are obtained have been checked by extensive static and projection tests with simulated rocket test vehicles which are described in this paper.

Vol. 273. A. 1232. (Price £1.60; U.S. $4.50) 13 [Published 28 September 1972

Introduction

Extensive investigations have been carried out in the last few decades on the factors responsible for the notorious random flight deviations of unguided rockets. The manner in which these occur is well known. The direction of the missile axis is changed by relatively small turning moments about its centre of gravity and the resulting departure of the thrust line from the intended direction is responsible for the flight deviation. It is known that the displacement of the line of thrust from the centre of gravity makes a major contribution to these turning moments. The effect of mechanical tolerances can be largely eliminated. These result in the centre of gravity being off the line of the nozzle exit cone axis but the malalinement can be removed by the simple expedient of balancing the rocket on a mandrel which is a good fit to the nozzle exit cone. In addition the design must be such that negligible distortion can arise from the pressure and temperature during burning. However it is found generally that the turning moments remain just as large and it has been established that these arise from the departure of the thrust line from the nozzle exit cone axis. Thus it is necessary to ascertain whether it is possible to design a nozzle such that the effective thrust line of the emergent jet lies along its exit cone axis even though the flow from the burning chamber is non-symmetric. The following notes outline the method of approach adopted in this paper to achieve such a design.

The validity of the classical equations of the one-dimensional flow in supersonic nozzles is well established and in this paper the two and three dimensional flows are treated as perturbations of these. In other words it is assumed that the lateral velocities are small compared with the axial values. By this means it is possible to linearize the equations in forms applicable to flows which are non-symmetric with respect to the nozzle exit cone axis.

The adequacy of the linearized equations in the supersonic phase are checked by comparing their solutions with the numerical values obtained by the method of characteristics. The throat region requires special treatment. If R is the radius of the boundary profile at the throat and D the throat diameter, the ratio R/D is a critical parameter for this determines the extent of the variations in the pressure and velocity across the throat section. It is generally necessary to maintain this ratio at as low a value as possible for, amongst other things, this reduces the length and weight of the nozzle. Symmetric flow in the throat region has been investigated by a number of workers and the solutions they obtained are used to provide a check on the linearized equations.

By these means it is established that the linearized theory predicts the mean value of the flow angles across a section with adequate accuracy, provided the ratio R/D is not too small. With this condition and using further equations derived from the force and moment diagrams, it is possible to obtain the lateral momentum and the parallel displacement of the axial component of the thrust to the second order of small quantities.

It is demonstrated theoretically that it is possible to design a nozzle such that the turning moment about the rocket centre of gravity arising from the thrust in the emergent jet is zero even though the flow at the throat section is asymmetric. The design is independent of the pressure in the burning chamber and of the magnitude of the asymmetry at the throat. Equations are derived by means of which this nozzle can be obtained.

The experimental programme was planned to check the validity of the principle and the accuracy of the equations in specifying the optimum nozzle. The initial experiments were carried out with small scale model rockets in which the flow asymmetry at the throat was obtained by machining the inlet cone at an angle to the exit cone axis. In the first experiment the nozzle

exit cone was 6.6° total angle and at this small value the linear theory could be expected to be valid. The close agreement between the theoretical and experimental results obtained is more remarkable when it is realized that the mean particle acceleration across the throat section exceeds 10^8 m/s^2. The subsequent experiments were carried out at larger cone angles and these were followed by flight tests with full scale test vehicles. The results confirm the theory to within the limits of the experimental errors.

1. The derivation of the linear equation of the flow in a two-dimensional nozzle

The one-dimensional solution of the equations of irrotational compressible flow in a Laval nozzle is well known. Briefly the solution may be expressed in the following form.

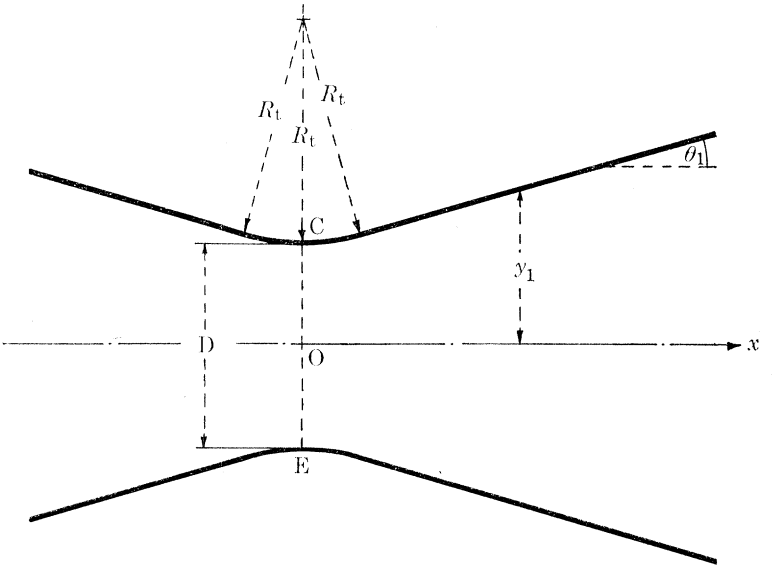

Figure 1. A typical Laval type nozzle configuration.

The contour of the gas conduit of the nozzle is given in figure 1. CE is the throat, i.e. the minimum cross-section at which the Mach number is unity. If A_t is the area of the throat and A the area at another section of the conduit, the Mach number M at that section is given by the relation

$$\left(\frac{A}{A_t}\right)^2 = \frac{1}{M^2}\left[\frac{2}{\gamma+1}\left(1+\frac{\gamma-1}{2}M^2\right)\right]^{(\gamma+1)/(\gamma-1)}, \tag{1.1}$$

γ being the ratio of the specific heats at constant pressure and constant volume.

The Mach number is the ratio of the local stream velocity to the local velocity of sound. The ratio of the local stream velocity at a given section to the stream velocity at the throat is denoted by w which is related to M by the equation

$$w^2 = (\gamma+1)\,M^2/\{2+(\gamma-1)\,M^2\}. \tag{1.2}$$

The pressure and density at the specified section are given by the equations

$$p = p_0\left[1-\frac{\gamma-1}{\gamma+1}w^2\right]^{\gamma/(\gamma-1)}, \quad \rho = \rho_0\left[1-\frac{\gamma-1}{\gamma+1}w^2\right]^{1/(\gamma-1)}, \tag{1.3}$$

where p_0 and ρ_0 are the stagnation values.

The exact equation of the two-dimensional irrotational inviscid flow may be expressed in the form (Shapiro 1953)

$$(a^2-u^2)\frac{\partial^2\phi_1}{\partial x^2}-2uv\frac{\partial^2\phi_1}{\partial x\,\partial y}+(a^2-v^2)\frac{\partial^2\phi_1}{\partial y^2}=0, \tag{1.4}$$

u and v are the stream velocities along the x and y directions respectively, ϕ_1 is the single-valued potential from which they are obtained, i.e.

$$u=\frac{\partial\phi_1}{\partial x}, \quad v=\frac{\partial\phi_1}{\partial y}, \tag{1.5}$$

and a is the local velocity of sound which is given by the equation

$$a^2=a_0^2-\tfrac{1}{2}(\gamma-1)\,(u^2+v^2), \tag{1.6}$$

a_0 being the velocity of sound in the reservoir. This is related to the velocity of sound at the throat, a_t by the equation

$$a_0^2=\tfrac{1}{2}(\gamma+1)\,a_t^2. \tag{1.7}$$

Equation (1.1) can be expressed in the form

$$\frac{A}{A_t}=\frac{1}{w}\left[\frac{\gamma+1}{2}-\frac{\gamma-1}{2}w^2\right]^{-1/(\gamma-1)}. \tag{1.8}$$

It is assumed that the slopes of the boundaries are continuous everywhere and, in addition, the curvature at the throat is continuous. The reason for the latter assumption is given later.

We write in the case of two-dimensional flow

$$w_1^2=(u^2+v^2)/a_t^2, \quad v_1^2=v^2/a_t^2, \quad \phi=\phi_1/a_t, \tag{1.9}$$

so that (1.4) may be written

$$h_1\phi_{xx}+2h_3\phi_{xy}-h_2\phi_{yy}=0, \tag{1.10}$$

where

$$h_1=w_1^2-1-2v_1^2/(\gamma+1), \quad h_2=1-(\gamma-1)\,w_1^2/(\gamma+1)-2v_1^2/(\gamma+1), \quad h_3=2\phi_x v_1/(\gamma+1). \tag{1.11}$$

We attempt to linearize this equation in such a manner that its physical characteristic lines agree closely with those of the linearized equation. The principal axis of flow is taken as $y=0$ and in the first instance it is assumed that the flow is symmetrical about this axis, the boundaries being given by

$$y=\pm y_1(x)$$

so that $A=2y_1$. The minimum section or throat at which $w=1$ is taken at $x=0$.

Differentiating (1.8) with respect to x we obtain

$$\frac{\mathrm{d}w}{\mathrm{d}x}=\frac{1-\{(\gamma-1)/(\gamma+1)\}w^2}{w^2-1}\frac{w}{y_1}\frac{\mathrm{d}y_1}{\mathrm{d}x}. \tag{1.12}$$

The gradient of the boundary at the throat section is zero so that for small values of x

$$w=1+w_t'x, \quad \mathrm{d}y_1/\mathrm{d}x=x/R_t,$$

and substituting these into (1.12) we find

$$w_t'=((\gamma+1)\,y_1R_t)^{-\frac{1}{2}} \quad (x=0). \tag{1.13}$$

If the derivatives of y_1 are of the first order of magnitude of small quantities, it is seen from (1.12) that w' is of the same order at positions away from the throat but near and at the throat it is a large quantity as shown by (1.13). The rate of mass flow m is

$$m = 2\int_0^{y_1} \rho u \, dy.$$

Writing

$$w_1^2 = w^2 + \lambda$$

and neglecting terms of order higher than λ^2 and ϕ_y^2 it is found that

$$\frac{m-m_0}{m_0} = -\frac{(w^2-1)\bar{\lambda}}{2w^2(1-\{(\gamma-1)/(\gamma+1)\}w^2)} + \beta\bar{\lambda^2} - \frac{\bar{v_1^2}}{2w^2},$$

where

$$\beta = \frac{(\gamma+1)[(3-\gamma)(w^2-1)^2-4]}{8w^2\{\gamma+1-(\gamma-1)w^2\}^2},$$

m_0 is the value calculated from one-dimensional theory and the bars denote the mean values across the sections perpendicular to the principal axis. Since $w = 1$ at the throat, m differs from m_0 by terms of the second order and away from the throat $\bar{\lambda}$, the mean value of λ across the section, is of the second order. The thrust of the flow crossing any section is

$$T = 2\int_0^{y_1} (p+\rho u^2)\, dy,$$

and neglecting terms higher than the second order, this becomes

$$T = T_0\left[1 - \frac{\bar{\lambda}\gamma(w^2-1)}{(w^2+1)\{\gamma+1-(\gamma-1)w^2\}} + \frac{\bar{\lambda^2}(\gamma w^2-3\gamma)}{2(w^2+1)\{\gamma+1-(\gamma-1)w^2\}^2} - \frac{2\gamma\bar{v_1^2}}{(\gamma+1)(w^2+1)}\right],$$

T_0 being the value calculated from one-dimensional theory.

The rate of mass flow is independent of x so that

$$\frac{d}{dx}\left(\frac{m-m_0}{m_0}\right) = 0,$$

and since the boundary gradient is zero at the throat

$$\frac{d}{dx}\left(\frac{T-T_0}{T_0}\right) = 0 \quad (x = 0).$$

From these two equations it is found that

$$\bar{\lambda} = -\frac{1}{4ww'}\frac{d\bar{\lambda^2}}{dx} + \frac{4-\gamma}{2}\bar{\lambda^2} + \frac{2}{\gamma+1}\bar{v_1^2} \quad (x = 0), \tag{1.14}$$

and

$$\frac{1}{2ww'}\frac{d\bar{v_1^2}}{dx} + \frac{\gamma+1}{4}\bar{\lambda^2} = 0,$$

so that $\bar{\lambda}$ is of the second order throughout.

The variable y is replaced by Y defined as

$$Y = y/\alpha, \tag{1.15}$$

where α is some function of x the derivatives of which are assumed to be of the first order. Along lines of constant Y

$$\Delta y = Y\Delta\alpha, \quad \Delta\phi = \frac{\partial\phi}{\partial x}\Delta x + Y\frac{\partial\phi}{\partial y}\Delta\alpha,$$

or
$$\left(\frac{\partial\phi}{\partial x}\right)_Y = \left(\frac{\partial\phi}{\partial x}\right)_y + Y\frac{\partial\phi}{\partial y}\frac{\mathrm{d}\alpha}{\mathrm{d}x},$$

and
$$\left(\frac{\partial^2\phi}{\partial x^2}\right)_Y = \left[\left(\frac{\partial}{\partial x}\right)_y + Y\frac{\mathrm{d}\alpha}{\mathrm{d}x}\frac{\partial}{\partial y}\right]\left[\left(\frac{\partial\phi}{\partial x}\right)_y + Y\frac{\partial\phi}{\partial y}\frac{\mathrm{d}\alpha}{\mathrm{d}x}\right],$$

or
$$\left(\frac{\partial^2\phi}{\partial x^2}\right)_y = \left(\frac{\partial^2\phi}{\partial x^2}\right)_Y - 2Y\frac{\mathrm{d}\alpha}{\mathrm{d}x}\frac{\partial^2\phi}{\partial x\partial y} - Y^2\left(\frac{\mathrm{d}\alpha}{\mathrm{d}x}\right)^2\frac{\partial^2\phi}{\partial y^2} - Y\frac{\partial\phi}{\partial y}\frac{\mathrm{d}^2\alpha}{\mathrm{d}x^2}. \tag{1.16}$$

Substituting this into (1.10) and equating the coefficient of ϕ_{xy} to zero gives

$$\frac{y}{\alpha}\frac{\mathrm{d}\alpha}{\mathrm{d}x}\left(w_1^2 - 1 - \frac{2v_1^2}{\gamma+1}\right) - \frac{2}{\gamma+1}(w_1^2 - v_1^2)^{\frac{1}{2}}v_1 = 0. \tag{1.17}$$

In the first instance we consider this equation at positions close to the axis $y = 0$. The slopes of the physical characteristics of (1.10) are given by

$$\mathrm{d}y/\mathrm{d}x = \tan(\theta + \psi),$$

and along these lines
$$\mathrm{d}f = \mathrm{d}\theta,$$

ψ, f and θ being the Mach angle, the Prandtl–Meyer expansion angle and the flow angle with respect to the principal axis respectively. At points close to the axis

$$v_1 = w_1\theta$$

so that
$$\frac{v_1}{y} = \frac{w_1\theta}{y} = \left(\frac{w_1}{\tan\psi}\frac{\mathrm{d}f}{\mathrm{d}x}\right)_{y=0}.$$

Also
$$\mathrm{d}f = \left(\frac{w_1^2 - 1}{1 - \{(\gamma-1)/(\gamma+1)\}w_1^2}\right)^{\frac{1}{2}}\frac{\mathrm{d}w_1}{w_1}, \quad \tan\psi = \left(\frac{1 - \{(\gamma-1)/(\gamma+1)\}w_1^2}{w_1^2 - 1}\right)^{\frac{1}{2}},$$

so that
$$\frac{v_1}{y} = \frac{w_1^2 - 1}{1 - \{(\gamma-1)/(\gamma+1)\}w_1^2}\frac{\mathrm{d}w_1}{\mathrm{d}x}.$$

Substituting this into (1.17) and neglecting v_1^2, we have

$$\left.\begin{aligned} \frac{1}{\alpha}\frac{\mathrm{d}\alpha}{\mathrm{d}x} &= \frac{2}{\gamma+1}\frac{w_1 w_1'}{1 - \{(\gamma-1)/(\gamma+1)\}w_1^2}, \\ \alpha &= k\left(1 - \frac{\gamma-1}{\gamma+1}w_1^2\right)^{-1/(\gamma-1)}. \end{aligned}\right\} \tag{1.18}$$

A similar result can be obtained if it is assumed that w_1 is sensibly equal to w and that v_1 is small and varies linearly across the section so that

$$v_1 = \frac{w}{y_1}y\frac{\mathrm{d}y_1}{\mathrm{d}x}.$$

Substituting this into (1.17) gives

$$\frac{1}{\alpha}\frac{\mathrm{d}\alpha}{\mathrm{d}x} = \frac{2}{\gamma+1}\frac{w^2}{w^2-1}\frac{1}{y_1}\frac{\mathrm{d}y_1}{\mathrm{d}x}.$$

Applying (1.12) and integrating produces the same form for α as (1.18) but with w_1 replaced by w and this can be written with the aid of (1.8),

$$\alpha = kwy_1, \tag{1.19}$$

the terms k being constants. A more detailed analysis suggests a closer value to be

$$\alpha = k\left(1-\frac{\gamma-1}{\gamma+1}\overline{w_1^2}-\frac{2}{\gamma+1}\overline{v_1^2}\right)^{-1/(\gamma-1)}, \tag{1.20}$$

the bars denoting the mean values across the sections perpendicular to the principal axis.

In the first instance we consider that region downstream of the throat in which the flow is supersonic. The variable x is replaced by X defined as

$$X = \int_\epsilon^x \frac{1}{\alpha}\left(\frac{h_2+h_3^2/h_1}{h_1}\right)^{\frac{1}{2}} \mathrm{d}x \quad (x > 0), \tag{1.21}$$

the term in the bracket in the integrand being given its mean value across the section and ϵ is a small quantity defined by

$$\mathrm{d}x/\mathrm{d}X = 0 \quad (x = \epsilon). \tag{1.22}$$

Consider the differential equation

$$\left(\frac{\partial^2\phi}{\partial X^2}\right)_Y - \left(\frac{\partial^2\phi}{\partial Y^2}\right)_X + F(X, Y) = 0. \tag{1.23}$$

X and Y are not independent variables and in terms of X and y the equation can be written with the aid of (1.16) and (1.17)

$$\left(\frac{\partial^2\phi}{\partial X^2}\right)_y + \frac{2h_3}{h_1}\frac{\mathrm{d}x}{\mathrm{d}X}\frac{\partial^2\phi}{\partial X\,\partial y} - \left[\alpha^2 - \frac{h_3^2}{h_1^2}\left(\frac{\mathrm{d}x}{\mathrm{d}X}\right)^2\right]\frac{\partial^2\phi}{\partial y^2} + \frac{y}{\alpha}\frac{\partial\phi}{\partial y}\frac{\mathrm{d}^2\alpha}{\mathrm{d}X^2} + F(X, Y) = 0. \tag{1.24}$$

The slopes of the physical characteristics of (1.10) are given by

$$\frac{\mathrm{d}y}{\mathrm{d}x} = [h_3 \pm (h_3^2 + h_1 h_2)^{\frac{1}{2}}]/h_1, \tag{1.25}$$

and those of (1.24) by

$$\frac{\mathrm{d}y}{\mathrm{d}X} = \frac{h_3}{h_1}\frac{\mathrm{d}x}{\mathrm{d}X} \pm \alpha,$$

or

$$\frac{\mathrm{d}y}{\mathrm{d}x} = \frac{h_3}{h_1} \pm \alpha\frac{\mathrm{d}X}{\mathrm{d}x}, \tag{1.26}$$

and from the definition of X we see this is of identical form to (1.25). The slopes given by (1.26) are independent of y but at each section the value is the mean of those of (1.25).

By applying (1.16), (1.17) and (1.21), we can write (1.23) as

$$h_1\phi_{xx} + 2h_3\phi_{xy} - h_2\phi_{yy} + \frac{h_2+h_3^2/h_1}{\alpha^2}\left[F(X, Y) - \left(\frac{\partial\phi}{\partial X}\right)_Y\left(\frac{\mathrm{d}x}{\mathrm{d}X}\right)^2\frac{\mathrm{d}^2X}{\mathrm{d}x^2} + Y\frac{\partial\phi}{\partial Y}\frac{\mathrm{d}^2\alpha}{\mathrm{d}x^2}\left(\frac{\mathrm{d}\alpha}{\mathrm{d}X}\right)^2\right] = 0. \tag{1.27}$$

At positions away from the throat, the differentials in the first three terms are of the first order and the last two terms are of the second order. Thus if we write $F(X, Y) = 0$ the equation is of the same form as equation (1.10) to the first order, the coefficients h having their mean values across the sections.

At positions close to the throat, the term ϕ_x is of the order w and, omitting second order terms, ϕ_{xx} is w_t' which has been shown to be a large quantity. Writing

$$w_1^2 = w^2 + \lambda, \quad h_1 = \overline{h_1} + \lambda,$$

then to the first order $\quad h_1\phi_{xx} = \overline{h_1}\phi_{xx} + \lambda w_t' = \overline{h_1}\phi_{xx} + 2ww_t'(\phi_x - w).$

The last term of (1.27) is of the second order at the throat, thus if we write

$$F(X, Y) = \left(\frac{\partial\phi}{\partial X}\right)_Y \left(\frac{dx}{dX}\right)^2 \frac{d^2X}{dx^2} + 2ww' \left(\frac{dx}{dX}\right)^2 \left[\frac{\partial\phi}{\partial X}\frac{dX}{dx} - w\right] \Big/ h_1,$$

(1.23) takes the same form as (1.10) to the first order. At positions close to $x = \epsilon$

$$X = \frac{2}{\alpha_t} \frac{(x-\epsilon)^{\frac{1}{2}}}{\{(\gamma+1)\, w_t'\}^{\frac{1}{2}}}, \quad \overline{h_1} = 2w_t'(x-\epsilon),$$

to the first order, and with these forms

$$F(X, Y) = \frac{1}{X}\left(\frac{\partial\phi}{\partial X}\right)_Y - (\gamma+1)\, \alpha_t^2 w^2 w_t'.$$

The equation (1.23) can be written

$$\left(\frac{\partial^2\phi}{\partial X^2}\right)_Y - \left(\frac{\partial^2\phi}{\partial Y^2}\right)_X + \frac{\xi}{X}\left(\frac{\partial\phi}{\partial X}\right)_Y = \xi(\gamma+1)\, \alpha_t^2 w^2 w_t', \tag{1.28}$$

where $\xi = 0$ away from the throat and $\xi = 1.0$ close to it.

It is advisable in problems of this type to obtain a solution which satisfies the boundary conditions exactly. This is the basis of the Galerkin method in which the solution is expressed as a series of simple polynomials each of which satisfies the boundary conditions exactly and the constants in the polynomials are chosen so as to give the best fit to the differential equation by the method of least squares. The boundary conditions to be satisfied are

$$\phi_y = \pm \phi_x\, dy_1/dx, \quad y = \pm y_1,$$

and (1.23) is not in a suitable form for satisfying these. We introduce a new function defined by

$$\Phi = w \int_0^y \frac{\phi_y}{w_1}\, dy. \tag{1.29}$$

If we omit third order terms this becomes

$$\Phi = [\phi]_0^y - \frac{1}{2w^2}\int_0^y \lambda\phi_y\, dy.$$

It is shown later that the second term on the right-hand side is of the third order when $y = y_1$ but in general it is a second order term. If it is omitted (1.23) takes the form

$$\left(\frac{\partial^2\Phi}{\partial X^2}\right)_Y - \left(\frac{\partial^2\Phi}{\partial Y^2}\right)_X + \frac{\xi}{X}\left(\frac{\partial\Phi}{\partial X}\right)_Y + F_1(X) = 0, \tag{1.30}$$

the last term being a function of X only.

By definition
$$\partial\Phi/\partial Y = \alpha w \sin\theta, \tag{1.31}$$
θ being the flow angle. Also

$$\left(\frac{\partial}{\partial X}(\alpha w \sin\theta)\right)_Y = \left(\frac{\partial}{\partial X}(\alpha w \sin\theta)\right)_y + \frac{Y}{\alpha}\frac{d\alpha}{dx}\frac{\partial}{\partial Y}(\alpha w \sin\theta)\frac{dx}{dX}$$

and since
$$\frac{dx}{dX} = 0 \quad (X = 0); \qquad \frac{\partial}{\partial X}(\alpha w \sin\theta) = \frac{\partial}{\partial x}(\alpha w \sin\theta)\frac{dx}{dX},$$

we have
$$\left(\frac{\partial}{\partial X}(\alpha w \sin\theta)\right)_Y = 0 \quad (X = 0). \tag{1.32}$$

The differential equation and boundary conditions can thus be written

$$\left(\frac{\partial^2(\alpha w\sin\theta)}{\partial X^2}\right)_Y+\frac{\xi}{X}\left(\frac{\partial(\alpha w\sin\theta)}{\partial X}\right)_Y=\left(\frac{\partial^2(\alpha w\sin\theta)}{\partial Y^2}\right)_X \quad (X>0,\ -y_1/\alpha<Y<y_1/\alpha), \tag{1.33}$$

$$\alpha w\sin\theta=\pm\alpha w\sin\theta_1, \quad Y=\pm y_1/\alpha, \tag{1.34}$$

$$\alpha w\sin\theta=g(Y) \quad (X=0). \tag{1.35}$$

These together with (1.32) are sufficient to obtain the flow angle throughout the exit cone where θ_1 is the flow angle at the boundary and the function in (1.35) is obtained from the subsonic region as will now be demonstrated.

The definition of X as given by (1.21) is valid only in the supersonic region for it assumes imaginary values with subsonic flow. A new variable is introduced for the latter case defined as

$$X_1=\int_\epsilon^x\frac{1}{\alpha}\left(-\frac{h_2+h_3^2/h_1}{h_1}\right)^{\frac{1}{2}}\mathrm{d}x \quad (x<\epsilon), \tag{1.36}$$

the term in the bracket in the integrand having the mean values across the sections perpendicular to the principal axis and ϵ has the same value as in (1.21) so that

$$X_1=\mathrm{d}x/\mathrm{d}X_1=0 \quad (x=\epsilon).$$

Equation (1.33) is replaced by

$$\left(\frac{\partial^2}{\partial X_1^2}(\alpha w\sin\theta)\right)_Y+\frac{\xi}{X_1}\left(\frac{\partial}{\partial X_1}(\alpha w\sin\theta)\right)_Y+\left(\frac{\partial^2(\alpha w\sin\theta)}{\partial Y^2}\right)_{X_1}=0 \quad (X_1<0,\ -y_1/\alpha<Y<y_1/\alpha). \tag{1.37}$$

The boundary conditions (1.32) and (1.34) remain the same but with X_1 replacing X but that given by (1.35) is no longer necessary since (1.37) is elliptic.

One further condition is necessary and it is generally sufficient to write this as

$$\alpha w\sin\theta=0 \quad (X_1\to-\infty). \tag{1.38}$$

Equations (1.32), (1.34), (1.37) and (1.38) are sufficient to obtain the complete solution in the subsonic region and in particular the value of θ can be obtained at $X_1=0$ which determines the function $g(Y)$ of (1.35).

The solutions are complicated by the form of ξ. The following procedure is adopted in the subsequent sections. In §§ 2 and 6 the numerical solutions obtained by the method of characteristics in the supersonic exit cone are compared with the values obtained by this linearized theory. The examples taken are hypothetical in so far that entirely parallel flow is assumed at the throat sections. In these cases all the terms of the differential equation are identically zero at the throat section. Further the values of ξ fall rapidly in value outside the curved portion of the nozzle and if small values of R_t/D are assumed, D being the throat diameter, it suffices to take $\xi=0$ throughout the exit cone. By this means trivial analytical solutions can be obtained from which the nature of the flow is easily appreciated.

The transonic region is investigated in §§ 3 and 7. It can be shown that the characteristics of the flow at the throat for a specified stagnation pressure are determined almost entirely by the local boundary conditions and ξ can be taken as unity.

The propagation of non-symmetries in the flow is investigated in some detail in §§ 4 and 8. In the approximate analysis ξ is taken as unity in the curved portion of the nozzle and zero thereafter. In the final analysis the correct values of ξ are employed which leads to equations which must be integrated numerically.

2. The validity of the linear equation in the two-dimensional nozzle exit cone

The limits of the variable Y are a complicated function of X and in general it is not possible to obtain the solution of (1.33) in analytical form. In this section some approximations are made to the linearized theory which enable us to obtain such solutions. The method of approach is best illustrated by expressing the slopes of the physical characteristics of (1.10) in the form

$$\mathrm{d}y/\mathrm{d}x = \tan(\theta \pm \psi),$$

ψ and θ being the local Mach angle and flow angle respectively. Thus the flow causes a net rotation of the characteristic lines through an angle θ. The variable y is replaced by Y to compensate for this as can be seen from (1.26). Approximately

$$\alpha = wy_1, \quad Y = y/wy_1,$$

as can be seen from (1.19). Both w and y_1 are increasing functions of x in the supersonic region and, apart from the throat region, y_1 increases more rapidly than w. For example increasing y_1 from y_t, the value at the throat, to $4y_t$ increases w from 1.0 to 2.07 approximately for $\gamma = 1.25$. Thus if we write

$$\alpha = y_1, \quad Y = y/y_1, \tag{2.1}$$

we partly compensate for the net rotation of the characteristics and also the limits of Y are

$$-1 \leqslant Y \leqslant 1.$$

This approximation is discussed further in § 8. If in addition we omit second order terms, we have

$$X = \int_0^x \frac{1}{y_1}\left(\frac{1-\{(\gamma-1)/(\gamma+1)\}w^2}{w^2-1}\right)^{\frac{1}{2}} \mathrm{d}x. \tag{2.2}$$

The solution of (1.37) with $\xi = 0$ subject to the boundary conditions (1.32), (1.34) and (1.35) takes the form

$$\begin{aligned} wy_1 \sin\theta = {} & \tfrac{1}{2}[g(Y+X)+g(Y-X)] \\ & +F_1(X-1+Y)-F_1(X-3-Y)+F_1(X-5+Y)-F_1(X-7-Y)\ldots \\ & +F_2(X-1-Y)-F_2(X-3+Y)+F_2(X-5-Y)-F_1(X-7+Y)\ldots, \end{aligned}$$

where $g(Y)$ specifies the conditions at the throat (eqn (1.35)) and

$$\begin{aligned} F_1(X) &= h(X) - \tfrac{1}{2}g(1-X), \\ F_2(X) &= -h(X) - \tfrac{1}{2}g(X-1), \\ h(X) &= wy_1 \sin\theta_1, \end{aligned}$$

and

$$g(Y) = 0 \quad (|Y| > 1.0). \tag{2.3}$$

A check on the analysis is obtained by comparing this solution with that obtained numerically by the method of characteristics. The example taken is illustrated in figure 2. The radius of curvature at and just after the throat is a constant value $R_t = \frac{1}{2}D$, D being the throat diameter, and the curved portion of the profile blends into the straight portion so that the slope is continuous, the cone semi-angle being sixteen degrees. The flow at the throat is taken as parallel so that $g(Y) = 0$. We compare the stream pressure variations across the semi-nozzle as obtained by the two methods, i.e. the difference in pressure between the axis and boundary at the various sections.

From (2.3) with $g = 0$ we obtain

$$\begin{aligned} w\int_0^{y_1} \sin\theta\,\mathrm{d}y &= \int_0^X h(u)\,\mathrm{d}u \quad (0 \leqslant X \leqslant 1), \\ &= \int_{X-1}^X h(u)\,\mathrm{d}u - \int_0^{X-1} h(u)\,\mathrm{d}u \quad (1 \leqslant X \leqslant 2), \\ &= \int_{X-1}^X h(u)\,\mathrm{d}u - \int_{X-2}^{X-1} h(u)\,\mathrm{d}u + \int_0^{X-2} h(u)\,\mathrm{d}u \quad (2 \leqslant X \leqslant 3), \end{aligned} \tag{2.4}$$

.....

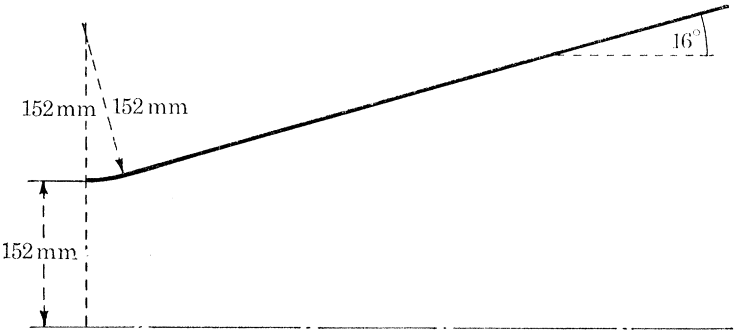

FIGURE 2. The nozzle configuration used in the calculations.

The velocity variation across the section is

$$\Delta q = (\phi_x^2 + \phi_y^2)^{\frac{1}{2}}{}_{y=y_1} - (\phi_x)_{y=0},$$

and to the second order this is

$$\begin{aligned} \Delta q &= (\phi_x)_{y=y_1} - (\phi_x)_{y=0} + \tfrac{1}{2}w\sin^2\theta_1, \\ &= \mathrm{d}\,[\phi(x, y_1) - \phi(x, 0)]/\mathrm{d}x - \tfrac{1}{2}w\sin^2\theta_1, \end{aligned}$$

since to the second order

$$\frac{\partial\phi}{\partial x} = \frac{\mathrm{d}\phi}{\mathrm{d}x} - w\sin^2\theta_1 \quad (y = y_1).$$

Omitting third order terms in (1.29) we obtain

$$\phi(x, y_1) - \phi(x, 0) = \int_0^{y_1} w\sin\theta\,\mathrm{d}y + \frac{1}{2w^2}\int_0^{y_1} \lambda\phi_y\,\mathrm{d}y.$$

The second term on the right-hand side is a third order term, thus to the second order

$$\Delta q = \frac{\mathrm{d}}{\mathrm{d}x}\left(w\int_0^{y_1} \sin\theta\,\mathrm{d}y\right) - \tfrac{1}{2}w\sin^2\theta_1,$$

the first term on the right-hand side of which is obtained from (2.4).

A large scale characteristic diagram was drawn with a throat diameter of 304.8 mm which is reproduced on a much reduced scale in figure 3, the rays representing 1° expansion waves. In each element of the grid, the flow angle and the Prandtl–Meyer expansion angle can be readily obtained; the latter is the minimum number of expansion waves that must be crossed in proceeding from the throat to the element. The values of w_1 can be obtained from these using the appropriate tables and thus the value Δq. The ratio of the specific heats is taken as 1.25.

The pressure difference across the section can be obtained from (1.3) and (1.8) in the form

$$\Delta p = -\left(\frac{2}{\gamma+1}\right)^{\gamma/(\gamma-1)} \gamma p_0 y_t \Delta q/y_1. \tag{2.5}$$

The continuous curve in figure 4 is obtained from the analytical theory and the discrete points from the characteristic diagram. The pressure difference is seen to be oscillatory. The agreement is reasonably good but there is clearly a systematic error, the positions of the two maxima being displaced from each other. This is probably due to the approximation made in α in (2.1). This is demonstrated more clearly by applying the analytical theory in the following manner.

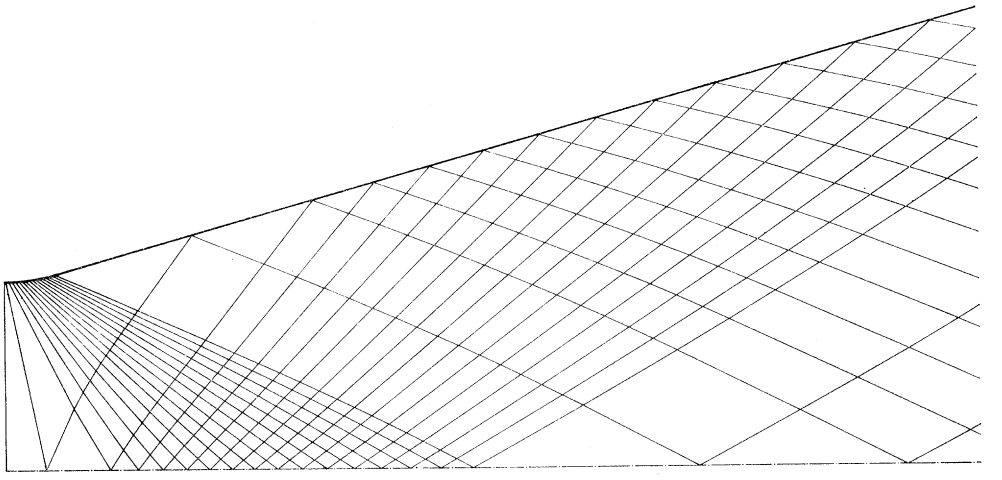

FIGURE 3. The characteristic diagram of the flow in the nozzle of figure 2 assuming parallel flow at the throat; 1° expansion waves, $\gamma = 1.25$.

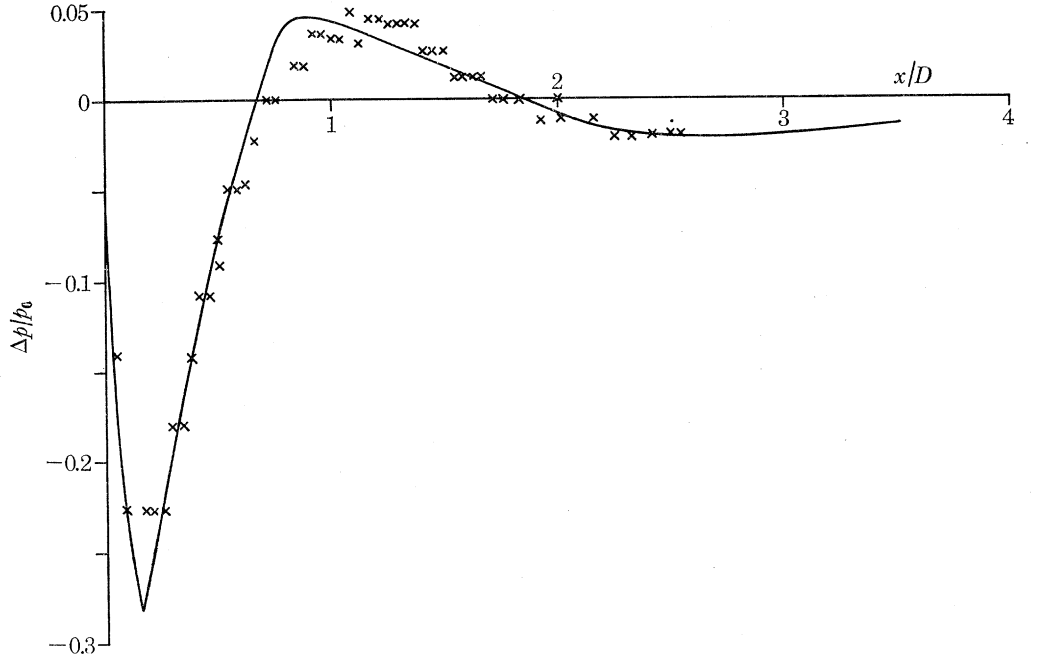

FIGURE 4. The pressure difference between the axis and the wall of the nozzle of figure 2 assuming parallel flow at the throat, stagnation pressure p_0.

In figure 5, the semi-nozzle of figure 3 is turned through 8° so that it represents a nozzle of 16° total angle but which is asymmetric in the region of the throat. The x axis is taken as the bisector of the exit cone. The method is illustrated in figure 5. The boundaries of the nozzle are taken to be O_1E_1 and O_2E_2 while O_1O_2 is taken to be the throat so that the flow angle at O_1 is that at O, namely, minus 8°, and the flow angle at any other point Q_1 is taken to be that at Q, the

displacements QQ_1 being quite small compared with the throat diameter. The value of w at the section Q_1Q_2 is obtained from the expansion ratio QQ_2/OO_2, i.e. we assume the mean Mach number across OO_2 is unity which is approximately correct as can be seen from the characteristic diagram. With this method of treatment the maximum values of the lateral velocity are halved so that the second order terms are reduced by a factor of the order of 4. The analysis is similar to that given previously with the boundary conditions

$$wy_1 \sin\theta = wy_1 \sin\theta_1 \equiv H_1(X) \quad (Y = 1),$$
$$wy_1 \sin\theta = -wy_1 \sin 8^\circ \equiv -H_2(X) \quad (Y = -1).$$

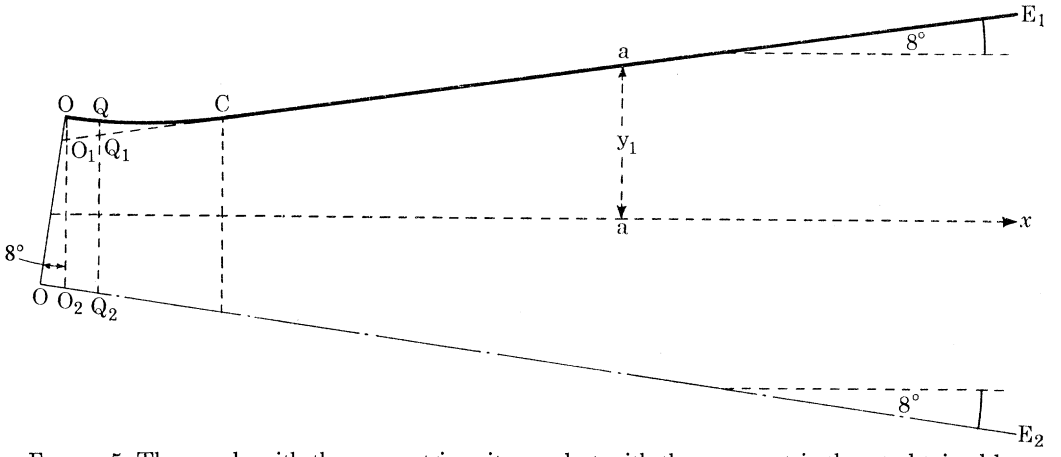

FIGURE 5. The nozzle with the symmetric exit cone but with the asymmetric throat obtained by the rotation of figure 2 through 8°.

The solution is given by (2.3) but with

$$F_1(X) = H_1(X) - [g(1-X)]/2,$$
$$F_2(X) = -H_2(X) - [g(X-1)]/2,$$

where
$$g(Y) = -y_t \sin 8^\circ \equiv H_3 \quad (-1 < Y < 1),$$
$$= 0 \quad (|Y| > 1), \tag{2.6}$$

y_t being the value of y_1 at the throat.

The solution can be expressed in the form

$$w\int_{-y_1}^{y_1} \sin\theta \, dy = \int_0^X H(u)\, du - 2(1-X)\, H_3 \quad (0 \leqslant X \leqslant 2),$$
$$= \int_0^X H(u)\, du - 2\int_0^{X-2} H(u)\, du - 2(X-3)\, H_3 \quad (2 \leqslant X \leqslant 4),$$
$$= \int_0^X H(u)\, du - 2\int_0^{X-2} H(u)\, du + 2\int_0^{X-4} H(u)\, du - 2(5-X)\, H_3 \quad (4 \leqslant X \leqslant 6),$$
$$= \int_0^X H(u)\, du - 2\int_0^{X-2} H(u)\, du + 2\int_0^{X-4} H(u)\, du - 2\int_0^{X-6} H(u)\, du - 2(X-7)\, H_3 \quad (6 \leqslant X \leqslant 8),$$
$$\ldots\ldots\ldots\ldots\ldots\ldots\ldots\ldots\ldots\ldots\ldots\ldots\ldots\ldots\ldots\ldots\ldots\ldots\ldots\ldots\ldots\ldots$$

where
$$H(X) = H_1(X) - H_2(X). \tag{2.7}$$

The mean values of θ, i.e. $\bar{\theta}$, across the sections so obtained are presented in figure 6 together with those obtained from the characteristic diagram; in the latter case they represent means across lines at 98° to the principal axis of the cone of figure 3. Beyond the point C in figure 3, i.e. the junction of the curved and straight portions of the boundary, the term H is zero since θ_1 is 8°. Thus beyond C the theoretical curve is periodic with the semi-wavelength given by $X = 2$. We find from the characteristic diagram that the mean values of $\sin\theta$ are zero at values of $2y_1$ of 172.3 mm and 248.5 mm and with the correct throat $2y_t = 152.4$ mm, the corresponding expansion ratios are 1.1305 and 1.6305 respectively and the Prandtl–Meyer expansion angles are 0.1746 and 0.4560 radian respectively. As we see later these give a semi-wavelength of (eqn (2.9))

$$X = \frac{1}{\tan 8°}[0.4560 - 0.1746] = 2.0022.$$

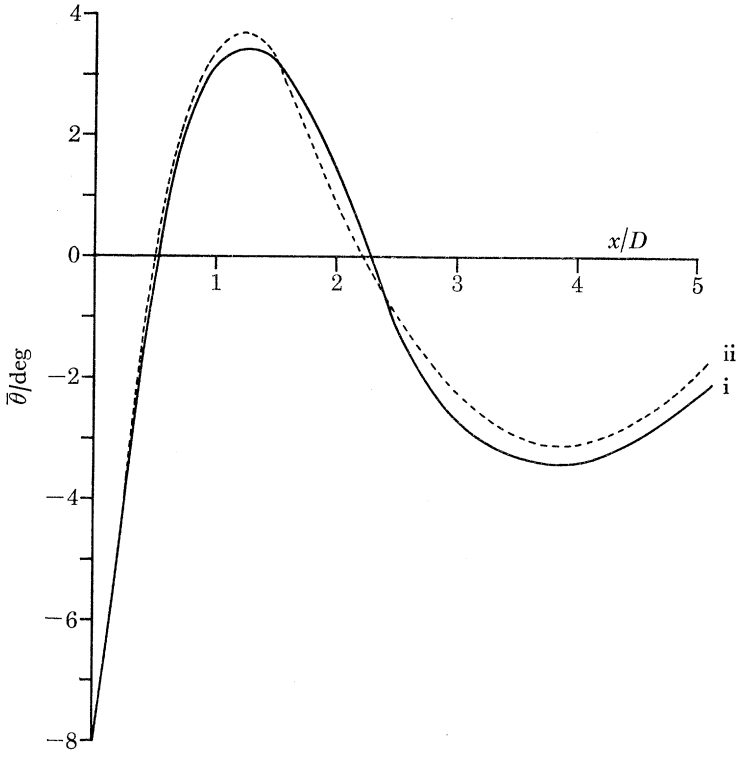

FIGURE 6. The mean value of the flow angle across the section of the nozzle of figure 5 assuming parallel flow at the throat. (i) Linearized theory, (ii) characteristic diagram.

This remarkable agreement is unlikely to be fortuitous. Two additional large scale characteristic diagrams have been constructed with $\gamma = 1.4$. The cone semi-angles are 8 and 16° respectively with $R_t/D = 1.0$ in both cases. A similar analysis was carried out with both of these and the results are given in table 1.

Figure 6 reveals further evidence of the systematic error due to the approximation of α, the discrepancy at the maximum being reversed at the minimum. Apart from this there appear to be no extraneous damping factors and the linearized equation reproduces the results of the more accurate treatment fairly closely.

In general it is necessary to compute X but in particular cases it can be expressed in functional form. For small values of x it becomes

$$X = \left(\frac{2}{\gamma+1}\right)^{\frac{1}{2}} \frac{1}{y_t} \int_0^x \frac{dx}{(2w_t' x)^{\frac{1}{2}}} = \frac{2}{y_t}\left(\frac{x}{(\gamma+1)w_t'}\right)^{\frac{1}{2}},$$

y_t being the throat semi-diameter and w_t' is given by (1.13). A more accurate form can be obtained by writing

$$w = 1 + w_t' x + \tfrac{1}{2} w_t'' x^2 + \ldots,$$

$$w_t'' = (w_t')^2 (1 - \tfrac{2}{3}\gamma),$$

and substituting it into (2.2).

TABLE 1

	8° semi-cone			16° semi-cone		
	y_1/y_t	X	ΔX	y_1/y_t	X	ΔX
1st zero	1.058	1.41	1.05	1.17	1.43	0.95
minimum	1.133	2.46	0.89	1.38	2.38	1.01
2nd zero	1.212	3.35	1.08	1.74	3.39	0.95
maximum	1.332	4.43	0.99	2.25	4.34	1.05
3rd zero	1.48	5.42	0.97	3.15	5.39	0.99
minimum	1.65	6.39	1.03	4.60	6.38	
4th zero	1.88	7.42	0.99	mean	$\Delta X =$	0.992
maximum	2.15	8.41	0.96			
5th zero	2.48	9.37	1.04			
minimum	2.94	10.41				
	mean	$\Delta X =$	1.000			

In the nozzle of figure 2, the radius of curvature R_t is constant and this fits into the straight portion, the slope being continuous at the junction at $x = x_0$. For values of x less than x_0, approximately

$$X = \frac{2}{y_t}\left(\frac{x}{(\gamma+1)w_t'}\right)^{\frac{1}{2}} (1 - \tfrac{1}{9}\gamma x w_t') \quad (0 \leqslant x \leqslant x_0). \tag{2.8}$$

Using (1.12) for values of x greater than x_0 we have

$$X = X_0 + \frac{dx}{dy_1} \int_{w_0}^{w} \left(\frac{w^2 - 1}{1 - \{(\gamma-1)/(\gamma+1)\}w^2}\right)^{\frac{1}{2}} \frac{dw}{w},$$

X_0 and w_0 being the values at x_0. This becomes

$$X = X_0 + [f(w) - f(w_0)] \Big/ \frac{dy_1}{dx} \quad (x > x_0), \tag{2.9}$$

$f(w)$ being the Prandtl–Meyer expansion angle. These are the values of X used in the analysis in this section.

3. THE VALIDITY OF THE LINEAR EQUATION IN THE THROAT REGION OF A TWO-DIMENSIONAL NOZZLE

The entry cone appears as in figure 1. The curved portions fit into the straight line generators which expand into a very large reservoir. The method of approach is similar to that used in the supersonic region. The values of α and Y are given by (2.1) and omitting second order terms

$$X_1 = \int_0^x \frac{1}{y_1}\left(\frac{1 - \{(\gamma-1)/(\gamma+1)\}w^2}{1 - w^2}\right)^{\frac{1}{2}} dx \quad (-\infty < x < 0), \tag{3.1}$$

so that $X_1 = 0$ at the throat with negative values in the entry cone.

The general solution is given in a later paper where it is shown that the throat region is of considerable importance and it is the purpose of this section to verify the analysis in this region. With the approximations already specified, (1.37) reduces to

$$\frac{\partial^2}{\partial X_1^2}(wy_1\sin\theta)+\frac{\xi}{X_1}\frac{\partial}{\partial X_1}(wy_1\sin\theta)+\frac{\partial^2}{\partial Y^2}(wy_1\sin\theta)=0 \quad (X_1\leqslant 0,\ -1\leqslant Y\leqslant 1), \tag{3.2}$$

with the boundary conditions

$$\partial(wy_1\sin\theta)/\partial X_1=0 \quad (X_1=0),$$
$$\sin\theta=\pm\sin\theta_1 \quad (Y=\pm 1).$$

This can be solved analytically for both $\xi=0$ and $\xi=1$ but the analysis is tedious. It has been carried out for the analogous problem in three dimensions and it has been found that the flow in the throat region is determined almost entirely by the boundary profile in this region and is unaffected by upstream conditions. Thus we should take $\xi=1.0$ and it is possible to solve the problem by series method.

Combining (1.12) and (3.1), we find

$$wy_1\sin\theta_1=-w'(\mathrm{d}x/\mathrm{d}X)^2\cos\theta_1. \tag{3.3}$$

Also at positions near the throat

$$w'=w'_t+w''_t x+\tfrac{1}{2}w'''_t x^2+\ldots, \tag{3.4}$$

$$w''_t=(w'_t)^2(1-2\gamma/3), \quad w'''_t=\tfrac{3}{2}(w'_t)^3\left[\frac{(3-\gamma)^2}{9}-\frac{7\gamma}{6}-\tfrac{1}{2}+y_t\frac{(\gamma+1)}{2R_t}\right].$$

Similarly for small values of x

$$X_1=-\frac{2}{y_t}\left(\frac{1}{(\gamma+1)\,w'_t}\right)^{\frac{1}{2}}(-x)^{\frac{1}{2}}\left[1-\frac{\gamma w'_t x}{9}-x^2\left\{\frac{(w'_t)^2}{720}(45+63\gamma+2\gamma^2)+\frac{1}{80R_t^2}\right\}\right],$$

and

$$x=-\frac{w'_t(\gamma+1)\,y_t^2X_1^2}{4}\left[1-\frac{\gamma y_t}{18R_t}X_1^2+\frac{X_1^4}{16}\left(\frac{y_t}{R_t}\right)^2\left\{\frac{45+63\gamma+2\gamma^2}{360}+\frac{7\gamma^2}{81}+\frac{\gamma+1}{40}\frac{y_t}{R_t}\right\}\right]. \tag{3.5}$$

Combining (3.3), (3.4) and (3.5), we have

$$wy_1\sin\theta_1=-aX_1^2+bX_1^4-cX_1^6\ldots, \tag{3.6}$$

where

$$a=y_t(\gamma+1)^{\frac{1}{2}}(y_t/R_t)^{\frac{3}{2}}/4,$$
$$b=ay_t(9+2\gamma)/36R_t,$$
$$c=a\left\{\left(\frac{y_t}{R_t}\right)^2\left(\frac{9}{128}+\frac{283\gamma}{5{,}760}+\frac{149\gamma^2}{25{,}920}\right)+\left(\frac{y_t}{R_t}\right)^3\frac{\gamma+1}{640}\right\}.$$

The solution is expressed in the form

$$wy_1\sin\theta=wy_1\sin\theta_1\,Y+S_1\sum_{n=0}^{\infty}A_{2n}X_1^{2n}+S_3\sum_{n=0}^{\infty}B_{2n}X_1^{2n}+\ldots, \tag{3.7}$$

where

$$S_1=Y^3-Y,$$
$$S_3=(3Y^5-10Y^3+7Y)/60,$$
$$S_5=(3Y^7-21Y^5+49Y^3-31Y)/2520,$$

so that
$$S_{2n+1} = 0, \quad Y = \pm 1, \quad (n > 0),$$
$$\mathrm{d}^2 S_{2n+1}/\mathrm{d}Y^2 = S_{2n-1} \quad (n \geqslant 1),$$

and the terms A, B, C... are constant.

Substituting this into (3.2) with $\xi = 1$ we obtain the recurrence relations

$$\left.\begin{aligned} 6A_0 &= 4a, & 4A_2 + B_0 &= 0, & 4B_2 + C_0 &= 0, & \ldots,\\ 6A_2 &= -16b, & 16A_4 + B_2 &= 0, & 16B_4 + C_2 &= 0, & \ldots,\\ 6A_4 &= 36c, & 36A_6 + B_4 &= 0, & 36B_6 + C_4 &= 0, & \ldots. \end{aligned}\right\} \tag{3.8}$$

At the throat
$$y_t \sin\theta = \tfrac{2}{3}aS_1 + \tfrac{32}{3}bS_3 + 384S_5 c \ldots. \tag{3.9}$$

The variation of the axial velocity across the section can be obtained from (1.29) and (1.31) in the form
$$\left(\frac{\partial\phi}{\partial x}\right)_y - \left(\frac{\partial\phi}{\partial x}\right)_0 = \frac{\partial}{\partial x}\int_0^y wy_1 \sin\theta \,\mathrm{d}Y + \frac{1}{2}\frac{\partial}{\partial x}\left(\frac{1}{w^2}\int_0^y \lambda\phi_y \,\mathrm{d}y\right). \tag{3.10}$$

The differential equation (3.2) with $\xi = 1$ can be written
$$\frac{\partial}{\partial X_1}\int_0^Y wy_1 \sin\theta \,\mathrm{d}Y = -\frac{1}{X_1}\int_0^{X_1} X_1 \left[\frac{\partial}{\partial Y}(wy_1 \sin\theta)\right]_0^Y \mathrm{d}X_1,$$

and thus
$$\frac{\partial}{\partial x}\int_0^Y wy_1 \sin\theta \,\mathrm{d}Y = -\frac{1}{2}\frac{\mathrm{d}X_1^2}{\mathrm{d}x}\left[K_1 \sum_{n=0}^{\infty} \frac{A_{2n} X_1^{2n}}{2n+2} + K_3 \sum_{n=0}^{\infty} \frac{B_{2n} X_1^{2n}}{2n+2} \ldots\right], \tag{3.11}$$

where
$$K_{2n+1} = [\mathrm{d}S_{2n+1}/\mathrm{d}Y]_0^Y,$$

and the differential of X_1^2 is obtained from (3.5).

Since $\bar{\lambda}$ is of the second order then from (3.9), (3.10) and (3.11)
$$\lambda/2w = (\tfrac{1}{2}Y^2 - \tfrac{1}{6})\, y_t/R_t,$$

and
$$\theta = Yx/R_t + (Y^3 - Y)\,(\gamma+1)^{\frac{1}{2}} y_t^{\frac{3}{2}}/6R_t^{\frac{3}{2}},$$

to the first order and these enable us to determine the second term on the right-hand side of (3.10) to the second order.

At the throat we find
$$\phi_x(y) - \phi_x(0) = y_t[36K_1 R_t + (144 + 32\gamma)\, K_3 y_t + (27Y^4 - 18Y^2)\, y_t]/216R_t^2 \tag{3.12}$$

to the second order.

The transonic region has received considerable attention from other investigators. Meyer (1908), Taylor (1930) and Hooker (1931) expressed their solutions in power series which terminated at the fourth order but these are not entirely satisfactory since the higher order terms of y are significant near the boundary. Their methods were developed by Sauer (1944) and Oswatitsch & Rothstein (1942) whose solutions agree to the first order and are a valid first approximation. This was later obtained by more sophisticated methods by Behrbohm (1950), Tomotika & Tamada (1950) and Tomotika & Hasimoto (1950). The nature of the flow was investigated in detail by Lighthill (1947) who pointed out that in the supersonic region y must be a three valued function of θ, a property possessed by Sauer's solution. More recently an extensive analysis was carried out by Hall (1962) and his results appear to be the best yet obtained in both two and three dimensional flow. He expresses the flow angle and velocity to the third order in $1/R_t$

whereas the earlier solutions are valid to the first order. Hall has evaluated the velocity distribution across the throat for $R_t/y_t = 5.0$ and his results are compared with those of (3.12) in table 2. The agreement is good. The solutions of Sauer and Hall are identical to (3.7) and (3.12) to the first order.

TABLE 2. VELOCITY VARIATION ACROSS THE THROAT

Y	Hall	equation (3.12)
0	0	0
0.2	0.0032	0.0032
0.4	0.0133	0.0130
0.6	0.0305	0.0303
0.8	0.0561	0.0563
1.0	0.0923	0.0929

It should be noted that the approximation made in α is reasonably correct in the exit cone. The velocity ratio w decreases in the subsonic region away from the throat and the approximation would appear to be invalidated. However, the conditions at the throat are determined by the profile slope in the immediate vicinity and little serious error arises. A more exact treatment is given in a later paper.

It is clear from the above analysis that ϕ_y is continuous provided the profile slope is continuous but the continuity of ϕ_x requires the curvature at the throat to be continuous also. This can be demonstrated by examining (3.11). The term in the square brackets is determined by the entry cone and

$$\frac{\mathrm{d}X_1^2}{\mathrm{d}x} = \frac{4}{w_t'(\gamma+1)\,y_t^2} \quad (X_1 = 0).$$

Equation (1.12) is valid in the entry and exit cones and by taking the limit as x approaches zero we obtain the value of w_t' given by (1.13). The limit can be reached from the entry or the exit side and if R_t is discontinuous at the throat, the two limiting values differ so that ϕ_x is discontinuous. It would appear that an isentropic solution requires that the curvature be continuous at the throat but elsewhere it is sufficient that the profile slope be continuous. The pattern of the flow that would otherwise occur is probably similar to that observed photographically by Fraser, Rowe & Coulter (1957). Small shock waves are attached to the boundary just ahead of the throat causing the flow to separate with re-attachment in the exit cone just after the throat. Slip streams parallel to the axis proceed into the exit cone from the throat boundaries, together with the characteristic diagonal shock pattern. These effects were observed with a discontinuity in profile slope at the throat but a similar phenomenon is likely with a discontinuity in curvature but to a lesser extent.

4. NON-SYMMETRIC FLOW IN A TWO-DIMENSIONAL NOZZLE; THE DERIVATION OF THE LATERAL FORCES AND COUPLES

It is assumed that the nozzle is symmetric but the flow is asymmetric due to upstream effects. That is, we require to determine the magnitude of the flow asymmetry at the exit of the nozzle when the entry flow is asymmetric.

The differential equation (1.10) is valid and ϕ can be expressed in the form

$$\phi = \phi' + \phi'', \tag{4.1}$$

where, with respect to the axis $y = 0$, ϕ' is symmetric and ϕ'' is the perturbation which is non-symmetric. The first term satisfies (1.10) as it represents the unperturbed flow which is discussed in § 1.

If we neglect the second order terms, the parameters h_2 and h_3 are the same as in the unperturbed flow because they contain the derivatives of ϕ' only. Also to the first order

$$h_1 = w^2 + \lambda - \frac{2}{\gamma+1} v^2 + 2w \frac{\partial \phi''}{\partial x} - 1,$$

λ and v having the values for the unperturbed flow. Thus

$$h_1 \phi''_{xx} + 2h_3 \phi''_{xy} - h_2 \phi''_{yy} + 2ww' \phi''_x = 0, \tag{4.2}$$

second order terms being neglected, and h_1, h_2 and h_3 being given the same values as those used in the unperturbed flow as expressed by (1.11). Equation (4.2) has the same characteristic lines as in the unperturbed flow so that it can be expressed in the form (1.23). In deriving the form for $F(X, Y)$, equation (1.27) with ϕ replaced by ϕ'' must be compared with (4.2). Thus

$$F(X, Y) = \frac{\partial \phi''}{\partial X} \left\{ \left(\frac{\mathrm{d}x}{\mathrm{d}X} \right)^2 \frac{\mathrm{d}^2 X}{\mathrm{d}x^2} + \frac{2ww'}{h_1} \frac{\mathrm{d}x}{\mathrm{d}X} \right\},$$

and for small values of x this becomes

$$F(X, Y) = \frac{1}{X} \frac{\partial \phi''}{\partial X}.$$

At distances away from the throat, $F(X, Y)$ is of the second order so that the function ϕ satisfies (1.28). The subsequent analysis of § 1 is valid and (1.33) and (1.37) apply to non-symmetric flow. This has already been assumed in § 2 and verified by the subsequent analysis.

The asymmetry of flow at the section at x perpendicular to the axis $y = 0$ can be expressed as a lateral momentum $-L$, and a parallel displacement from the axis $y = 0$ of the thrust T by a distance z. The term Tz is effectively a clockwise couple which is denoted by C_{T}.

The thrust per unit cross-sectional area is

$$T_1 = p_1 + \rho_1 (w_1^2 - v_1^2) a_{\mathrm{t}}^2 = \rho_1 a_{\mathrm{t}}^2 (w_1^2 + 1)(\gamma + 1)/2\gamma - \rho_1 v_1^2 a_{\mathrm{t}}^2,$$

p_1 and ρ_1 being the pressure and density respectively,

$$w_1^2 = \left(\frac{\partial \phi}{\partial x} \right)^2 + \left(\frac{\partial \phi}{\partial y} \right)^2 \quad \text{and} \quad v_1^2 = \left(\frac{\partial \phi}{\partial y} \right)^2.$$

If $w_1^2 = w^2 + \lambda_1$ and $v_1 = v + \Delta v$ where, with respect to the axis $y = 0$, w and v are symmetric while λ_1 and Δv are the non-symmetric parts, and it is assumed that λ_1, Δv and v^2 are first order terms so that their products and squares are neglected, then from (1.3)

$$\rho_1 = \rho \left[1 - \frac{\lambda_1}{\gamma + 1 - (\gamma - 1) w^2} \right].$$

Thence $$T_1 = a_{\mathrm{t}}^2 \rho (w^2 + 1)(\gamma + 1)/2\gamma - a_{\mathrm{t}}^2 \rho (M^2 - 1) \lambda_1 / 2 - \rho a_{\mathrm{t}}^2 (v^2 + 2v\Delta v),$$

and $$C_{\mathrm{T}} = \int_{-y_1}^{y_1} T_1 y \, \mathrm{d}y = -\tfrac{1}{2}(M^2 - 1) \rho a_{\mathrm{t}}^2 \int_{-y_1}^{y_1} \lambda y \, \mathrm{d}y - \rho a_{\mathrm{t}}^2 \int_{-y_1}^{y_1} 2v \Delta v y \, \mathrm{d}y. \tag{4.3}$$

The perturbations in the flow angles at the boundaries are zero and at $y = \pm y_1$,

$$2w\Delta v = -\lambda_1 \sin \theta_1,$$

so that the integrand of the second integral on the right-hand side of (4.3) can be neglected at the boundary while y and v are zero at the axis. It can be expected that the perturbation $\Delta\theta$ in the flow angle is of an order less than $\sin\theta_1$ so that the second integral on the right-hand side of (4.3) can be neglected. This is confirmed by the numerical analysis discussed later. The mean value of M across the throat is unity so that

$$C_T = 0 \quad (x = 0). \tag{4.4}$$

The lateral momentum is
$$L = -a_t^2 \int_{-y_1}^{y_1} \rho_1 \phi_x \phi_y \, dy, \tag{4.5}$$

and since
$$\rho_1 \phi_x = w\rho \left(1 - \frac{\lambda_1}{\gamma + 1 - (\gamma - 1)w^2}\right)\left(1 + \frac{\lambda_1 - v_1^2}{2w^2}\right),$$

$$\phi_y = w(1 + \lambda_1/2w^2)\sin\theta,$$

this may be written
$$L = -a_t^2 \int_{-y_1}^{y_1} \rho w^2 \sin\theta \, dy + \rho a_t^2 \frac{M^2 - 2}{2w} \int_{-y_1}^{y_1} \lambda_1 v \, dy. \tag{4.6}$$

The second term on the right-hand side is of the second order and in this it suffices to write

$$v = wy \sin\theta_1 / y_1,$$

so that
$$\int_{-y_1}^{y_1} \lambda_1 v \, dy = \frac{w \sin\theta_1}{y_1} \int_{-y_1}^{y_1} \lambda_1 y \, dy. \tag{4.7}$$

Thus from (4.3), (4.6) and (4.7)
$$L = -a_t^2 \int_{-y_1}^{y_1} \rho w^2 \sin\theta \, dy - \frac{M^2 - 2}{M^2 - 1} \frac{\sin\theta_1}{y_1} C_T. \tag{4.8}$$

It has been shown in § 1 that the mean value of w_1^2 across the section differs from the one-dimensional value by terms of the order v^2. Also from one-dimensional theory the rate of mass flow is m where

$$m = 2y_1 w \rho a_t,$$

so that
$$L = -\frac{m a_t}{2y_1} \int_{-y_1}^{y_1} w \sin\theta \, dy - \frac{M^2 - 2}{M^2 - 1} \frac{C_T}{y_1} \frac{dy_1}{dx}. \tag{4.9}$$

TABLE 3

x/D	$10^3 L/T$	$10^3 L_1/T$
0.664	22.03	22.28
0.774	−9.83	−9.76
0.885	2.13	2.33
0.996	11.87	10.71
1.106	18.46	18.76
2.655	11.35	11.44
2.765	8.53	8.57
2.876	4.03	4.04
2.987	0.29	0.22
3.097	−2.47	−2.55
7.522	−6.30	−6.44
7.633	−5.22	−5.38
7.743	−4.81	−4.93
7.854	−4.31	−4.48
7.965	−3.39	−3.55
8.075	−2.24	−2.38
8.186	−1.47	−1.62

This formula has been checked using the characteristic diagram of figure 3 turned through 8° as in figure 5 so that it corresponds to the flow in a symmetric exit cone of 16° total angle but with a skew throat. The couple C_T is maximum near the zeros of L and the computations have been carried out around these positions. The lateral momentum L has been calculated by using (4.5), the terms in the integrand being obtained from the characteristic diagram.

Also it has been calculated in a similar manner from (4.9), this value being denoted by L_1. The results are contained in table 3, in which the two values of the lateral momentum are expressed as ratios to the axial thrust in the jet at that section.

The agreement is seen to be good, the differences being of the order of possible numerical errors.

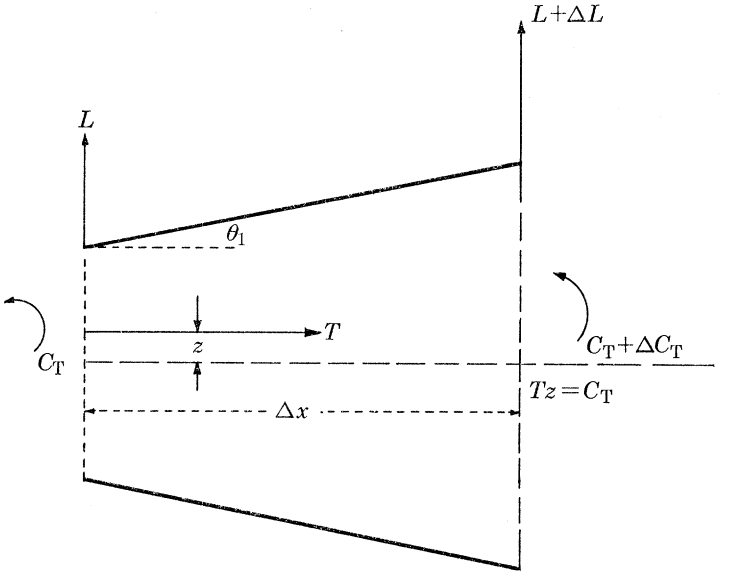

FIGURE 7. The force system on a section of a two-dimensional nozzle.

One further relation between L and C_T can be derived from geometrical considerations. Figure 7 is a section of a two-dimensional nozzle. If the nozzle terminates at x the lateral force is L, if it terminates at $x+\delta x$ the lateral force is $L+(\mathrm{d}L/\mathrm{d}x)\,\delta x$.

Clearly
$$\mathrm{d}L/\mathrm{d}x = (p_1)_{y_1} - (p_1)_{-y_1}.$$

Taking moments about O of the forces on the elementary section

$$-y_1\,\delta y_1 \frac{\mathrm{d}L}{\mathrm{d}x} + \left(L + \frac{\mathrm{d}L}{\mathrm{d}x}\,\delta x\right)\delta x + \frac{\mathrm{d}C_T}{\mathrm{d}x}\,\delta x = 0,$$

so that
$$\frac{\mathrm{d}C_T}{\mathrm{d}x} = -L + y_1 \frac{\mathrm{d}y_1}{\mathrm{d}x}\frac{\mathrm{d}L}{\mathrm{d}x}. \tag{4.10}$$

Equations (4.4), (4.9) and (4.10) enable us to express L and C_T in terms of I where

$$I = \int_{-y_1}^{y_1} w \sin\theta \,\mathrm{d}y. \tag{4.11}$$

As an example we take the case of flow in the exit cone when flow in the throat is non-symmetric owing to upstream effects. The solution of the differential equation with boundary conditions given by (2.3) corresponds to the case when $\xi = 0$ throughout. In this the flow is entirely parallel at the throat and also R_t/D is small so that this approximation is valid apart from a zero error.

The results obtained from the analysis are in close agreement with those obtained by the method of characteristics, and in all examples it would appear that the values of $w \sin\theta$ deduced can be considered as correct to the second order, even though the differential equation is correct only to the first order. This may be accepted as a semi-empirical result.

An alternative form of the solution given by (2.3) can be derived. As in § 2 we take $\alpha = y_1$ and $\xi = 0$. The differential equation is given by (1.33) and the boundary conditions are given by (1.32) and (1.34). The solution is

$$wy_1 \sin\theta = \sum_{n=0}^{\infty} A_n \cos\{(n+\tfrac{1}{2})\pi Y\} \cos\{(n+\tfrac{1}{2})\pi X\} + f(X, Y) \quad (n = 0, 1, 2, 3, \ldots), \tag{4.12}$$

where the coefficients A_n are obtained from the Fourier expansion

$$g(Y) = \sum_{n=0}^{\infty} A_n \cos\{(n+\tfrac{1}{2})\pi Y\}, \tag{4.13}$$

and the function $f(X, Y)$ is the part of the solution arising from the boundary condition (1.34) and is symmetrical with respect to the axis $Y = 0$. Thus

$$I = 2 \sum_{n=0}^{\infty} (-1)^n A_n \cos\{(n+\tfrac{1}{2})\pi X\}/(n+\tfrac{1}{2})\pi. \tag{4.14}$$

In general the flow is not parallel at the throat and the analysis cannot be confined to small values of R_t/D so the assumption $\xi = 0$ is not valid. The general solution takes the form

$$wy_1 \sin\theta = \sum_{n=0}^{\infty} A_n \cos\{(n+\tfrac{1}{2})\pi Y\} K_n(X) + f(X, Y), \tag{4.15}$$

where the functions $K_n(X)$ are the solutions of the equations

$$\frac{\mathrm{d}^2 K_n}{\mathrm{d}X^2} + \frac{\xi}{X}\frac{\mathrm{d}K_n}{\mathrm{d}X} + (n+\tfrac{1}{2})^2 \pi^2 K_n = 0 \tag{4.16}$$

with the conditions $$K_n = 1 \quad \text{and} \quad \mathrm{d}K_n/\mathrm{d}X = 0 \quad \text{at} \quad X = 0. \tag{4.17}$$

It is seen in § 1 that w'_t is a large term but w''_t is a small term. Thus w' is fairly constant in that region bounded by the curved profile of the nozzle but it falls rapidly in magnitude beyond. This suggests the following approximation.

$$\xi = 1, \quad (0 < X < X_0); \qquad \xi = 0, \quad (X > X_0), \tag{4.18}$$

X_0 being the value of X at the intersection of the curved and straight positions of the nozzle. Thus

$$\begin{aligned} K_n(X) &= J_0\{(n+\tfrac{1}{2})\pi X\} \quad (0 < X < X_0), \\ &= a_n \cos\{(n+\tfrac{1}{2})\pi X\} + b_n \sin\{(n+\tfrac{1}{2})\pi X\} \quad (X > X_0), \end{aligned} \tag{4.19}$$

the terms a_n and b_n being obtained from the conditions that $K_n(X)$ and its derivative are continuous at $X = X_0$. Away from the curved portion of the profile the semi-wavelength is again $X = 2.0$.

It is not possible to express L and C_T in simple analytical form in terms of I. An adequate approximation can be found in the following manner. To the first order

$$\mathrm{d}C_T/\mathrm{d}x = -L, \tag{4.20}$$

and substituting this into (4.9) using (1.2) and (1.12) we find

$$\frac{\mathrm{d}C_{\mathrm{T}}}{\mathrm{d}x} = \frac{ma_{\mathrm{t}}}{2y_1} I + \frac{C_{\mathrm{T}}}{y_1}\frac{\mathrm{d}y_1}{\mathrm{d}x} - \frac{w'}{w} C_{\mathrm{T}}. \tag{4.21}$$

Integrating this and using the initial condition given by (4.4) we have

$$C_{\mathrm{T}} = \frac{ma_{\mathrm{t}} y_1}{2w} \int_0^x \frac{w}{y_1^2} I \,\mathrm{d}x. \tag{4.22}$$

Substituting this value of C_{T} into (4.20) or (4.9) yields the value of L to the second order. Thus

$$L = -\frac{ma_{\mathrm{t}}}{2}\frac{\mathrm{d}}{\mathrm{d}x}\left\{\frac{y_1}{w}\int_0^x \frac{w}{y_1^2} I \,\mathrm{d}x\right\}. \tag{4.23}$$

This could be substituted into (4.10) to obtain C_{T} to the second order.

5. The derivation of the linear equation in an axisymmetric nozzle

The procedure is similar to that in the two-dimensional case. The equations of motion are linearized in an analogous manner and the numerical solutions so obtained are compared with those derived from the method of characteristics. A section of the conical nozzle containing the principal axis is as in figure 1. Ox is the axis and r_1 the radius of the section normal to this axis at x so that

$$A/A_{\mathrm{t}} = r_1^2/r_{\mathrm{t}}^2,$$

r_{t} being the radius of the throat section at which x is zero and A_{t} being the throat area.

It is assumed in the first instance that the flow is cylindrically symmetric with respect to the Ox axis and the equation of flow becomes (Shapiro 1953)

$$(1-u^2/a^2)\frac{\partial^2\phi_1}{\partial x^2} + (1-v^2/a^2)\frac{\partial^2\phi_1}{\partial r^2} - \frac{2uv}{a^2}\frac{\partial^2\phi_1}{\partial x\,\partial r} + \frac{1}{r}\frac{\partial\phi_1}{\partial r} = 0, \tag{5.1}$$

u and v being the velocity components parallel and perpendicular to the axis respectively so that

$$u = \frac{\partial\phi_1}{\partial x}, \quad v = \frac{\partial\phi_1}{\partial r}.$$

This can be expressed in terms of the non-dimensional velocities of (1.11) in the form

$$h_1\phi_{xx} + 2h_3\phi_{xr} - h_2\left(\phi_{rr} + \frac{1}{r}\phi_r\right) - \frac{2}{\gamma+1}\frac{v_1^2}{r}\phi_r = 0, \tag{5.2}$$

the coefficients h having the values given by (1.11). From (1.8)

$$w' = \frac{1-\{(\gamma-1)/(\gamma+1)\}w^2}{w^2-1}\frac{2w}{r_1}\frac{\mathrm{d}r_1}{\mathrm{d}x}, \tag{5.3}$$

and taking the limit as x approaches zero

$$w'_{\mathrm{t}} = \{\tfrac{1}{2}(\gamma+1)\, r_{\mathrm{t}} R_{\mathrm{t}}\}^{-\frac{1}{2}}, \tag{5.4}$$

R_{t} again being the radius of the boundary profile at the throat as in figure 1.

Proceeding as in § 1, we replace the variable r by R defined as

$$R = r/\alpha_1, \tag{5.5}$$

in which α_1 is some function of x, the derivatives of which are of the first order. By differentiating along lines of constant R we obtain an equation similar to (1.16) but with y, Y and α replaced by r, R and α_1 respectively. By substituting this into (5.2) and equating the resulting coefficient of ϕ_{xr} to zero, we obtain

$$r_1\{w_1^2-1-2v_1^2/(\gamma+1)\}\frac{\mathrm{d}\alpha_1}{\mathrm{d}x} = 2(w_1^2-v_1^2)^{\frac{1}{2}}\alpha_1 v_1/(\gamma+1). \tag{5.6}$$

The mean value of w_1 across the section differs from w by a term of the second order. On the assumption that v_1 is small and varies linearly across the diameter, so that away from the throat

$$v_1 = \frac{wr}{r_1}\frac{\mathrm{d}r_1}{\mathrm{d}x},$$

(5.6) reduces to

$$\frac{1}{\alpha_1}\frac{\mathrm{d}\alpha_1}{\mathrm{d}x} = 2w^2\frac{\mathrm{d}r_1}{\mathrm{d}x}\Big/(\gamma+1)\,(w^2-1)\,r_1$$

and with (5.3) this can be written

$$\frac{\mathrm{d}\alpha_1}{\mathrm{d}x} = \frac{\alpha_1 ww'}{\gamma+1-(\gamma-1)\,w^2}.$$

or

$$\alpha_1 = k\{1-(\gamma-1)\,w^2/(\gamma+1)\}^{-1/2(\gamma-1)},$$

and from (1.8)

$$\alpha_1 = kw^{\frac{1}{2}}r_1, \tag{5.7}$$

the terms k being arbitrary constants.

In the supersonic region, the variable x is replaced by X defined as

$$X = \int_c^x \frac{1}{\alpha_1}\left(\frac{h_2+h_3^2/h_1}{h_1}\right)^{\frac{1}{2}}\mathrm{d}x, \tag{5.8}$$

the term in brackets being given the appropriate mean value across the section and c is a small quantity defined by

$$\mathrm{d}x/\mathrm{d}X = 0 \quad (x = c). \tag{5.9}$$

A difficulty arises in the method of averaging the integrand in (5.8). To obtain the correct mean slope of the characteristics we should average across a diameter but it may be better to weight the slope by the mass flow, in which case averaging across the section would be appropriate. Since $\bar{\lambda}$ is a second order term when averaged over the section (eqn (1.14)) and a first order term when averaged over a diameter, the values of X so obtained differ by terms of the first order but the discrepancy is largely confined to the throat region.

Proceeding as in § 1 we obtain the linearized equation in the form

$$\left(\frac{\partial^2\phi}{\partial X^2}\right)_R + \frac{\xi}{X}\left(\frac{\partial\phi}{\partial X}\right)_R - \left(\frac{\partial^2\phi}{\partial R^2}\right)_X - \frac{1}{R}\left(\frac{\partial\phi}{\partial R}\right)_X = -F(X), \tag{5.10}$$

$F(X)$ being a function only of X, $\xi = 0$ away from the throat and $\xi = 1$ close to it.

In order to satisfy the boundary condition to the second order we introduce the function Φ defined by

$$\Phi = [\phi]_0^r - \frac{1}{2w^2r_1}\int_0^r r_1\lambda\phi_r\,\mathrm{d}r, \tag{5.11}$$

so that

$$\frac{\partial\Phi}{\partial r} = w\frac{\partial\phi}{\partial r}\Big/(w^2+r\lambda/r_1)^{\frac{1}{2}}, \tag{5.12}$$

to the second order. It is shown later that the integral term on the right-hand side is of the third order at $r = r_1$ at positions away from the throat.

The linearized equation then takes the form

$$\left(\frac{\partial^2\Phi}{\partial X^2}\right)_R + \frac{\xi}{X}\left(\frac{\partial\Phi}{\partial X}\right)_R - \left(\frac{\partial^2\Phi}{\partial R^2}\right)_X - \frac{1}{R}\left(\frac{\partial\Phi}{\partial R}\right)_X = F_1(X),$$

and this can be written

$$\left(\frac{\partial^2\Phi_1}{\partial X^2}\right)_R + \frac{\xi}{X}\left(\frac{\partial\Phi_1}{\partial X}\right)_R = \left(\frac{\partial^2\Phi_1}{\partial R^2}\right)_X + \frac{1}{R}\left(\frac{\partial\Phi_1}{\partial R}\right)_X - \frac{\Phi_1}{R^2}. \tag{5.13}$$

where

$$\Phi_1 = \partial\Phi/\partial R. \tag{5.14}$$

The boundary conditions to be satisfied are as in § 1.

$$\left.\begin{aligned} \partial\Phi/\partial R &= w\alpha_1 \sin\theta_1 \quad (R = r_1/\alpha_1 \equiv R_1,\ X \geqslant 0);\\ &= 0 \quad (R = 0,\ X \geqslant 0),\\ \partial\Phi/\partial X &= 0 \quad (X = 0,\ 0 < R < R_1). \end{aligned}\right\} \tag{5.15}$$

We need in addition the value of Φ at $X = 0$ and this is obtained from the analysis in the subsonic region as follows. The variable x is replaced by X_1, defined as

$$X_1 = \int_c^x \frac{1}{\alpha_1}\left(\frac{h_2 + h_3^2/h_1}{-h_1}\right)^{\frac{1}{2}} \mathrm{d}x, \tag{5.16}$$

and proceeding as above we find

$$\left(\frac{\partial^2\Phi_1}{\partial X_1^2}\right)_R + \frac{\xi}{X}\left(\frac{\partial\Phi_1}{\partial X}\right) + \frac{\partial^2\Phi_1}{\partial R^2} + \frac{1}{R}\frac{\partial\Phi_1}{\partial R} - \frac{\Phi_1}{R^2} = 0, \tag{5.17}$$

together with the boundary conditions (5.15).

The analysis of § 6 is applied to the hypothetical case of the nozzle with parallel flow at the throat with small values of R_t/D. Thus, as in the two-dimensional case, ξ can be taken as zero. In § 7 the analysis is confined to the throat region with non-parallel flow so that ξ can be taken as unity.

6. The validity of the linear equation in the exit cone of an axisymmetric nozzle

The method of approximation is similar to that in § 2. The radius r_1 increases more rapidly than $w^{\frac{1}{2}}$. For example, with $\gamma = 1.25$, expanding r_1 from r_t to $2r_t$ increases $w^{\frac{1}{2}}$ from 1.0 to 1.44. Thus we take

$$\alpha_1 = r_1, \quad R = r/r_1, \quad 0 \leqslant R \leqslant 1, \tag{6.1}$$

and, neglecting second order terms, (5.8) can be written as

$$X = \int_0^x \frac{1}{r_1}\left[\frac{1 - \{(\gamma-1)/(\gamma+1)\}w^2}{w^2 - 1}\right]^{\frac{1}{2}} \mathrm{d}x. \tag{6.2}$$

The solution of (5.13) with $\xi = 0$ is

$$\frac{\partial\Phi}{\partial R} = wr_1 R\sin\theta_1 + \sum_m \frac{2}{\lambda_m^2}\frac{J_1(\lambda_m R)}{J_0(\lambda_m)}\int_0^X \frac{\mathrm{d}^2 C(u)}{\mathrm{d}u^2}\sin\lambda_m(X-u)\,\mathrm{d}u + \sum_m B_m J_1(\lambda_m R)\cos\lambda_m X, \tag{6.3}$$

the summation being over the positive roots λ_m of

$$J_1(\lambda_m) = 0,$$

while
$$C(X) = wr_1 \sin\theta_1, \tag{6.4}$$

and the coefficients B_m are obtained from the Fourier–Bessel expansion.

$$\sum_m B_m J_1(\lambda_m R) = (\partial\Phi/\partial R)_{X=0} \quad (0 < R < 1).$$

The difference in pressure Δp between the boundary and the axis is given by (2.5) with

$$\Delta q = \frac{\mathrm{d}}{\mathrm{d}x}[(\Phi)_{R=1}] - \tfrac{1}{2}w\left(\frac{\mathrm{d}r_1}{\mathrm{d}x}\right)^2,$$

and since
$$\int_0^1 J_1(\lambda_m R)\,\mathrm{d}R = (1 - J_0(\lambda_m))/\lambda_m,$$

we find

$$\Delta q = \frac{\mathrm{d}X}{\mathrm{d}x}\left[\frac{1}{2}\frac{\mathrm{d}C}{\mathrm{d}X} + \int_0^X \frac{\mathrm{d}^2C(u)}{\mathrm{d}u^2} S(X-u)\,\mathrm{d}u - \sum_m B_m \frac{1-J_0(\lambda_m)}{J_0(\lambda_m)} \sin\lambda_m X\right] - \tfrac{1}{2}w\left(\frac{\mathrm{d}r_1}{\mathrm{d}x}\right)^2, \tag{6.5}$$

where
$$S(X-u) = \sum_m \frac{2}{\lambda_m^2} \frac{1-J_0(\lambda_m)}{J_0(\lambda_m)} \cos\lambda_m (X-u). \tag{6.6}$$

The convergence of this series is slow and it has been evaluated by the following method. For large values of m

$$\lambda_m = m\pi + \pi/4, \quad J_0(\lambda_m) = (2/m)^{\frac{1}{2}} \cos m\pi,$$

so that approximately

$$\frac{2}{\lambda_m^2} \frac{1-J_0(\lambda_m)}{J_0(\lambda_m)} \cos\lambda_m X = \left(\frac{2^{\frac{1}{2}}}{\pi} \frac{1}{m^{\frac{3}{2}} \cos m\pi} - \frac{2}{m^2\pi^2}\right) \cos(m\pi + \tfrac{1}{4}\pi) X.$$

The series S can be written

$$S(X) = \sum_m \left\{\frac{2}{\lambda_m^2} \frac{1-J_0(\lambda_m)}{J_0(\lambda_m)} \cos\lambda_m X - \left(\frac{2^{\frac{1}{2}}}{\pi} \frac{1}{m^{\frac{3}{2}} \cos m\pi} - \frac{2}{m^2\pi^2}\right) \cos(m\pi + \tfrac{1}{4}\pi) X\right\}$$
$$- (F_1 - G_1) \cos(\tfrac{1}{4}\pi X) + (F_2 - G_2) \sin(\tfrac{1}{4}\pi X),$$

where
$$F_1 = 2 \sum_{m=1}^{\infty} \frac{\cos m\pi X}{m^2\pi^2}, \qquad F_2 = 2 \sum_{m=1}^{\infty} \frac{\sin m\pi X}{m^2\pi^2}.$$

$$G_1 = \frac{2^{\frac{1}{2}}}{\pi} \sum_{m=1}^{\infty} \frac{\cos m\pi X}{m^{\frac{3}{2}} \cos m\pi}, \quad G_2 = \frac{2^{\frac{1}{2}}}{\pi} \sum_{m=1}^{\infty} \frac{\sin m\pi X}{m^{\frac{3}{2}} \cos m\pi},$$

The series F and G can be calculated in the following manner. We have

$$F_1 = \tfrac{1}{3} + \tfrac{1}{2}(X^2 - 2X) \quad (0 \leqslant X \leqslant 1),$$

while the series F_2 can be obtained from the Fourier expansion

$$\sum_{m=1}^{\infty} \frac{\cos m\pi X}{m} = -\tfrac{1}{2} \ln(2 - 2\cos\pi X) \quad (|X| < 1),$$

the integration of which gives

$$\sum_{m=1}^{\infty} \frac{\sin m\pi X}{m^2\pi^2} = -\frac{1}{2\pi} X \ln(2 - 2\cos\pi X) + \frac{1}{2}\int_0^X X \cot(\tfrac{1}{2}\pi X)\,\mathrm{d}X.$$

Also
$$X\cot(\tfrac{1}{2}\pi X) = 2/\pi\,\{1 - \tfrac{1}{3}(\tfrac{1}{2}\pi X)^2 - \tfrac{1}{4\,5}(\tfrac{1}{2}\pi X)^4 - \tfrac{2}{9\,4\,5}(\tfrac{1}{2}\pi X)^6 \ldots\} \quad (X < 2)$$

so that

$$F_2 = -1/\pi\{X\ln(2-2\cos\pi X)\}$$
$$+2/\pi\{X-0.2742X^3-0.02706X^5-0.00454X^7-0.00087X^9-0.000177X^{11}\ldots\}$$

a form which converges rapidly for $X < 1$.

The series G_1 and G_2 can be expressed in the integral forms

$$G_1 = -\left(\frac{2}{\pi}\right)^{\frac{3}{2}}(I_1+I_2\cos\pi X); \quad G_2 = -\left(\frac{2}{\pi}\right)^{\frac{3}{2}} I_2\sin\pi X \quad (|X|<1),$$

where

$$I_1 = \int_0^\infty \frac{x^{\frac{1}{2}}\,\mathrm{e}^{-2x}\,\mathrm{d}x}{1+2\,\mathrm{e}^{-x}\cos\pi X+\mathrm{e}^{-2x}}, \quad I_2 = \int_0^\infty \frac{x^{\frac{1}{2}}\,\mathrm{e}^{-x}\,\mathrm{d}x}{1+2\,\mathrm{e}^{-x}\cos\pi X+\mathrm{e}^{-2x}}.$$

These integrals have been evaluated in the range $0 \leqslant X \leqslant 1$ and for values $1 \leqslant X \leqslant 2$ we use the formulae

$$F_1(2-u) = F_1(u), \quad F_2(2-u) = -F_2(u),$$
$$G_1(2-u) = G_1(u), \quad G_2(2-u) = -G_2(u).$$

The function $S(X)$ is continuous at $X = 1.0$ but its differential coefficient is discontinuous. The values are given in table 4.

TABLE 4

X	$S(X)$	X	$S(X)$	X	$S(X)$	X	$S(X)$
0.00	−0.500	0.50	0.071	1.00	0.835	1.50	−0.379
0.05	−0.452	0.55	0.138	1.05	0.283	1.55	−0.393
0.10	−0.399	0.60	0.206	1.10	0.102	1.60	−0.399
0.15	−0.345	0.65	0.276	1.15	−0.022	1.65	−0.399
0.20	−0.290	0.70	0.349	1.20	−0.115	1.70	−0.391
0.25	−0.233	0.75	0.423	1.25	−0.188	1.75	−0.376
0.30	−0.176	0.80	0.500	1.30	−0.246	1.80	−0.352
0.35	−0.116	0.85	0.580	1.35	−0.293	1.85	−0.317
0.40	−0.056	0.90	0.662	1.40	−0.330	1.90	−0.270
0.45	0.007	0.95	0.747	1.45	−0.358	1.95	−0.204
		1.00	0.835			2.00	−0.087

The analysis is applied to the conical nozzle of figure 1. The boundary profile at the throat is of radius R_t and this mates into the straight line generators of the exit cone, the slope being continuous. The values of the parameters at this intersection are denoted by the suffix zero. The terms w, w', r_1 and θ_1 are continuous at this position so that the function $C(X)$ of (6.4) is continuous but the derivative has a discontinuity such that

$$\lim_{\epsilon\to 0}\left\{\left(\frac{\mathrm{d}C}{\mathrm{d}x}\right)_{x_0+\epsilon} - \left(\frac{\mathrm{d}C}{\mathrm{d}x}\right)_{x_0-\epsilon}\right\} = -w_0(r_1)_0/R_t. \tag{6.7}$$

As we see from (6.2) both X and its first derivative with respect to x are continuous. Using the approximations of (6.1) we can obtain the values of X in the forms (cf. § 2)

$$X = \frac{2}{r_t}\left(\frac{x}{(\gamma+1)w_t'}\right)^{\frac{1}{2}}(1-\tfrac{1}{9}\gamma w_t' x) \quad (0 \leqslant x \leqslant x_0)$$
$$= X_0 + [f(w)-f(w_0)]\Big/2\frac{\mathrm{d}r_1}{\mathrm{d}x} \quad (x \geqslant x_0), \tag{6.8}$$

X_0 and w_0 being the values of X and w at $x = x_0$. The values of w' and w_t' are given by (5.3) and (5.4) and $f(w)$ is the Prandtl–Meyer expansion angle.

In view of the discontinuity in C at $x = x_0$, (6.5) must be written in the following form for values of X exceeding X_0.

$$\Delta q = -\tfrac{1}{2}w\left(\frac{dr_1}{dx}\right)^2 + \frac{dX}{dx}\left[\frac{1}{2}\frac{dC}{dX} - \left(\frac{dx}{dX}\right)_0 \frac{w_0(r_1)_0}{R_t} S(X-X_0) + \int_0^{X_0-\epsilon} \frac{d^2C(u)}{du^2} S(X-u)\,du + \int_{X_0+\epsilon}^{X} \frac{d^2C(u)}{du^2} S(X-u)\,du\right] \tag{6.9}$$

taking the limit as $\epsilon \to 0$. In this the constants B_m are taken as zero, for we consider the case in which the flow at the throat is parallel to the axis as in § 2. The function $S(X)$ is numerically -0.5 at $X = 0$ so that Δq is continuous at $x = x_0$.

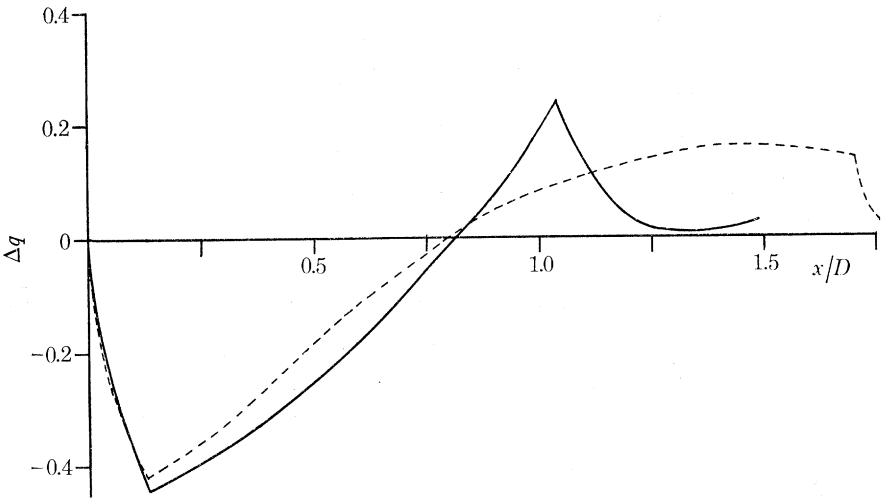

FIGURE 8. The velocity variation between the boundary and the axis of an axisymmetric nozzle assuming parallel flow at the throat, 15° cone semi-angle, $\gamma = 1.25$.

In the numerical example considered the value of the profile radius of curvature at the throat is $R_t = 0.5$ and the radius of the throat section is also 0.5. The semi-angle of the exit cone is 15°. The values of Δq calculated from the formula in which the first term on the right hand side is omitted, i.e. the linearized form, are given by the continuous curve in figure 8. In addition, (5.1) has been solved numerically by the method of characteristics and the values of Δq so obtained are given by the discontinuous curve in figure 8. The agreement is good between the throat and that position at which Δq changes sign. Thereafter there is a marked discrepancy. We see that the slope of the curve Δq is discontinuous at two positions. The first of these is at the intersection of the curved profile and the straight line generators of the exit cone. This corresponds to a value of $X = 0.6717$ ($x = 0.2588$). The second discontinuity occurs at the value $X = 1.6717$. Since the boundary is represented by $R = 1$ and the slopes of the characteristics of (5.13) are ± 1, the latter value of X corresponds to that position at which the characteristic line from the intersection of the curved profile and the straight line generator cuts the central axis. In the same manner the discontinuities in the slopes of Δq obtained by the method of characteristics are also at the corresponding positions and the discrepancy in the values of Δq is associated with these discrepancies in the characteristic lines.

By using the method of characteristics it is found that the characteristic ray which leaves the

boundary at the intersection of the curved and straight portions cuts the central axis at $x = 1.70$ whereas according to the above analysis the value of x is 1.03. The velocity at the axis increases with increasing distance from the throat up to this position but falls on passing through the cusp that is formed due to the discontinuity in the curvature at the source of the ray on the profile. This drop in velocity is reflected in the values of Δq on both curves in figure 8 but they occur at different positions. There are two reasons for the marked discrepancy which are now discussed.

In the foregoing linearized theory the approximation $\alpha_1 = r_1$ has been used as this gives $R = 1$ at the boundary. The second approximation is obtained by taking

$$X = \int_0^x \frac{1}{w^{\frac{1}{2}} r_1} \left(\frac{1 - \{(\gamma-1)/(\gamma+1)\} w^2}{w^2 - 1} \right)^{\frac{1}{2}} \mathrm{d}x \quad (R = r/w^{\frac{1}{2}} r_1), \tag{6.10}$$

so that the boundary is represented by $R = w^{-\frac{1}{2}}$. The characteristic ray leaving the boundary at X arrives at the axis at $X + w^{-\frac{1}{2}}$, w having the value at X, and on this basis the critical characteristic is found to cut the axis at $x = 1.28$.

The velocity at a point on the boundary not far removed from the throat is markedly larger than that at the axis and is also greater than the value of w for that section. For example, at the section containing the discontinuity, the velocity ratio w_1 is 1.48 at the wall, 1.06 at the axis and 1.25 as calculated from one-dimensional theory. Thus the characteristic ray leaving the boundary has a slope markedly less than that calculated for the mean over the section. Also, at the section at which the critical characteristic cuts the axis, the velocity at the axis is greater than that at the wall. Thus the mean slope of the critical characteristic between the wall and the intersection with the axis is appreciably smaller in magnitude than that obtained from the change in the value of X as determined above. Also, to a very good approximation, the change in the Prandtl–Meyer expansion angle as the ray proceeds from the curved portion of the wall to the intersection with the axis is twice the angle of turn of the flow, i.e. $2\theta_1$, where θ_1 is the angle at the wall where the ray begins. This rule breaks down beyond the critical characteristic due to the formation of the cusp. In two-dimensional flow the change in the Prandtl–Meyer expansion angle is θ_1 throughout the nozzle. The discrepancy observed above is associated with this smaller slope of the critical characteristic and this arises from the marked variation across the section. The discrepancy rapidly diminishes with increasing values of R_t/r_t and at values above 2.0 it cannot be distinguished from the numerical errors.

If some feature of the flow had been examined which is more representative of a mean effect across the section, then the discrepancies would be much less marked. This is typified by the remarkably good agreement between the wavelengths of § 2. This is discussed further in § 8.

7. The validity of the linear equation in the throat region of an axisymmetric nozzle

The subsonic region in the entry cone is bounded as in figure 1. The curved portions of the profile fit into the straight line generators which expand into a very large reservoir. The approximations used are given by (6.1) and (6.2) and neglecting second order terms

$$X_1 = \int_0^x \frac{1}{r_1} \left(\frac{1 - \{(\gamma-1)/(\gamma+1)\} w^2}{1 - w^2} \right)^{\frac{1}{2}} \mathrm{d}x, \tag{7.1}$$

x and thus X_1 assuming negative values.

The solution of (5.17) with $\xi = 1.0$ subject to the boundary conditions

$$\frac{\partial}{\partial X_1}(\Phi_1(X_1, R)) = 0 \qquad (X_1 = 0,\ 0 \leqslant R \leqslant 1),$$
$$= \frac{\mathrm{d}C(X_1)}{\mathrm{d}X_1} \qquad (R = 1,\ X_1 \leqslant 0) \tag{7.2}$$

can be written

$$\frac{\partial}{\partial X_1}(\Phi_1(X_1, R)) = R\frac{\mathrm{d}C(X_1)}{\mathrm{d}X_1} + \sum_m \frac{1}{\lambda_m}\frac{J_1(\lambda_m R)}{J_0(\lambda_m)}\left\{\int_0^{X_1+\epsilon}\frac{\mathrm{d}^2C(u)}{\mathrm{d}u^2}[K_1(\lambda_m(u-X_1)) - K_1(-\lambda_m(X_1+u))]\,\mathrm{d}u\right.$$
$$\left. + \int_{X_1-\epsilon}^{-\infty}\frac{\mathrm{d}^2C(u)}{\mathrm{d}u^2}[K_1(-\lambda_m(X_1+u)) - K_1(\lambda_m(X_1-u))]\mathrm{d}u\right\}, \tag{7.3}$$

where ϵ is a small positive quantity, the limit being taken as ϵ approaches zero. The terms λ_m are the positive zeros of the Bessel function $J_1(\lambda_m)$ and the function $K_1(z)$ is the Macdonald form of the Bessel function of the second kind. The function $C(X_1)$ is defined as

$$C(X_1) = wr_1 \sin\theta_1. \tag{7.4}$$

The solution is evaluated for small values of x in order to compare it with the results obtained by Hall (1962). For small values of x

$$x = a_0 X_1^2\left\{1 - \frac{\gamma}{9}\frac{r_t}{R_t}X_1^2 + \left[\left(\frac{r_t}{R_t}\right)^2\left(\frac{3}{120} + \frac{7\gamma}{320} + \frac{149\gamma^2}{6480}\right) + \frac{\gamma+1}{320}\left(\frac{r_t}{R_t}\right)^3\right]X_1^4\ldots\right\}, \tag{7.5}$$

where

$$a_0 = -\tfrac{1}{4}r_t\left(\frac{2(\gamma+1)\,r_t}{R_t}\right)^{\frac{1}{2}}.$$

Also

$$C(X_1) = -aX_1^2 + bX_1^4 + cX_1^6 + \ldots,$$

where

$$\left.\begin{aligned} a &= r_t^{\frac{5}{2}}\{2(\gamma+1)\}^{\frac{1}{2}}/4R_t^{\frac{3}{2}}, \\ b &= (9+2\gamma)\,r_t a/18R_t, \\ &\ldots\ldots\ldots\ldots\ldots\ldots \end{aligned}\right\} \tag{7.6}$$

The following Fourier–Bessel expansions are required. The first is

$$Q_1 \equiv \sum_m \frac{1}{\lambda_m}\frac{J_1(\lambda_m R)}{J_0(\lambda_m)} = -\tfrac{1}{2}R \qquad (0 \leqslant R < 1).$$

Integrating both sides of this with respect to R between zero and R gives

$$\sum_m \frac{J_0(\lambda_m R)}{\lambda_m^2 J_0(\lambda_m)} = \tfrac{1}{4}R^2 + \sum_m \frac{1}{\lambda_m^2 J_0(\lambda_m)}.$$

Multiplying both sides of this latter equation by R and integrating between zero and R we obtain

$$Q_3 \equiv \sum_m \frac{J_1(\lambda_m R)}{\lambda_m^3 J_0(\lambda_m)} = \frac{R^3}{16} + \frac{R}{2}\sum_m \frac{1}{\lambda_m^2 J_0(\lambda_m)} = \frac{R^3 - R}{16},$$

since the series on the left-hand side converges in the range $0 \leqslant R \leqslant 1$ and is zero at $R = 1$ so that

$$\sum_m \frac{1}{\lambda_m^2 J_0(\lambda_m)} = -\frac{1}{8}.$$

By repeating the procedures it is found that

$$Q_5 = \sum_m \frac{J_1(\lambda_m R)}{\lambda_m^5 J_0(\lambda_m)} = \frac{-2R + 3R^3 - R^5}{384} \qquad (0 \leqslant R \leqslant 1),$$

and
$$Q_7 = \sum_m \frac{J_1(\lambda_m R)}{\lambda_m^7 J_0(\lambda_m)} = \frac{-7R + 12R^3 - 6R^5 + R^7}{18\,432}. \tag{7.7}$$

Also
$$\int_0^\infty K_n(z)\, z^{m-1}\, \mathrm{d}z = 2^{m-2}\, \Gamma\left(\frac{m-n}{2}\right) \Gamma\left(\frac{m+n}{2}\right).$$

For small values of X_1 it is found that (7.3) becomes

$$\left.\begin{aligned} \partial(\Phi_1(X_1, R))/\partial X_1 = {} & [4aX_1 + 6bX_1^3 - 6cX_1^5 \ldots]\, Q_1 \\ & + [-24b\pi X_1 + 120c\pi X_1^3 \ldots]\, Q_3 \\ & + [360\pi X_1 c + \ldots]\, Q_5 \\ & \ldots\ldots\ldots\ldots\ldots\ldots\ldots\ldots\ldots \end{aligned}\right\} \tag{7.8}$$

For small values of X_1
$$\frac{\partial \Phi_1}{\partial X_1} = X_1 \frac{\partial^2 \Phi_1}{\partial X_1^2},$$

so that (5.17) can be written

$$\frac{\partial^2 \Phi_1}{\partial R^2} + \frac{1}{R}\frac{\partial \Phi_1}{\partial R} - \frac{\Phi_1}{R^2} = -2\frac{\partial^2 \Phi_1}{\partial X_1^2} \quad (X_1 = 0). \tag{7.9}$$

From (7.7), (7.8) and (7.9) it is found that

$$\Phi_1(0, R) = 8aQ_3 - 48b\pi Q_5 + 720c\pi Q_7 + \ldots, \tag{7.10}$$

and $\Phi_1(X_1, R)$ is obtained by integrating (7.8) with respect to X_1 between zero and X_1 with the value at zero given by (7.10).

The expression
$$\frac{\partial \Phi_1(X_1, R)}{\partial R} - \frac{\partial}{\partial R}\Phi_1(X_1, 0), \tag{7.11}$$

can be obtained by integrating (7.8) with respect to R between zero and R. This function and $\Phi_1(X_1, R)$ together express the variations across the section and it is the validity of these that we require to check. Hall (1962) expresses the velocity q and the angle of flow θ in the form

$$q = 1 + q_1/R_t + q_2/R_t^2 + \ldots,$$

$$\theta = \left(\frac{\gamma+1}{2R_t}\right)^{\frac{1}{2}} (\theta_1/R_t + \theta_2/R_t^2 + \ldots).$$

The foregoing linearized theory produces identical values of q_1 and θ_1 to those derived by Hall but the second order terms q_2 and θ_2 are discrepant. In table 5 the values of θ_2 are obtained for $\gamma = 1.25$ and $R_t/r_t = 3.5$ at the throat section.

TABLE 5

R	Hall	linearized theory
0	0	0
0.2	0.0707	0.047
0.4	0.1097	0.076
0.6	0.0987	0.079
0.8	0.0460	0.049
1.0	0	0

The discrepancy can be shown to be due to the approximation made in the term α_1 of (5.7), namely $\alpha_1 = r_1$. This is not valid in the entry cone since w falls rapidly with increasing distance from the throat. A more accurate theory can be developed under these circumstances but this is

not discussed here since we are primarily concerned with the flow at the throat and in the exit cone.

8. Non-symmetric flow in an axisymmetric nozzle; the derivation of the lateral forces and couples and the optimum nozzle design

It is assumed, as in § 4, that the nozzle itself is cylindrically symmetric but the flow is asymmetric due to upstream effects. Again it is required to determine the nature and magnitude of the flow asymmetry at the exit of the nozzle when the entry flow is asymmetric.

The equation of flow in cylindrical coordinates x, r and ψ become (Shapiro 1953)

$$(1-u^2/a^2)\frac{\partial^2\phi_1}{\partial x^2}+(1-v^2/a^2)\frac{\partial^2\phi_1}{\partial r^2}-\frac{2uv}{a^2}\frac{\partial^2\phi_1}{\partial x\,\partial r}+(1-\eta^2/a^2)\frac{1}{r^2}\frac{\partial^2\phi_1}{\partial\psi^2}$$
$$-\frac{2u\eta}{a^2}\frac{1}{r}\frac{\partial^2\phi_1}{\partial x\,\partial\psi}-\frac{2v\eta}{a^2}\frac{\partial^2\phi_1}{\partial r\,\partial\psi}+\frac{v^2}{r^2}(1+\eta^2/a^2)=0, \tag{8.1}$$

where the notation is as in § 5 and $\eta=\dfrac{1}{r}\dfrac{\partial\phi_1}{\partial\psi}$.

It is assumed that the non-symmetries are small terms so that their squares can be neglected. Proceeding as in § 5, the equation becomes

$$h_1\frac{\partial^2\phi}{\partial x^2}+2h_3\frac{\partial^2\phi}{\partial x\,\partial r}-h_2\left(\frac{\partial^2\phi}{\partial r^2}+\frac{1}{r}\frac{\partial\phi}{\partial r}\right)-\frac{h_2}{r^2}\frac{\partial^2\phi}{\partial\psi^2}-\frac{2}{\gamma+1}\frac{v_1^2}{r}\frac{\partial\phi}{\partial r}-\frac{2}{\gamma+1}\frac{v_1^2}{r^2}\frac{\partial^2\phi}{\partial\psi^2}=0. \tag{8.2}$$

The last two terms in this equation are small and can be neglected. Multiplying throughout by $\sin\psi$ and integrating with respect to ψ from $\psi=0$ to 2π we obtain

$$h_1\frac{\partial^2H}{\partial x^2}+2h_3\frac{\partial^2H}{\partial x\,\partial r}-h_2\left[\frac{\partial^2H}{\partial r^2}+\frac{1}{r}\frac{\partial H}{\partial r}-\frac{H}{r^2}\right]=0,$$

where
$$H=\int_0^{2\pi}\phi\sin\psi\,\mathrm{d}\psi. \tag{8.3}$$

In order to satisfy the boundary conditions exactly, the function H is replaced by H_1, where

$$H_1=\int_0^{2\pi}\sin\psi\int_0^r\frac{w(\partial\phi/\partial r)\,\mathrm{d}r\,\mathrm{d}\psi}{(w^2+r\lambda/r_1)^{\frac{1}{2}}}, \tag{8.4}$$

so that H_1 satisfies the same differential equation as H to the first order and also satisfies the boundary condition

$$\partial H/\partial r=0\quad(r=r_1). \tag{8.5}$$

It is assumed that the flow is symmetric with respect to the plane $z=0$ which contains the principal axis of the nozzle, so that the lateral momentum at the section at x is

$$-L=\int_0^{r_1}r\int_0^{2\pi}\rho_1uv\,\mathrm{d}\psi\,\mathrm{d}r, \tag{8.6}$$

where $u=\partial\phi_1/\partial x$ and $v=\partial\phi_1/\partial y$ as in § 1, or

$$-L=a_t^2\int_0^{r_1}r\int_0^{2\pi}\rho_1\phi_x\phi_y\,\mathrm{d}\psi\,\mathrm{d}r.$$

The negative sign has been introduced so that L is the lateral force on the nozzle if it terminated at this section x.

The procedure is as in § 4. The term $\rho_1\phi_x$ is as in that section and

$$\phi_y = \phi_r \sin\psi + \frac{1}{r}\frac{\partial\phi}{\partial\psi}\cos\psi.$$

Thus $$L = -w\rho a_t^2 \int_0^{r_1} r \int_0^{2\pi} \left(\phi_r \sin\psi + \frac{1}{r}\frac{\partial\phi}{\partial\psi}\cos\psi\right) \mathrm{d}\psi\,\mathrm{d}r + \frac{M^2-1}{2w}\rho a_t^2 \int_0^{r_1} r \int_0^{2\pi} \lambda\phi_y \,\mathrm{d}\psi\,\mathrm{d}r.$$

We have

$$\int_0^r r\int_0^{2\pi}\left(\phi_r\sin\psi + \frac{1}{r}\frac{\partial\phi}{\partial\psi}\cos\psi\right)\mathrm{d}\psi\,\mathrm{d}r = \int_0^{2\pi}\sin\psi\int_0^r (r\phi_r+\phi)\,\mathrm{d}r\,\mathrm{d}\psi = r\int_0^{2\pi}\phi\sin\psi\,\mathrm{d}\psi.$$

Also
$$H_1 = \int_0^{2\pi}\sin\psi\int_0^r \frac{\partial\phi}{\partial r}\left(1-\frac{r\lambda}{2r_1w^2}\right)\mathrm{d}r\,\mathrm{d}\psi$$
$$= \int_0^{2\pi}\phi\sin\psi\,\mathrm{d}\psi - \int_0^{2\pi}\sin\psi\int_0^r \frac{\partial\phi}{\partial r}\frac{r\lambda}{2r_1w^2}\mathrm{d}r\,\mathrm{d}\psi, \tag{8.7}$$

so that

$$L = -w\rho r_1 a_t^2\left[(H_1)_{r=r_1} + \int_0^{2\pi}\sin\psi\int_0^{r_1}\frac{\partial\phi}{\partial r}\frac{r\lambda}{2r_1w^2}\mathrm{d}r\,\mathrm{d}\psi\right] + \frac{M^2-1}{2w}\rho a_t^2\int_0^{r_1} r\int_0^{2\pi}\lambda\phi_y\,\mathrm{d}\psi\,\mathrm{d}r. \tag{8.8}$$

The moment of thrust about the plane $z = 0$ is, as in § 4,

$$C_T = \int_0^{r_1} r\int_0^{2\pi} T_1 r\sin\psi\,\mathrm{d}\psi\,\mathrm{d}r$$
$$= -\tfrac{1}{2}(M^2-1)\rho a_t^2\int_0^r r\int_0^{2\pi} r\lambda\sin\psi\,\mathrm{d}\psi\,\mathrm{d}r. \tag{8.9}$$

Away from the throat the term λ is small and in the second and third integrals in the expression for L it suffices to write

$$\phi_y = \phi_r\sin\psi, \quad \phi_r = \frac{wr}{r_1}\frac{\mathrm{d}r_1}{\mathrm{d}x}.$$

Also the rate of mass flow across any section is m where

$$m = \rho w a_t \pi r_1^2.$$

Thus
$$L = -\frac{m}{\pi r_1}a_t(H_1)_{r=r_1} - \frac{M^2-2}{M^2-1}\frac{C_T}{r_1}\frac{\mathrm{d}r_1}{\mathrm{d}x}. \tag{8.10}$$

As in § 4, there is a further relation between L and C_T. Figure 9 is a section of the exit cone of a three-dimensional nozzle. Clearly

$$r_1\int_0^{2\pi}\{(\Delta p)_y - (\Delta p)_{-y}\}_{r=r_1}\sin\psi\,\mathrm{d}\psi = \frac{\mathrm{d}L}{\mathrm{d}x}.$$

Also
$$-\int_0^{\pi} r\frac{\mathrm{d}r_1}{\mathrm{d}x}\{(\Delta p)_y - (\Delta p)_{-y}\}\Delta x y\,\mathrm{d}\psi + \left(L + \frac{\mathrm{d}L}{\mathrm{d}x}\Delta x\right)\Delta x + \Delta C_T = 0,$$

or
$$\frac{\mathrm{d}C_T}{\mathrm{d}x} + L - r_1\frac{\mathrm{d}r_1}{\mathrm{d}x}\frac{\mathrm{d}L}{\mathrm{d}x} = 0. \tag{8.11}$$

At $x = 0$, i.e. the throat, $M = 1$ so that from (8.9)

$$C_T = 0 \quad (x = 0). \tag{8.12}$$

Equations (8.10), (8.11) and (8.12) enable us to express L and C_T in terms of H_1. Proceeding as in § 4,

$$\frac{dw}{dx} = \frac{1-\{(\gamma-1)/(\gamma+1)\}w^2}{w^2-1}\frac{2w}{r_1}\frac{dr_1}{dx}, \tag{8.13}$$

and to the first order

$$dC_T/dx = -L. \tag{8.14}$$

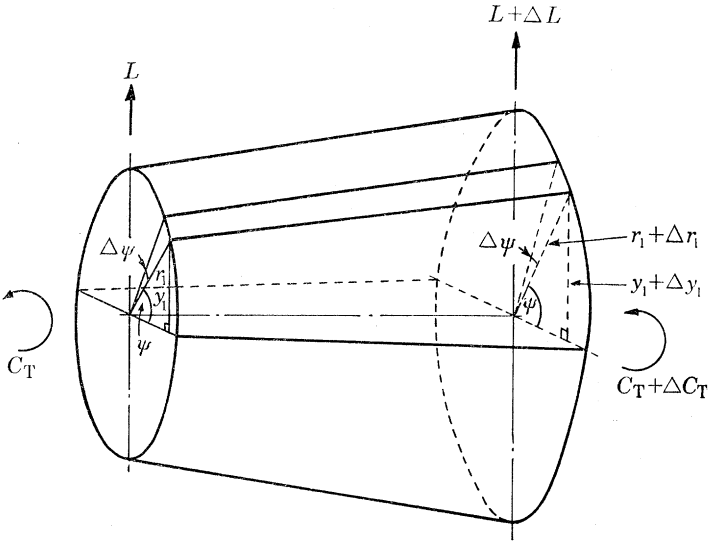

FIGURE 9. The force system on a section of an axi-symmetric nozzle.

Substituting these into (8.10) gives

$$\frac{d}{dx}\left(\frac{w^{\frac{1}{2}}}{r_1}C_T\right) = \frac{ma_t w^{\frac{1}{2}}}{\pi r_1^2}H_1, \tag{8.15}$$

or

$$C_T = \frac{ma_t r_1}{\pi w^{\frac{1}{2}}}\int_0^x \frac{w^{\frac{1}{2}}H_1}{r_1^2}dx, \tag{8.16}$$

to the first order, and

$$L = -\frac{ma_t}{\pi}\frac{d}{dx}\left\{\frac{r_1}{w^{\frac{1}{2}}}\int_0^x \frac{w^{\frac{1}{2}}}{r_1^2}H_1\,dx\right\}, \tag{8.17}$$

to the second order. This value L could be substituted into (8.11) to give C_T to the second order.

It is assumed in the first instance that the throat and the exit cone are axially symmetric so that the non-symmetry in the flow arises upstream of the throat. The flow across the throat is thus non-symmetric. It is also assumed that the non-symmetry in the flow is sufficiently small not to affect the mean slope of the characteristic lines at each section.

Equation (8.3) can be linearized in the manner described in § 5 and using the approximation for α given in § 6, the solution for H_1 can be written

$$H_1 = \sum_n A_n J_1(\beta_n R)\, I(\beta_n X), \tag{8.18}$$

the terms β_n being the roots of the Bessel function

$$J_1'(\beta_n) = 0,$$

so that

$$\beta_1 = 1.841, \quad \beta_2 = 5.331, \quad \beta_3 = 8.536, \quad \ldots,$$

and for large values $\beta_n = n\pi - \frac{1}{4}\pi$. The coefficients A_n are obtained from the Fourier–Bessel expansion

$$A_n = 2\beta_n^2 \int_0^1 R f_1(R)\, J_1(\beta_n R)\, \mathrm{d}R \Big/ (\beta_n^2 - 1)\,[J_1(\beta_n)]^2, \tag{8.19}$$

where $f_1(R)$ is the value of $H_1(R)$ at the throat. The function $I(\beta_n X)$ satisfies the differential equation

$$\frac{\mathrm{d}^2 I}{\mathrm{d}X^2} + \frac{\xi}{X}\frac{\mathrm{d}I}{\mathrm{d}X} + \beta_n^2 I = 0, \tag{8.20}$$

with the initial conditions

$$I(\beta_n X) = 1.0, \quad \frac{\mathrm{d}I(\beta_n X)}{\mathrm{d}X} = 0 \quad (X = 0)$$

and

$$\frac{\xi}{X} = \left(\frac{\mathrm{d}x}{\mathrm{d}X}\right)^2 \left(\frac{\mathrm{d}^2 X}{\mathrm{d}x^2} + \frac{2ww'}{w^2 - 1}\frac{\mathrm{d}X}{\mathrm{d}x}\right). \tag{8.21}$$

It is seen in § 4 that all of the terms in the series for the two-dimensional form of L are identically zero for odd integral values of X. The separate terms of H_1 are not zero at the same values of X and the values which make H_1 zero depend to a small extent on the function $f_1(R)$. It is usual in vibration problems for the amplitude of the fundamental to be markedly greater than that of any of the harmonics, and the fundamental of H_1 contains $I(\beta_1 X)$ only. In the first instance we concentrate on this fundamental.

At the throat $\xi = 1.0$, and in the region between the throat and the junction of the curved and straight portions of the nozzle ξ departs only slightly from unity. Beyond this it falls rapidly in value. Thus as a first approximation

$$\begin{aligned} I(\beta_1 X) &= J_0(\beta_1 X) \quad (X \leqslant X_0), \\ &= J_0(\beta_1 X_0)\cos\beta_1(X - X_0) - J_1(\beta_1 X_0)\sin\beta_1(X - X_0) \quad (X \geqslant X_0), \end{aligned} \tag{8.22}$$

X_0 being the value of X at the intersection, and both $I(\beta_1 X)$ and $I'(\beta_1 X)$ are continuous at $X = X_0$. A closer approximation is obtained by numerical integration of (8.20). This has been carried out with a variety of values of R_t/r_t and it has been found that the first approximation is in good agreement with the numerical solution.

Some justification for the predominance of the fundamental is provided by the following analysis. The function $f_1(R)$ satisfies the conditions

$$f_1(R) = 0 \quad (R = 0),$$
$$\mathrm{d}f_1(R)/\mathrm{d}R = 0 \quad (R = 1),$$

and we can expect to be able to express it with fair accuracy as a series of polynomials of the form

$$f_1(R) = b(R - 0.5R^2) + c(R^3 - 1.5R^2) + \ldots,$$

$b, c, \ldots$, being constants. The coefficients A_n in the Fourier–Bessel expansions of these polynomials are as follows

$f_1(R)$	A_1	A_2	A_3	A_4
$R - 0.5R^2$	0.5139	−0.0113	0.0020	−0.0008
$R^3 - 1.5R^2$	−0.4479	−0.0547	0.0031	−0.0031

Further, the first approximation for $I(\beta_n X)$ contains the Bessel functions as seen in (8.22). These fall off in amplitude with increasing values of β_n for given values of X. Thus the fundamental can be expected to dominate the solution particularly at the larger values of X.

The lateral force and couple are obtained from (8.16) and (8.17) in which H_1 is expressed in the form

$$H_1 = A_1 J_1(\beta_1)\, I(\beta_1 X). \tag{8.23}$$

If l is the distance between the centre of gravity of the rocket and the nozzle exit then the turning moment about the centre of gravity due to the non-symmetry of the flow is

$$Ll + C_T. \tag{8.24}$$

Thus X, and hence x, is determined from (8.16), (8.17) and (8.23) which makes this turning moment zero. The values of X and x so derived are independent of A_1, that is, the nature of the asymmetry of flow at the throat. Typical values of L and C_T are given in figure 10 in which the function $I(\beta_1 X)$ has been deduced by numerical integration of (8.20).

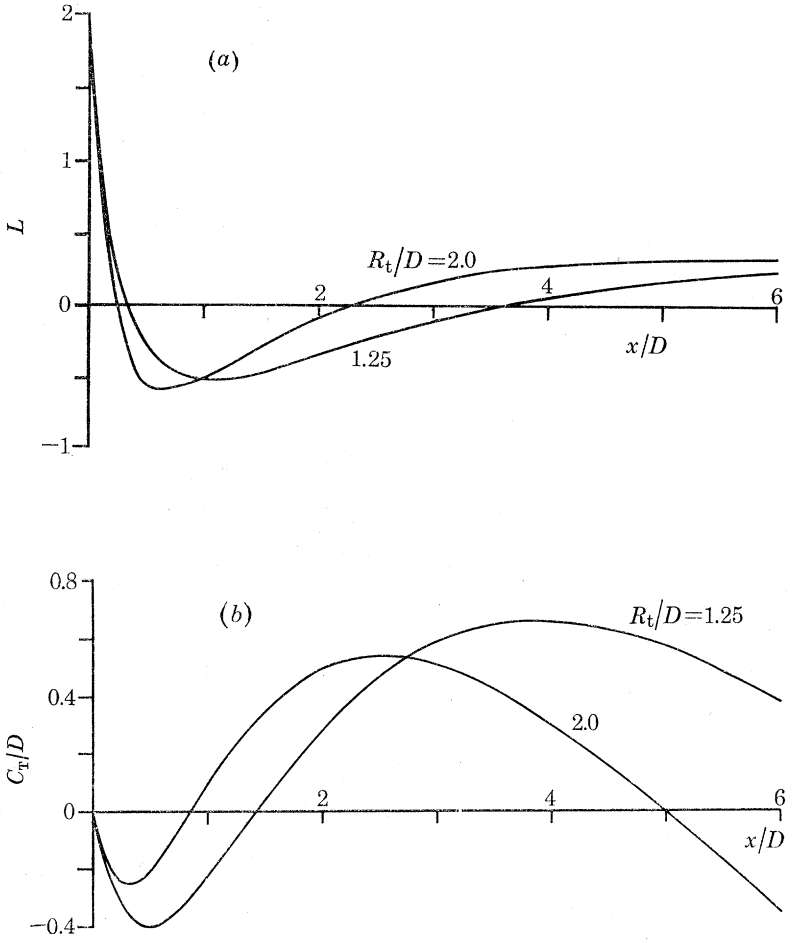

FIGURE 10 (*a*). The variation of the lateral force L with exit cone length.
(*b*). The variation of the couple C_T with exit cone length.

The foregoing analysis is concerned with the design of a nozzle which eliminates the turning moment about the centre of gravity which would otherwise arise from the non-symmetry of flow into the nozzle, the nozzle itself being perfectly symmetric. When hot propellants or long times of burning are employed, it is necessary to introduce into the throat region an insert of a refractory or other suitable material. This extends some distance into the exit cone and even though it is mated into the exit cone with very close tolerances, it is found that the hot gases produce very

severe erosion at the intersection. This appears as a deep jagged-edged pit around the circumference and is unlikely to be symmetric. It thus creates non-symmetry in the downstream flow. The turning moments which can arise from this can also be eliminated by correct design as demonstrated in the following paragraphs.

Using the approximations for X and R given in § 6 we suppose the erosion is around the circumference at $X = X_c$. At this position the flow is assumed to be symmetric. Thus

$$H_1 = \partial H_1/\partial X = 0, \quad (X = X_c), \tag{8.25}$$

and we specify the asymmetry by

$$\left.\begin{aligned} \partial H_1/\partial R &= K, \quad X_c < X < X_c + \Delta X, \quad (R = 1), \\ &= 0, \quad X > X_c + \Delta X, \quad (R = 1). \end{aligned}\right\} \tag{8.26}$$

First it is necessary to solve the equation subject to condition (8.25) and

$$\partial H_1/\partial R = K, \quad X > X_c, \quad R = 1.$$

The solution is given by $H_1 = KR + \sum_n A_n J_1(\beta_n R)\, I\{\beta_n(X - X_c)\}$,

the summation being over the positive roots β_n obtained earlier and

$$A_n = -2\beta_n^2 \int_0^1 R^2 J_1(\beta_n R)\, \mathrm{d}R \Big/ (\beta_n^2 - 1)\,[J_1(\beta_n)]^2.$$

We have $$\int_0^1 R^2 J_1(\beta_n R)\, \mathrm{d}R = J_2(\beta_n)/\beta_n,$$

and since $$J_1'(\beta_n) = 0$$

the recurrence relations for the Bessel functions give

$$J_2(\beta_n) = J_1(\beta_n)/\beta_n.$$

Thus $$A_n = -2/(\beta_n^2 - 1)\, J_1(\beta_n).$$

Similarly, the solution H_1 satisfying the boundary conditions

$$\partial H_1/\partial R = -K, \quad X > X_c + \Delta X \quad (R = 1),$$

$$H_1 = \partial H_1/\partial X = 0, \quad X = X_c + \Delta X \quad (0 < R < 1),$$

is $$H_1 = -KR + 2K \sum_n \frac{J_1(\beta_n R)}{(\beta_n^2 - 1)\, J_1(\beta_n)}\, I\{\beta_n(X - X_c - \Delta X)\}.$$

Taking ΔX as small, the value of H_1 satisfying the conditions (8.26) is

$$H_1 = -2K\Delta X \sum_n \frac{\beta_n J_1(\beta_n R)}{(\beta_n^2 - 1)\, J_1(\beta_n)} \frac{\mathrm{d}}{\mathrm{d}(\beta_n X)}\, I\{\beta_n(X - X_c)\}. \tag{8.27}$$

It is convenient to take $2K\Delta X = 1$, i.e. the unit of the asymmetry. In the previous analysis it was found sufficient to take only the first term of the series but this series for H_1 converges very slowly; it is in fact conditionally convergent when $X_c > X_0$ for in this ξ can be taken as zero and $I(\beta_n X)$ becomes $\cos \beta_n X$.

At $R = 1$ assuming $X_c > X_0$, $$H_1 = \sum_n \frac{\beta_n}{\beta_n^2 - 1} \sin \beta_n X. \tag{8.28}$$

In the first instance it is necessary to know the values of X at which this is zero. The larger roots β_n are given by

$$\beta_n = n\pi - \tfrac{1}{4}\pi.$$

Consider the series

$$S = \sum_{n=1}^{\infty} \frac{1}{n\pi} \sin(n\pi - \tfrac{1}{4}\pi) X.$$

Thus

$$H_1 - S = \sum_n \left[\frac{\beta_n}{\beta_n^2 - 1} \sin \beta_n X - \frac{1}{n\pi} \sin(n - \tfrac{1}{4})\pi X \right]. \tag{8.29}$$

This converges much more rapidly. The first five terms are given in table 6 for $X = 1.73$ and $X = 1.83$.

TABLE 6

n	$X = 1.73$	$X = 1.83$
1	0.2227	0.1194
2	0.0528	0.0314
3	0.0229	0.0211
4	0.0047	0.0127
5	−0.0032	0.0070

The series converges absolutely. Also

$$S = \frac{1}{\pi} S_1 \cos \tfrac{1}{4}\pi X - \frac{1}{\pi} C_1 \sin \tfrac{1}{4}\pi X,$$

where

$$S_1 = \sum_{n=1}^{\infty} \frac{1}{n} \sin n\pi X, \quad C_1 = \sum_{n=1}^{\infty} \frac{1}{n} \cos n\pi X.$$

These are

$$S_1 = \tfrac{1}{2}\pi(1 - X), \quad C_1 = -\tfrac{1}{2} \ln[2 - 2\cos \pi X].$$

Thus S can be evaluated and H_1 is obtained by using the first five terms of the series for $H_1 - S$. Some values are shown in table 7.

TABLE 7

X	H_1
1.67	0.4202
1.69	0.3869
1.71	0.3507
1.73	0.3111
1.75	0.2675
1.77	0.2192
1.79	0.1665
1.81	0.1077
1.83	0.0402

By extrapolation the zero of H_1 is found to be at $X = 1.841$. The zeros of the turning moment can be obtained by an analysis as above but this is lengthy and is not reproduced here. The conditions under which these results are valid are discussed in the following paragraphs.

If the terms in ϕ_y^4 are neglected in the expression for X given by (5.8), it can be written with $\alpha_1 = r_1$,

$$X = \int_0^x \frac{1}{r_1} \left(\frac{1 - \{(\gamma - 1)/(\gamma + 1)\} w^2}{w^2 - 1} \right)^{\frac{1}{2}} \left[1 + \frac{w^2 \sin^2 \theta_1}{(\gamma + 1)(w^2 - 1)} \right] dx, \tag{8.30}$$

in which the mean value of ϕ_y^2 across the section has been written

$$\overline{\phi_y^2} = \tfrac{1}{2} w_1^2 \sin^2 \theta_1,$$

θ_1 being the flow angle at the boundary of the section.

The mean value of w_1 across the section differs only very slightly from the value of w obtained from one-dimensional theory. This has been confirmed by determining w_1 from the characteristic diagram with $R_t/r_t = 1.0$ and a total exit cone angle of 40°. Typical values are given in table 8.

TABLE 8

$x/2r_t$	mean velocity across a diameter	mean velocity across the area	one-dimensional theory
0	1.0068	1.0068	1.000
0.08682	1.107	1.155	1.165
0.1294	1.166	1.226	1.246
0.1710	1.228	1.298	1.328
0.25	1.360	1.440	1.451
0.35	1.454	1.536	1.563
0.45	1.554	1.625	1.649
0.60	1.679	1.703	1.750
0.80	1.809	1.832	1.854
1.00	1.912	1.918	1.934

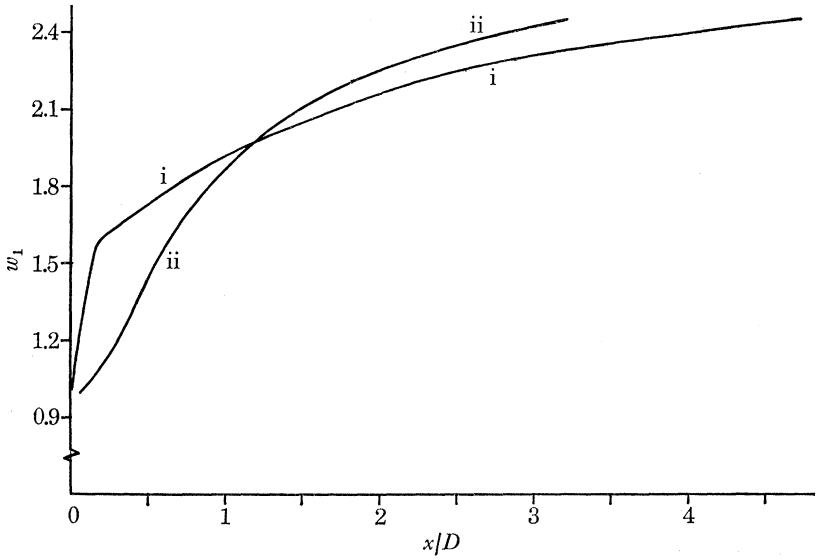

FIGURE 11. The velocities in the exit cone of an axi-symmetric nozzle assuming parallel flow at the throat as determined by the method of characteristics; (i) on the boundary, (ii) on the axis; $R_t/D = 0.5$, $\gamma = 1.25$, cone semi-angle 20°, $w_t = 1.0065$.

The values of w_1 on the axis and at the boundary are given graphically in figure 11. The example considered in § 6 is hypothetical, since parallel sonic flow is assumed across the throat whereas in general there is a large variation in w_1 across the throat section as is shown in § 7. The mean value of w_1 across the throat section is not unity, and thus the term ϵ which defines the zero of X in (5.8), is not zero. The throat section makes a large disproportionate contribution to X and thus relatively small values of ϵ can introduce significant errors. Also, since w_1 varies significantly across the throat, the mean value of the integrand in (5.8) for X differs markedly from that obtained by using the mean value of w_1 in the integrand. Further, it is seen in § 6 that the large variations in w_1 give rise to a large variation in the slopes of the characteristic rays crossing a section and the position for zero lateral thrust could then be influenced by the form of asymmetry of the flow at the throat. The variation of w_1 across the sections reduces rapidly with increasing values of R_t/r_t and for values above 2.0 the errors do not appear to be serious. The conditions for

isentropic flow at the throat require the curvature of the boundary profile to be continuous at the throat section. The discontinuity in curvature at the intersection of the curved profile and the straight line generators of the exit cone affects the entropy only in that part of the flow beyond the cusp on the axis and this is of little concern in practical nozzles.

The term $w^{\frac{1}{2}}$ in the expression for α_1 has been ignored and, as is shown in § 6, this significantly changes the slopes of the characteristics. However the above formulae for L and C_T remained unchanged as is now demonstrated. The nozzle length is divided into segments over each of which $w^{\frac{1}{2}}$ can be taken as constant. In one such segment

$$R = r/r_1\overline{w^{\frac{1}{2}}}, \quad X_1 = (X - X_0)/\overline{\omega^{\frac{1}{2}}}$$

$\overline{w^{\frac{1}{2}}}$ being the mean value along the length, X is defined as in (6.2) and X_0 is the value of X at the leading face of the segment. The solution for H_1 becomes

$$H_1 = \sum_n A_n J_1(\delta_n R)\, I_1(\delta_n X_1) + \sum_n \beta_n J_1(\delta_n R)\, I_2(\delta_n X_1),$$

where $I_1(\delta_n X_1)$ and $I_2(\delta_n X_1)$ are solutions of (8.20) in which X and β_n have been replaced by X_1 and δ_n respectively and

$$I_1(\delta_n X_1) = 1.0, \quad \mathrm{d}I_1(\delta_n X_1)/\mathrm{d}X_1 = 0, \quad (X_1 = 0),$$
$$I_2(\delta_n X_1) = 0, \quad \mathrm{d}I_2(\delta_n X_1)/\mathrm{d}X_1 = 1.0 \quad (X_1 = 0),$$

the constants A_n and B_n being determined by conditions at $X_1 = 0$. The terms δ_n are determined from the boundary equation

$$\frac{\mathrm{d}J_1(\delta_n R)}{\mathrm{d}R} = 0, \quad R = \frac{1}{\overline{w^{\frac{1}{2}}}},$$

thus

$$\delta_n = \beta_n \overline{w^{\frac{1}{2}}},$$

so that

$$H_1 = \sum_n A_n J_1(\beta_n r/r_1)\, I_1\{\beta_n(X - X_0)\} + \sum_n B_n J_1(\beta_n r/r_1)\, I_2\{\beta_n(X - X_0)\}$$

and this is identical to the value of H_1 given by (8.18) for the equation takes the same form when expressed in terms of X or X_1.

It is concluded from the analysis that the formulae for L and C_T given by (8.16) and (8.17) are valid provided that the variations in w_1 across the sections are not excessive. This requires that $R_t/r_t > 2.0$ and the exit cone angle should not exceed 30° total angle. However, greater cone angles can be accommodated with greater values of R_t/r_t.

9. Experimental investigation of non-symmetric flow in axisymmetric nozzles and the validity of the optimum nozzle

The static experiments were carried out with the 'all forces dynamometer' which was designed to measure the complete thrust vector on the rocket model employed. The model comprised a steel tube of 336.6 mm length, 69.9 mm outside diameter and 6.35 mm wall thickness into which was inserted a solid cylindrical steel nozzle with machined entry and exit cones. The propellant charge of 291 g of cordite burned at a pressure of approximately 69 bar for one second, producing a fairly constant thrust of 580 N. The nozzle throat diameter was 10.41 mm. By taking suitable precautions during assembly and cleaning, the model was fired repeatedly with negligible changes in mechanical tolerances.

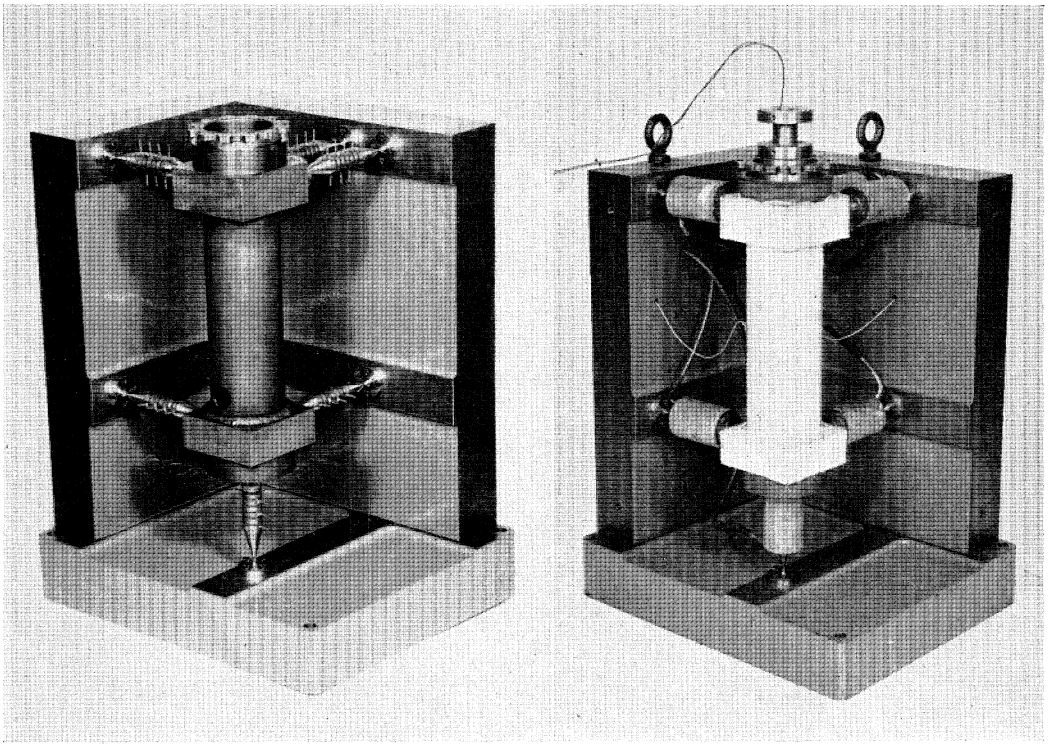

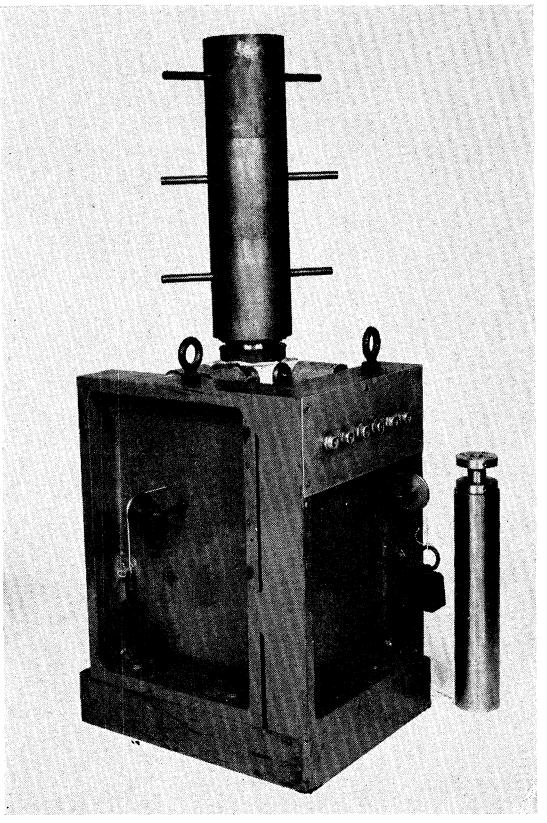

FIGURE 12. The 'all forces dynamometer'.

(*Facing p.* 224)

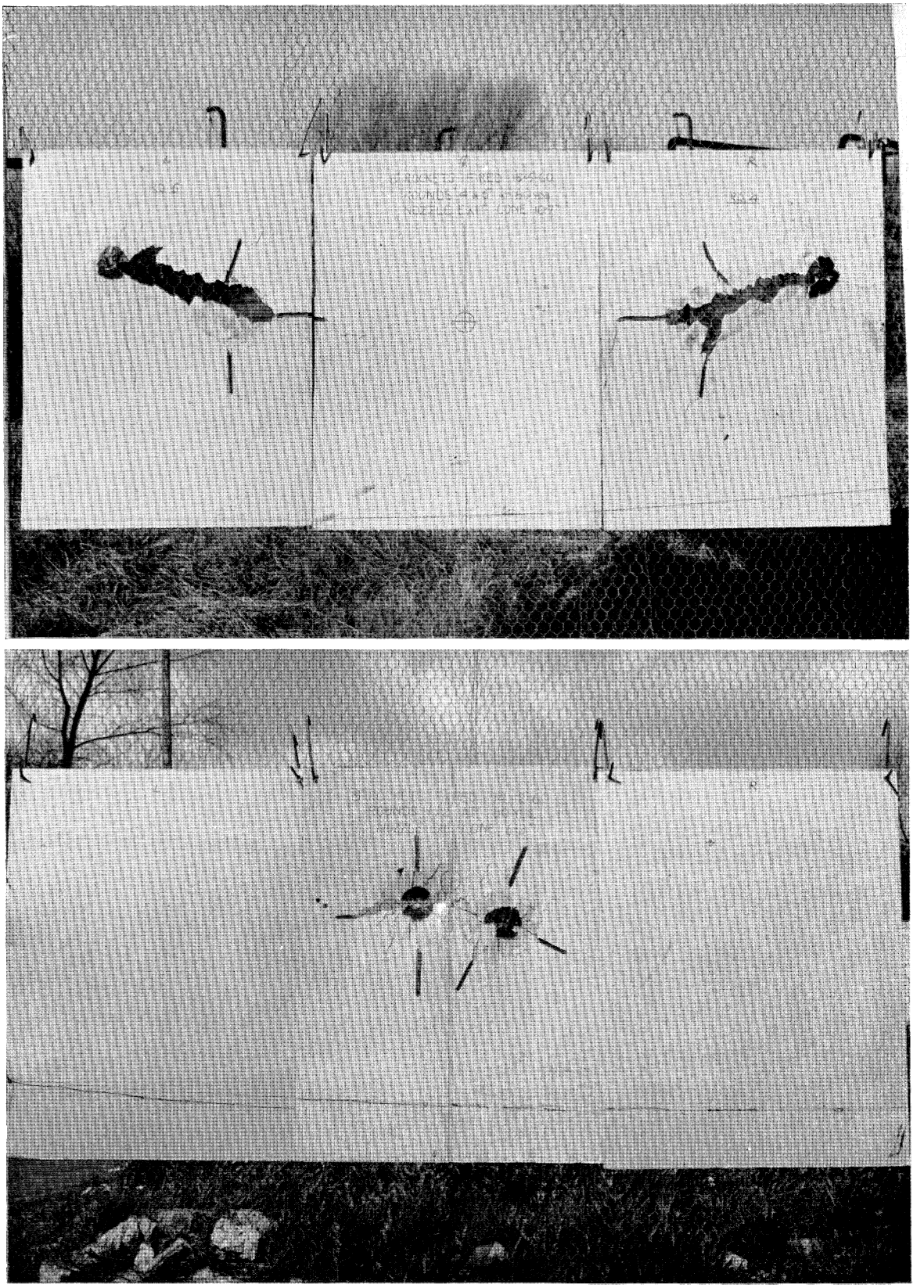

FIGURE 25. Targets showing the yaws and flight deviations of the 8 in (20 cm) test vehicle with the asymmetric entry cone and with exit cone lengths of (top) 272 mm and (bottom) 157 mm.

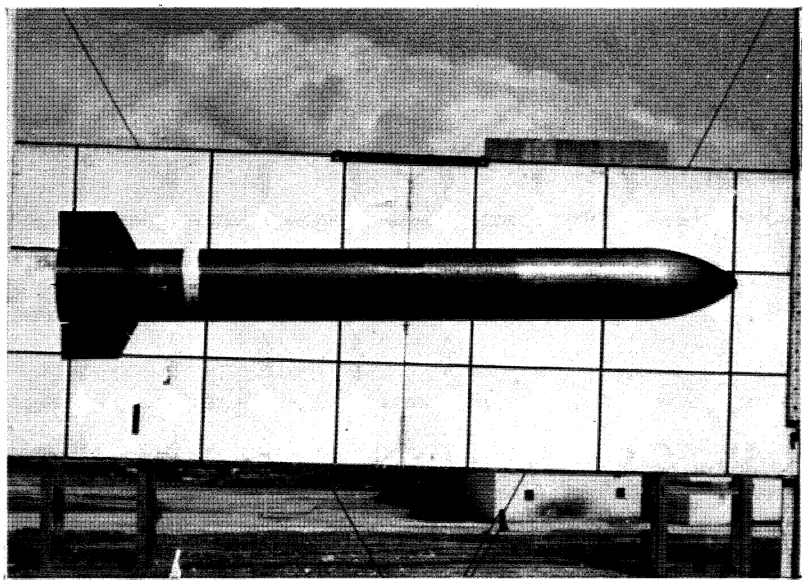

FIGURE 22. The 200 mm test vehicle.

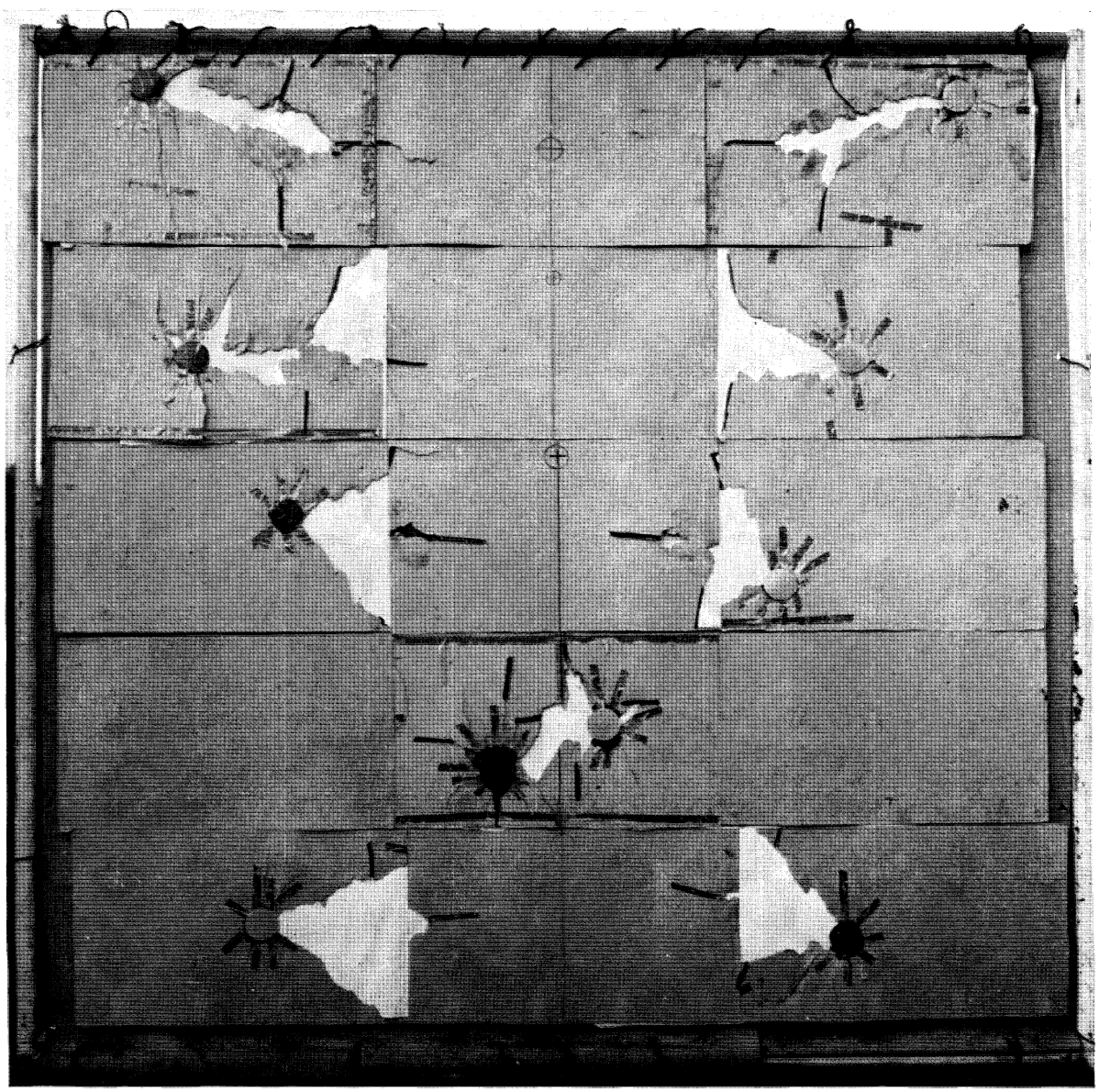

FIGURE 26. Composite picture of the targets showing the variation of the flight deviation with nozzle exit cone length. ◯, Orientation left; ●, orientation right.

The dynamometer is shown in figure 12, plate 1. The rocket model is mounted vertically downward to eliminate the effect of the charge weight during burning. The complete specification of the thrust vector requires three forces and three couples in orthogonal directions and thus six gauges are required. The output from these was measured on a six-channel photographic galvanometer recorder, the calibration being a system of weights over pulleys. The apparatus was checked by bevelling the exit plane of a nozzle and measuring the thrust malalinement so produced. This agreed with the calculated value to better than 5%.

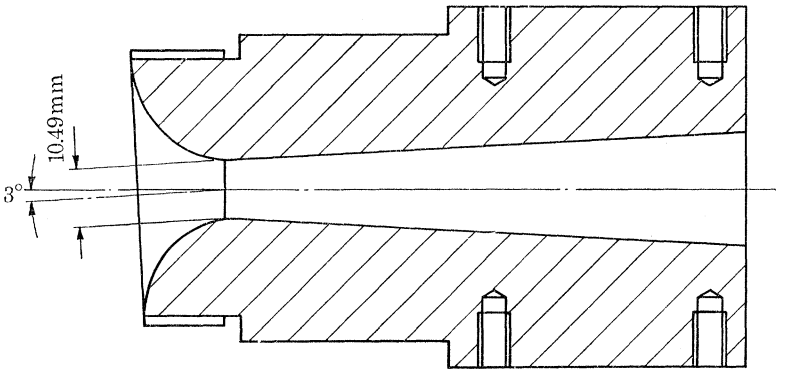

FIGURE 13. The experimental nozzle with total exit cone angle of 6.6° and canted inlet cone.

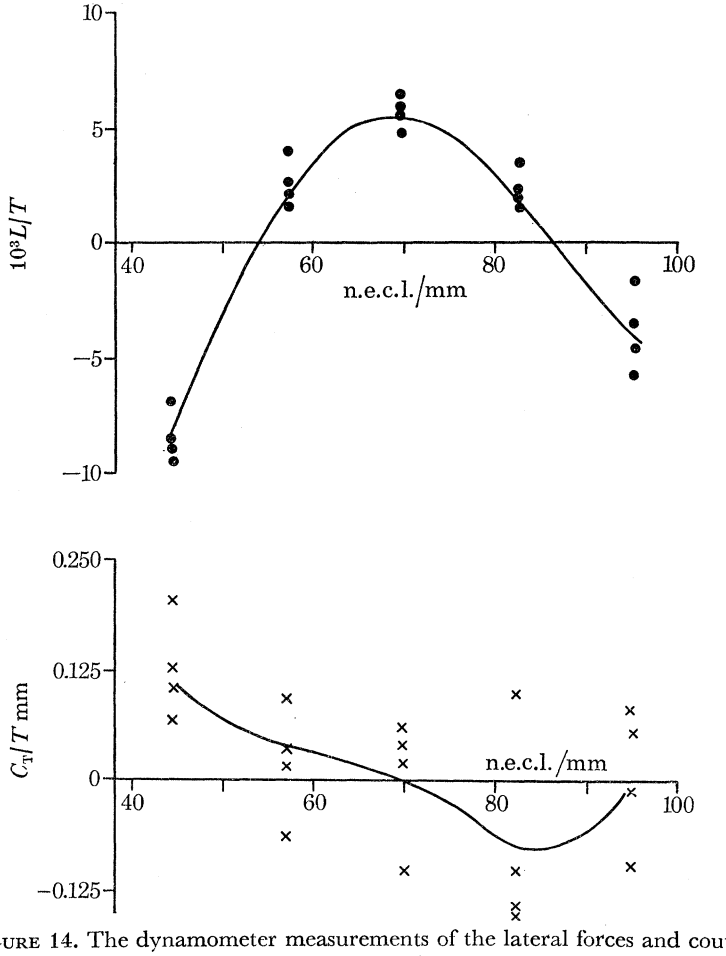

FIGURE 14. The dynamometer measurements of the lateral forces and couples with the nozzle of figure 13.

The first experiments were carried out with a nozzle of 6.6° total exit cone angle. The inlet cone was made skew by machining it up to the throat as illustrated in figure 13. Four firings were carried out with the full length nozzle. In each case the plane of symmetry of the nozzle was placed in the plane of one of the gauges, the orientation in the second and fourth firings being at 180° to the first and third to remove any dynamometer bias. The length of the nozzle was subsequently shortened by 12.7 mm at each of four stages, the firing procedure described for the full-length nozzle being repeated at each stage. Thus we obtained four thrust malalinement measurements at each of five nozzle exit cone lengths, the final being 50.8 mm shorter than the original. At this stage the limit was reached, for with further shortening the nozzle became recessed into the tube and so the results would have been affected by the projection of the tube beyond the nozzle exit.

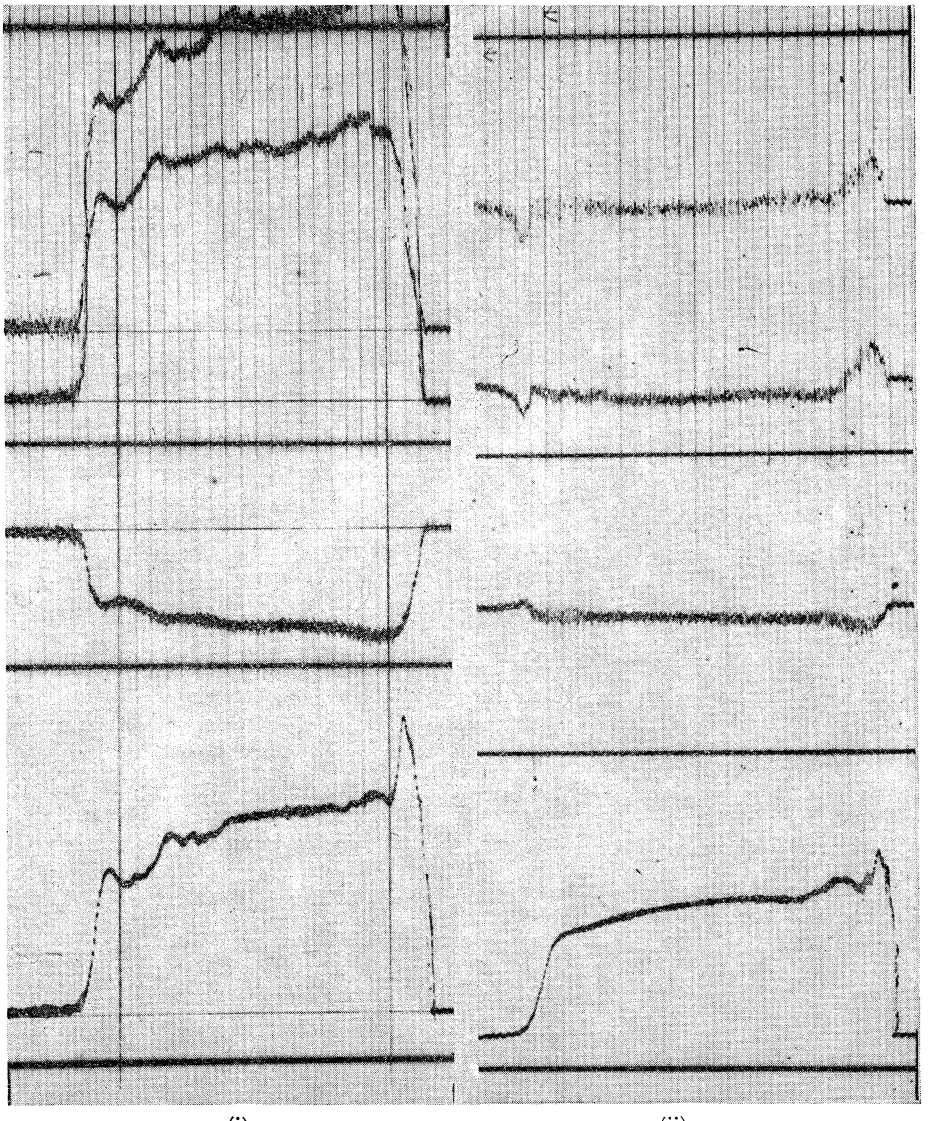

(i) (ii)

FIGURE 15. Typical dynamometer records. (i) At the maximum of the curve of figure 17; (ii) at the near-zero of the curve of figure 17. The bottom curve in each case is the axial thrust, the second being with a reduced scale to allow greater magnification of the lateral thrust.

In the text the thrust malalinement is resolved into a lateral force L acting at the exit plane of the nozzle, and the couple C_T which is the product of the axial thrust and the displacement of this parallel to the nozzle exit cone axis. These are usually expressed as ratios of the axial thrust and are quoted in milliradians and millimetres respectively. The lateral thrusts so obtained with the 6.6° total exit cone angle are given in figure 14, a smooth curve being drawn through the mean points at each length. The galvanometer traces are remarkably consistent within themselves and could be analysed without much difficulty. The records and results show the performance of the dynamometer to be satisfactory. Each experimental point in figure 14 is obtained from the mean lateral force during burning, omitting the two transient stages, i.e. the initial rise to the working thrust and the concluding fall-off. During these transient stages the velocity at the throat is not sonic so that the theoretical analysis is not valid. Typical records are given in figure 15 which show the smoothness of the traces.

The conclusions from the experiments are evident from figure 14. The curve of the lateral thrust against the exit cone length exhibits the oscillatory form expected theoretically with zero values at exit cone lengths of 53.6 and 86.6 mm.

In the nozzle used in the above experiments, the exit cone fitted into the throat with no radiusing after the throat (figure 13), while the profile of the entry cone had a radius of 10.41 mm. On linearized theory the condition for zero lateral thrust is

$$\frac{f(w)}{2\tan(3.3°)} = \frac{(n+\frac{1}{2})\,\pi}{1.841} \quad (n = 0, 1, 2, 3, \ldots),$$

where $f(w)$ is the Prandtl–Meyer expansion angle at the exit of the nozzle as calculated from one-dimensional theory. Thus

$$\left.\begin{aligned} f(w) &= 0.1965(n+\tfrac{1}{2}), \\ \text{and} \qquad A/A_t &= (1+0.01106x)^2, \end{aligned}\right\} \tag{9.1}$$

the term on the left-hand side of (9.1) being the expansion ratio of the nozzle from which w is obtained and x is the exit cone length in mm, the throat diameter being 10.41 mm. The theoretical zeros are given in table 9.

TABLE 9

zero (as numbered from the throat)	X	$f(w)$	A/A_t	x/mm
1	0.853	0.098	1.055	2.44
2	2.56	0.295	1.294	12.5
3	4.27	0.491	1.728	28.5
4	5.97	0.688	2.49	52.3
5	7.68	0.884	3.90	88.1
6	9.39	1.081	6.61	142.2

The fourth and fifth zeros are at 52.3 and 88.1 mm which are remarkably close to the experimental values of 53.6 and 86.6 mm. Also the direction of the lateral force is in agreement with the theory. The experiments were repeated in part with a second nozzle to check that the agreement was not fortuitous. Firings were carried out with this at the two longer exit cone lengths and the zero lateral thrust position was found to be at the exit cone length of 87.6 mm which confirms the first measurement.

An examination of the records and experimental technique indicated that the ratio lateral force to axial thrust could be measured to within 0.25 mrad. The exit cone was inserted into the motor body with screw thread attachment extending to the length of 38.1 mm. Measurements

of a batch of tubes and nozzles of this type gave a mean value of the mechanical malalinement between the axes of the nozzle exit cone and the tube of 0.3 mrad circular error. In these experiments the nozzle orientation relative to the tube was fairly constant from round to round so that this mechanical malalinement probably enters as a systematic error.

The lateral force measurements are obtained from the sum of the forces on the gauges whereas the couple C_T is obtained from the differences of the moments. The measured ratios of the couple to the lateral thrust, i.e. the parallel displacement, is of the order of a few hundredths of a mm and it has been found that the measured values are not sufficiently precise. The values given in figure 14 show the random scatter arising. Nevertheless the mean curve does exhibit the features expected from the linear theory, i.e. the oscillatory nature of the curve and the zero value at the maximum value of the lateral thrust.

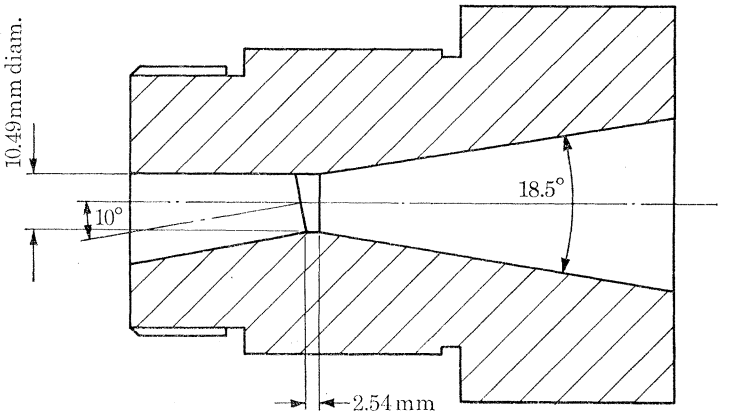

FIGURE 16. The experimental nozzle with the total exit cone angle of 18.5° with canted inlet.

The subsequent programme was designed to check the theory at large exit cone angles. The model rocket is a convenient vehicle for this investigation from the point of view of economy and ease of manipulation but its small scale exacts a penalty in the increased importance of mechanical tolerances. These tolerances can be classified into two types. The first type produces lateral forces but does not affect the value of X to a significant extent at downstream sections. The second type can change the mean Mach number in some region and thus change the value X to a significant extent. The latter type need not arise in service nozzles, but in small scale nozzles very considerable care must be taken in manufacture, particularly in the region of the throat. The nozzle chosen for the second series of experiments is illustrated in section in figure 16. The throat was located by means of the short parallel-walled section and the inlet and exit cones were mated into this at sharp junctions. The inlet cone was offset ten degrees to produce the systematic lateral force, the exit cone angle being 18.5°. The manufactured nozzle appeared satisfactory, having a smooth exit cone and a well defined throat of length 2.0 mm. The results are given in figure 17. The measured maximum lateral force ratio is 15 mrad, and it is zero at an exit cone length of 22.2 mm. The records and results are satisfactory and the lateral force exhibits the oscillatory form expected. The spread in the individual values at the lateral thrust zero is one milliradian as against a spread of the order of five milliradians at the maximum position. Thus it would appear that the random lateral forces arising from malalined gas flow into the nozzle are also minimum at the lateral force zero.

On linear theory, the lateral thrust is zero at exit cone lengths satisfying the equation

$$\frac{f(w)}{2\tan(9.25°)} = \frac{(n+\frac{1}{2})\pi}{1.841} \quad (n = 0, 1, 2, 3, \ldots), \tag{9.2}$$

and the values are

X	0.853	2.56	4.27
x/mm	4.06	27.4	88.9

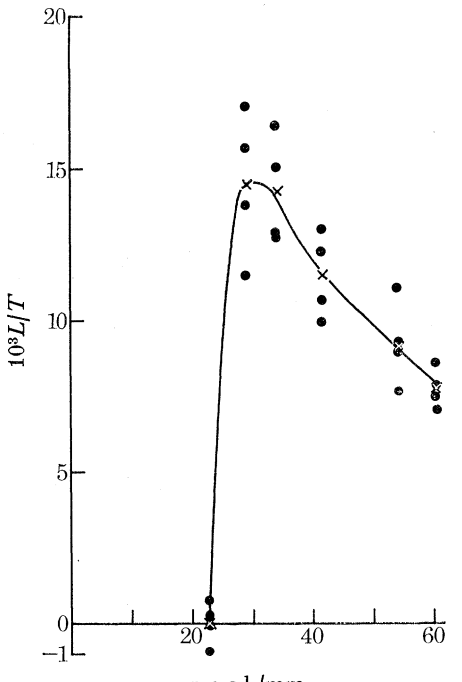

FIGURE 17

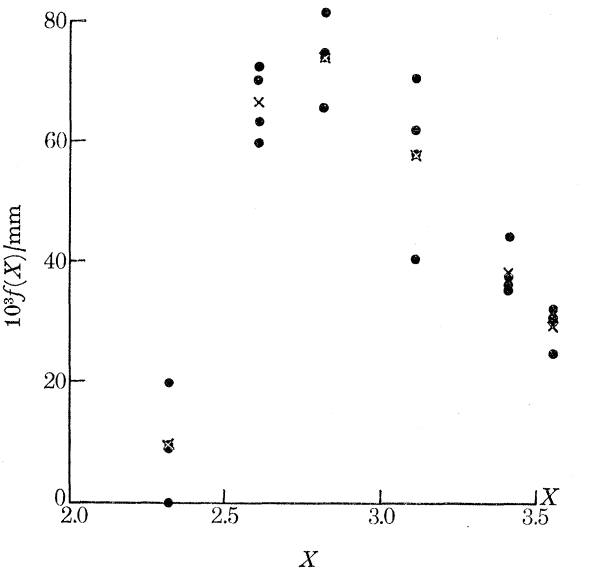

FIGURE 18

FIGURE 17. The dynamometer measurements of the lateral forces with the nozzle of figure 16.

FIGURE 18. The curve derived from the right-hand side of (9.3) with the experimental values of L and C_T from figure 17.

From the directions of the lateral forces it appears that the experimentally observed zero corresponds to $X = 2.56$ and $x = 27.4$ mm. Thus the observed value is discrepant with the theoretical value based on linear theory. To compare the results with nonlinear theory, the values of the lateral forces and couples are substituted into the right-hand side of the following equation which is derived from (8.10).

$$\frac{A}{T}\cos(1.841X) = -r_1\left[\frac{L}{T} + \frac{M^2-2}{M^2-1}\frac{1}{r_1}\frac{\mathrm{d}r_1}{\mathrm{d}x}\frac{C_T}{T}\right] \equiv f(X), \tag{9.3}$$

and the resulting curve is given in figure 18. The best estimates of the zero positions are at $X = 2.28$ and 4.0, the latter being approximate. The left-hand side of (9.3) is zero at values of 2.56 and 4.27. Thus both zeros are displaced, the wavelength being approximately correct, which would suggest a zero error.

The experiments were repeated with a similar nozzle but which had a throat length of 3.5 mm and a total exit cone angle of 14°. The results are given in figure 19. The values of the lateral thrusts and couples are substituted into the right-hand side of (9.3) and the resulting curve is

given in figure 20. It is seen that the expression is zero at $X = 3.60$ and the directions of the lateral thrust indicate that this corresponds to the theoretical zero $X = 4.27$. Again there is a marked discrepancy between theory and experiment.

It is unlikely that this is due to the failure of the theory at the larger cone angles since the discrepancy is greater with the fourteen-degree cone, which, however, has the longer throat. To examine this, the experiments were repeated with the total exit cone of 18.5° but with some modifications. The entry cone of figure 16 was replaced by the standard type entry cone of figure 13 which was machined asymmetrically to produce the systematic lateral flow at the throat. The length of the throat section was reduced to 0.50 mm and there was a smooth junction of the inlet cone with the throat to reduce the possibility of the formation of a vena contracta at the throat. The results are given in figure 21. The exit cone length for zero lateral force is 25.1

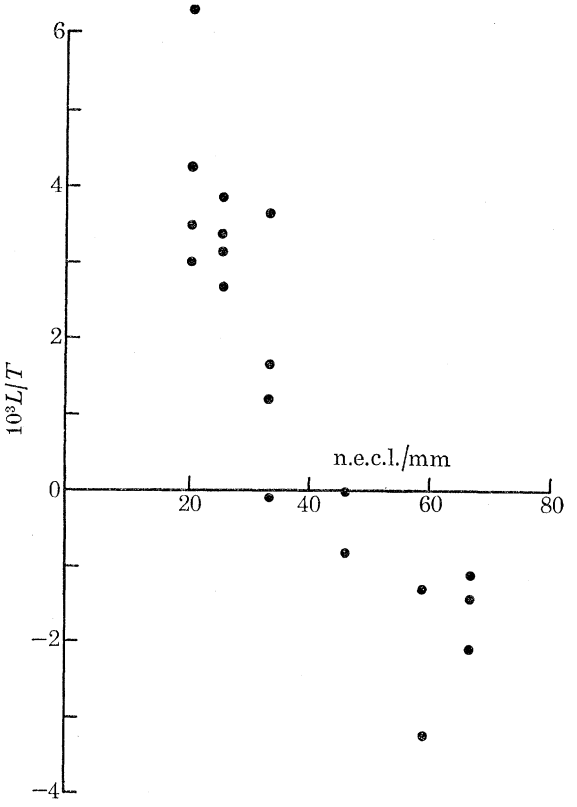

FIGURE 19

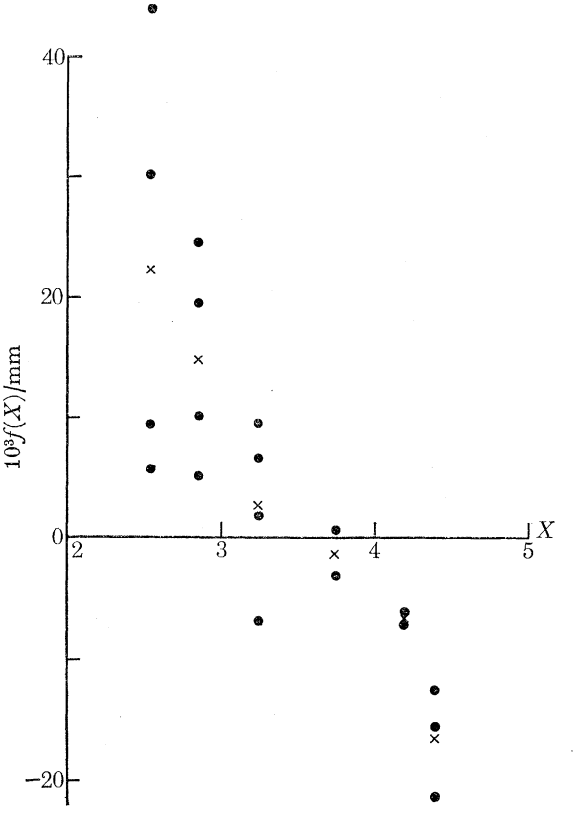

FIGURE 20

FIGURE 19. The dynamometer measurements with the nozzle of 14° total exit cone angle.

FIGURE 20. The curve derived from the right-hand side of (9.3) with the experimental values of L and C_T from figure 19.

which is closer to the theoretical value of 27.4 mm obtained from linear theory. The nonlinear expression on the right-hand side of equation (9.3) is zero at $X = 2.44$ which is closer to the theoretical value 2.56. A small correction should be applied to these latter figures to allow for the slight erosion of the originally sharp junction of the throat with the exit cone. Examination of the sectioned nozzle showed that the junction was eroded into a smooth curve 0.25 mm long which corresponds to a radius of curvature $R_t = 1.8$ mm. From formula (6.8) it can be shown that this increases the value of X by an amount 0.14 so that the experimental value of $X = 2.44$

becomes 2.58 which compares favourably with the theoretical value of $X = 2.56$. The close agreement is possibly fortuitous but it is clear that the theory and experiment agree within experimental error. This nozzle was of mild steel and showed greater erosion at the junction than that made of standard nozzle material.

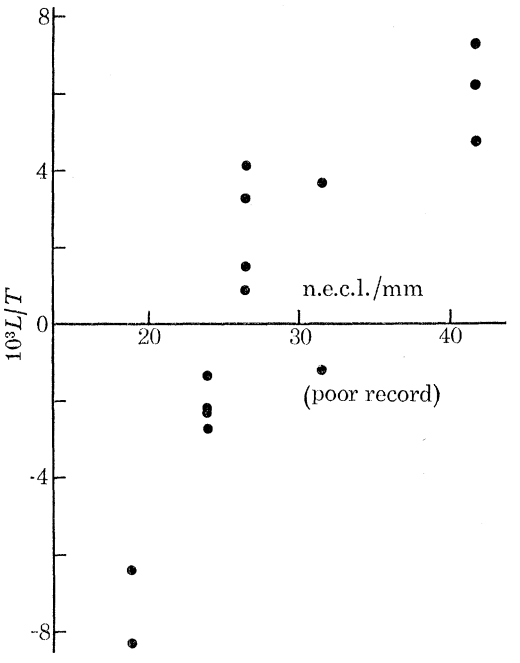

FIGURE 21. The dynamometer measurements with the nozzle of 18.5° total exit cone angle but with the short throat.

The reason for the discrepancy with the 14° cone and the first 18.5° cone is now clear. The phenomenon by means of which it occurs is undoubtedly that observed by Fraser, Rowe & Coulter (1957) at Imperial College. With a sharp junction at the throat, the flow separates from the wall just upstream of the throat and reattaches just downstream. There is a significant drop in thrust due to the reduced flow and velocity coefficients at the throat so that the effective throat is less than the mechanical value. With the parallel-walled throat its position is also upstream of the junction with the exit cone. This gives rise to the zero error noted earlier.

Thus it would appear that the experiments confirm the theoretical analysis, provided the throat configuration is as assumed in the theory, i.e. profile slope and curvature continuous at the throat.

Small scale experiments such as these are not suitable for precise quantitative measurement and so these experiments were followed by flight tests with 200 mm test vehicles simulating a flight rocket (figure 22, plate 3). These were constructed from discarded nitrogen cylinders which were adapted to take a conventional conical head and nozzle. The charge mass was 6.72 kg with burning time 0.25 s and working pressure 69 bar and delivering a fairly constant thrust of 53 kN. The burning chamber wall-thickness was 4.19 mm with an internal polyethylene lining 2.5 mm thick for heat insulation. Consequently there was negligible bending of the tube due to such factors as non-symmetric heating and wall-thickness variation. Before projection each vehicle was balanced by adjusting a system of weights in the head so that the nozzle exit cone axis was alined to pass through the centre of gravity of the complete vehicle. The overall

weight was 93 kg, there being some variation in this due to the different nozzle designs. The round-to-round variation in launch angular velocity was reduced to acceptable limits by using a carefully made launcher 4.05 m in length. The launch velocity was 71.3 m/s and the distance of free flight during burning was 15.2 m.

Denoting the aerodynamic restoring moment at yaw δ and velocity V by $K(V, \delta)$, the restoring moment coefficient n is defined by

$$n^2 = K(V, \delta)/IV^2\delta,$$

I being the moment of inertia about a transverse axis through the centre of gravity. The value of n for the test vehicle was 0.050 m^{-1} with the fins employed. The deviations in the directions of motion of the centre of gravity at the end of burning relative to the line of launch due to

(i) a thrust malalinement of 1 mrad,
(ii) a launch angular velocity of 1°/s,
(iii) a cross-wind of 1 m/s,

were calculated to be 0.10, 0.023 and 0.020° respectively. The dispersion in flight due to the random effects was found to be 0.028° linear mean deviation. This would result from a thrust malalinement of 0.28 mrad or a launch angular velocity variation of 1.2°/s linear mean values. The first of these corresponds to a circular mean value of 0.46 mrad.

The systematic lateral force was obtained by offsetting the entry cone axis as in the model tests. Thus the throat and exit cone axis were symmetrical to the rocket and the systematic gas malalinement was due to asymmetry previous to the throat. The offset in the entry cone was designed to give a thrust malalinement of 10 mrad maximum value so that systematic flight deviations were much greater than the random values.

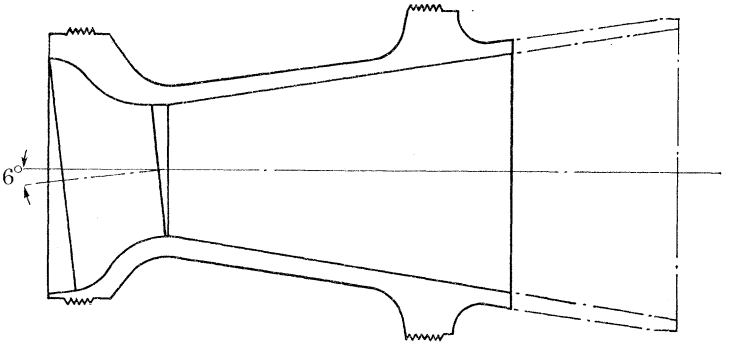

FIGURE 23. Sketch of the nozzle used with the 200 mm test vehicle.

The test vehicles were projected at cardboard targets supported on wire-netting screens at a range of 55 m. Just previous to firing, the nose was daubed with black paint which became imprinted on the target. This, together with the fin cuts, enabled us to obtain the position of the centre of gravity of the vehicle when it struck the target to ± 12 mm laterally. The nozzle was placed in the tube with its entry cone axis in the plane of two fins which were placed horizontally on the launcher so that the systematic deviations were entirely in the horizontal plane, with the rounds orientated alternatively right and left to remove any systematic launcher and wind effects. The sand bay behind the target collected the rounds which suffered negligible damage and could be used repeatedly.

Eight nozzles were made with exit cone total angles of 18.5° as in figure 23. The eight were first fired with an exit cone length of 272 mm and subsequently four were fired at each of the

lengths 246, 221, 196, 157 and 145 and eight at 170 mm. The results are shown graphically in figure 24 which gives the separation between the positions of strike at the target of the centre of gravity of pairs of rounds fired with the orientation alternatively right and left. It is seen that the separation is zero with an exit cone length of 161 mm. It is convenient to express the orientation by the thinnest side of the wall of the entry cone looking along the line of flight. With this to the left, the rockets deviate right when the exit cone length exceeds 161 mm but deviate left when below this length. At 246 mm the entry cone axes were inadvertently not placed in the plane of a pair of fins but were inclined to it by angles up to 25° which explains the departure of these results from the general pattern, the horizontal deviations only being measured. Figures 25 and 26,

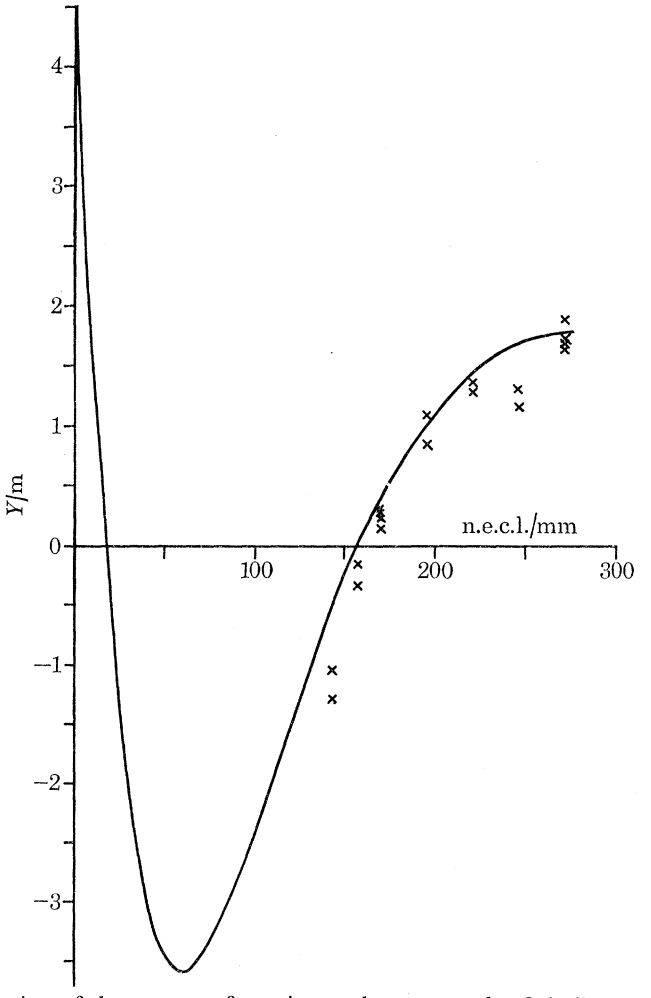

FIGURE 24. The separation of the centres of gravity at the yaw cards of similar rounds with their orientation alternately left and right. Comparison of the theoretical curve with the experimental points for different nozzle exit cone lengths.

plates 2 and 3, show typical target photographs. Figure 26 is a photograph of the targets placed one above the other starting with 272 mm at the top to 145 mm at the bottom. Circular disks are placed over the imprints of the nose, dark disks with the orientation right and white disks with it left. The effect of the length of the exit cone on the magnitude and direction of the deviation is thus made evident.

The deviating forces on the test vehicle comprise the turning couples Ll and C_T and the lateral

force L acting at the centre of gravity which is at the distance l from the exit plane of the nozzle. The contribution from the latter can be neglected. It is convenient to express the couple in terms of the ratio

$$\beta = (Ll + C_T)/lL_t,$$

where L_t is the value of L at the throat and is thus independent of the exit cone, C_T being zero at the throat section. The ratios L/L_t and C_T/L_t are calculated from (8.16) and (8.17). The deviation of the path of the centre of gravity at the end of burning is

$$0.10 \times 10^3 \beta L_t / T \text{ degrees},$$

T being the axial thrust. The deviation is zero when $\beta = 0$ and this is calculated to be 155 mm exit cone length which agrees well with the experimental value of 161 mm. L_t could have been calculated from the inlet cone configuration but this has not been done. The value of L_t can be chosen so as to give the correct deviation at 272 mm exit cone length and the theoretical curve with this value is given in figure 24. The form of the curve is the same as that of the experimental points. The directions of the deviations are also in accord with theory.

The experiments were continued with nozzles of 30° total angle. Four nozzles were constructed all having expansion ratios of 6:1 but with different throat configurations. Two had a throat profile curvature such that $R_t/D = 1.0$ and two such that $R_t/D = 1.5$. In each case systematic malalined flow at the throat was obtained by non-symmetry in the entry cone. These were projected against targets as in the previous trial with the paired rounds orientated alternatively right and left. The measured angles of turn at the targets were

$R_t/D = 1.0$: -63 mrad $\quad -60$ mrad

$R_t/D = 1.5$: $\quad 19$ mrad $\quad 22$ mrad

The positive direction is that which would have been obtained with zero exit cone length. Linear interpolation indicates that zero turning moment is obtained at $R_t/D = 1.37$. With a value of $\gamma = 1.25$ the theoretical null point is at $R_t/D = 1.43$ and with $\gamma = 1.20$, $R_t/D = 1.36$. The actual value of γ lies between these two values. This good agreement must, however, be qualified.

The asymmetries in the entry cones were designed to give the same lateral momentum at the throat section but these could not be achieved due to interference between the tool and the nozzle; at the higher value R_t/D it was completed manually. Plaster casts of the entry cone were not sufficiently precise in the important region approaching the throat to make the necessary correction but qualitatively they indicated a smaller lateral momentum at the throat of the nozzles with $R_t/D = 1.5$ so that the inferred null point is at a value $R_t/D < 1.37$. This lower value is not unexpected. The propellant charges were built from thin sheets which broke up appreciably during burning. It is unlikely that the lateral momentum of the particles of charge is reversed in the nozzle and also the resulting non-isentropic flow produces lower Mach numbers at the various sections of the exit cone. Both of these factors lower the value of R_t/D for zero turning moment. Within the limits of the experiments the agreement with theory is satisfactory.

Finally some limited trials were carried out with the flight test vehicle to examine the correctness of the optimization of the nozzle exit cone in removing any thrust malalinement arising from non-symmetric erosion at a section of the exit cone as discussed in § 8. Four nozzles with exit cones of 30° total angle, expansion ratio 4:1 and $R_t/D = 1.56$ were constructed with symmetric entry cones. The exit cones were gouged to simulate non-symmetric erosion. The gouge was in a plane

perpendicular to the exit cone axis; it was 38 mm long, 6.4 mm wide and approximately 3.2 mm deep. The vehicles were projected at yaw cards at 24.4 m range in a closed tunnel. The resulting yaws were immeasureably small and it would appear that the thrust malalinements were less than 0.2 mrad. The position of the gouge was at a distance from the exit plane of the nozzle corresponding to a difference in X of 1.80 so that theoretically the yaws would be expected to be zero. The tests should have been continued to determine the effect of the gouge at other positions but this was not possible owing to other commitments. Thus it is uncertain to what extent the optimization was responsible for the very low values of the yaws.

The author thanks Dr R. J. Rosser for his constant encouragement during the investigation and his advice on the experimental programme. The 'all forces dynamometer' was designed by Mr J. F. Waddington who also supervised the initial experiments. Mr B. Trenear and Mr B. Bodimeade also assisted in the experimental programme while a large part of the numerical work was carried out by Miss J. M. Yendall. The author wishes to express his thanks to these colleagues for their invaluable assistance.

References

Behrbohm, H. 1950 *Z. angew. Math. Mech.* **30**, 101.
Fraser, R. P., Rowe, P. N. & Coulter, M. O. 1957 *Proc. Inst. Mech. Engrs* **171**, 553–580.
Hall, I. M. 1962 *Quart. J. Mech. Appl. Math.* **15**, 487.
Hooker, S. G. 1931 *Rep. Memor. Aero Res. Comm., London*, no. 1429.
Lighthill, M. J. 1947 *Proc. R. Soc. Lond.* A **191**, 323.
Meyer, T. L. 1908 *Verh. dt Ing. Forschungsheft*, p. 62.
Oswatitsch, K. & Rothstein, W. 1942 *Jahrbuch Luftfahrtforschung* **1**, 91–102.
Sauer, R. 1944 *Dt. Luftfahrtforschung, Forschungsbericht*, p. 1992.
Shapiro, A. H. 1953 *The dynamics and thermodynamics of compressible fluid flow*, Ch. 4 and 9. New York: The Ronald Press Co.
Taylor, G. I. 1930 *Rep. Memor. Aero. Res. Comm. London*, no. 1381.
Tomotika, S. & Hasimoto, Z. 1950 *J. math. Phys.* **29**, 105.
Tomotika, S. & Tamada, K. 1950 *Q. appl. Maths.* **7**, 338.

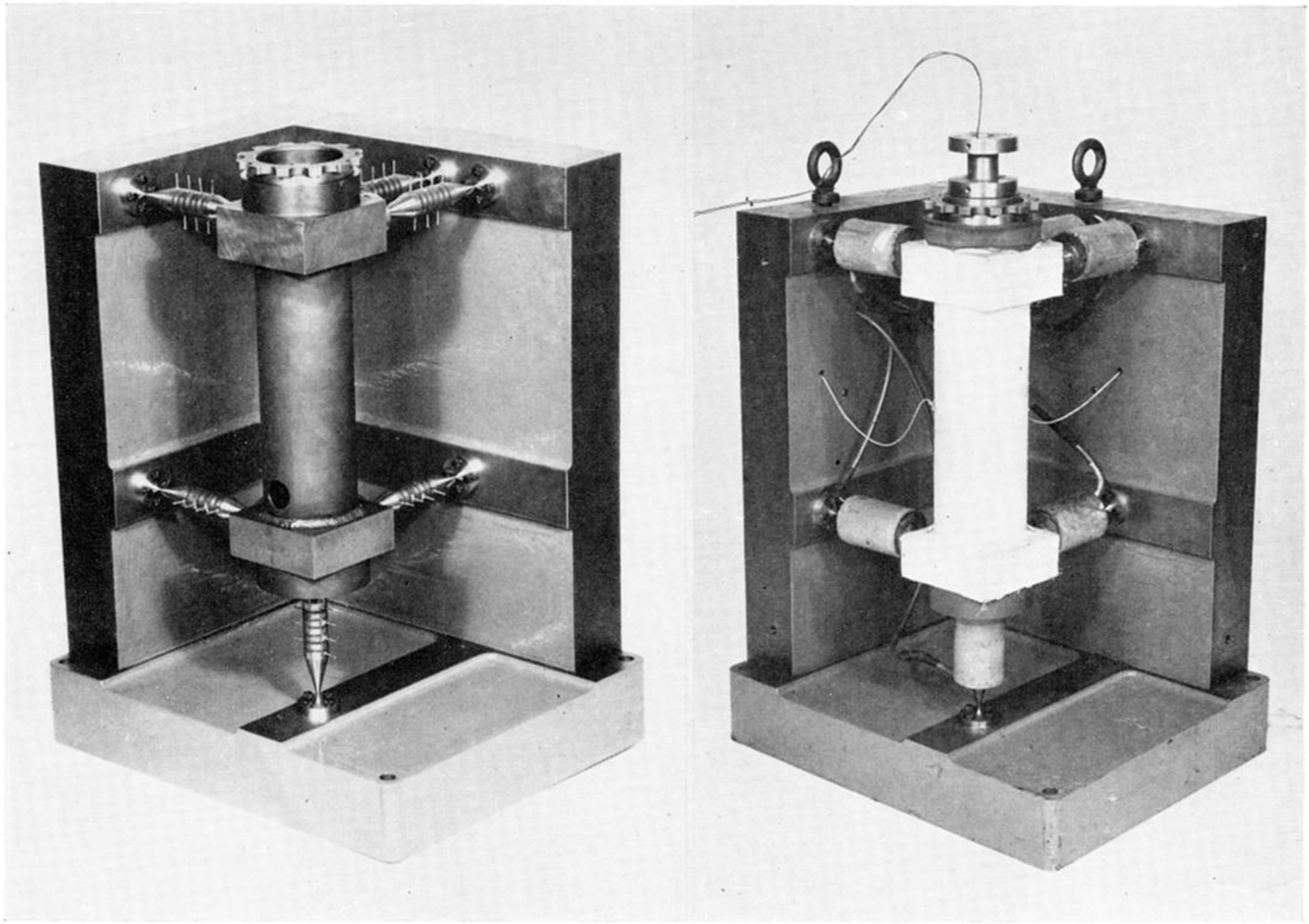

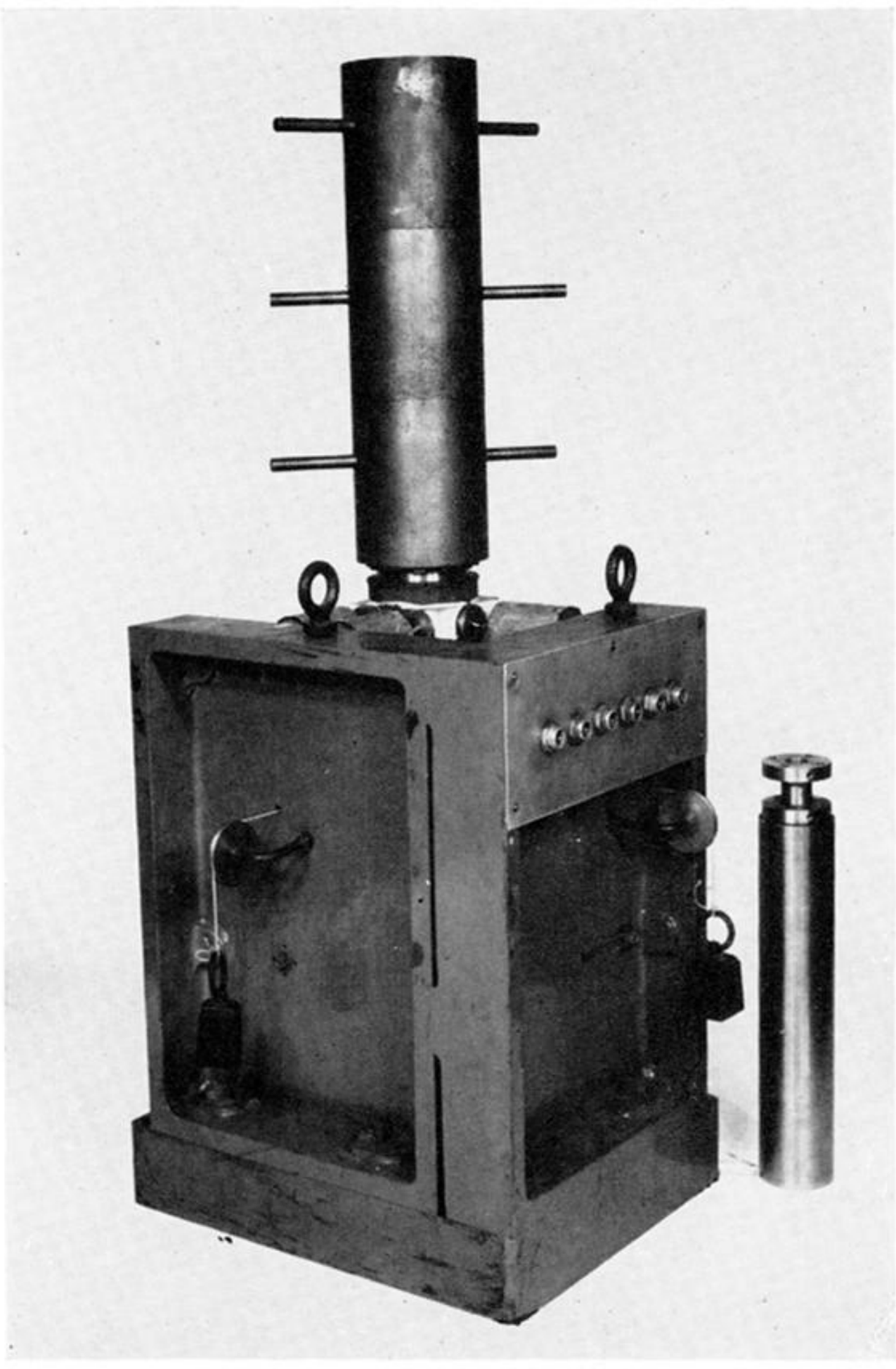

FIGURE 12. The 'all forces dynamometer'.

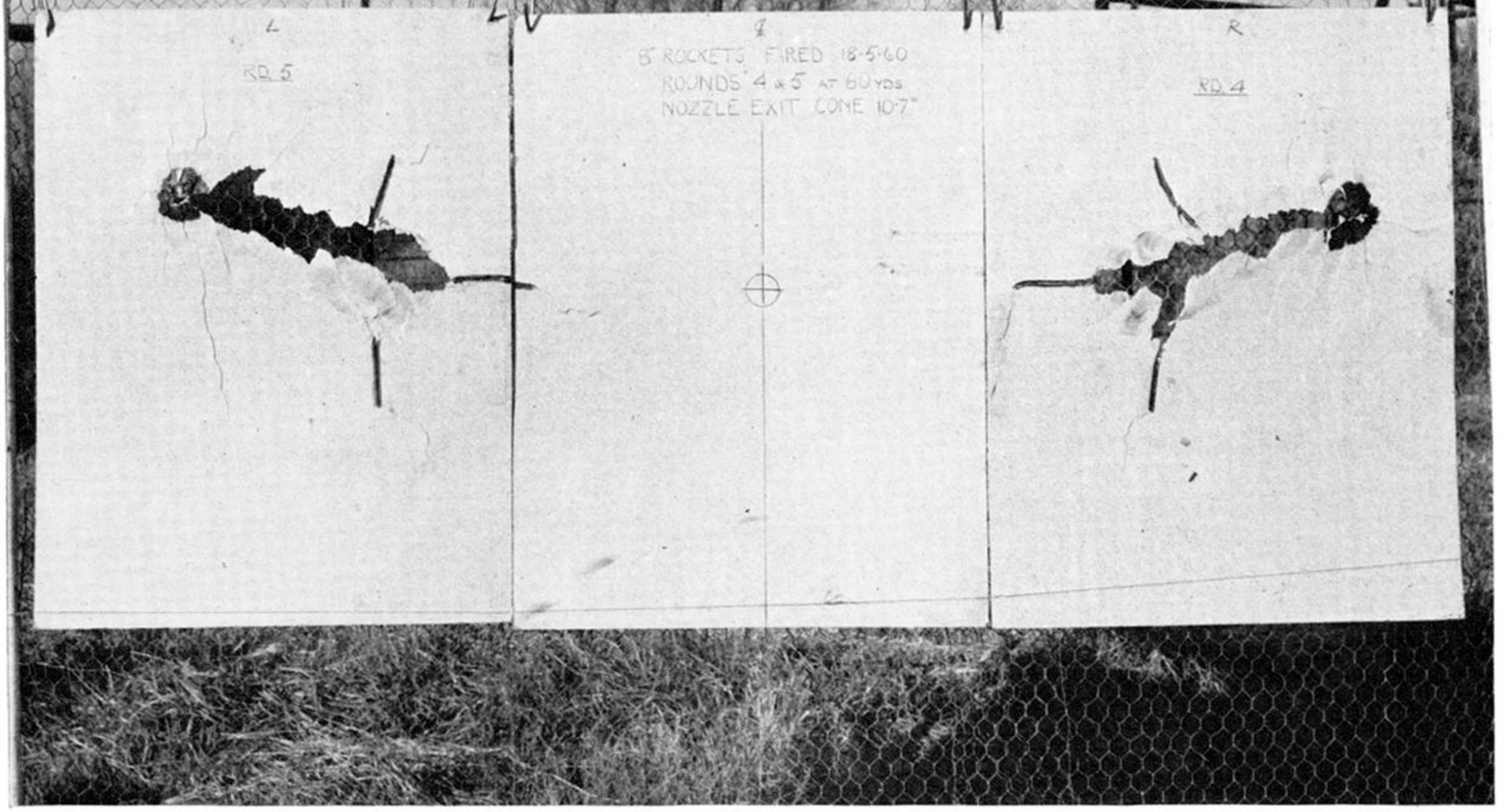

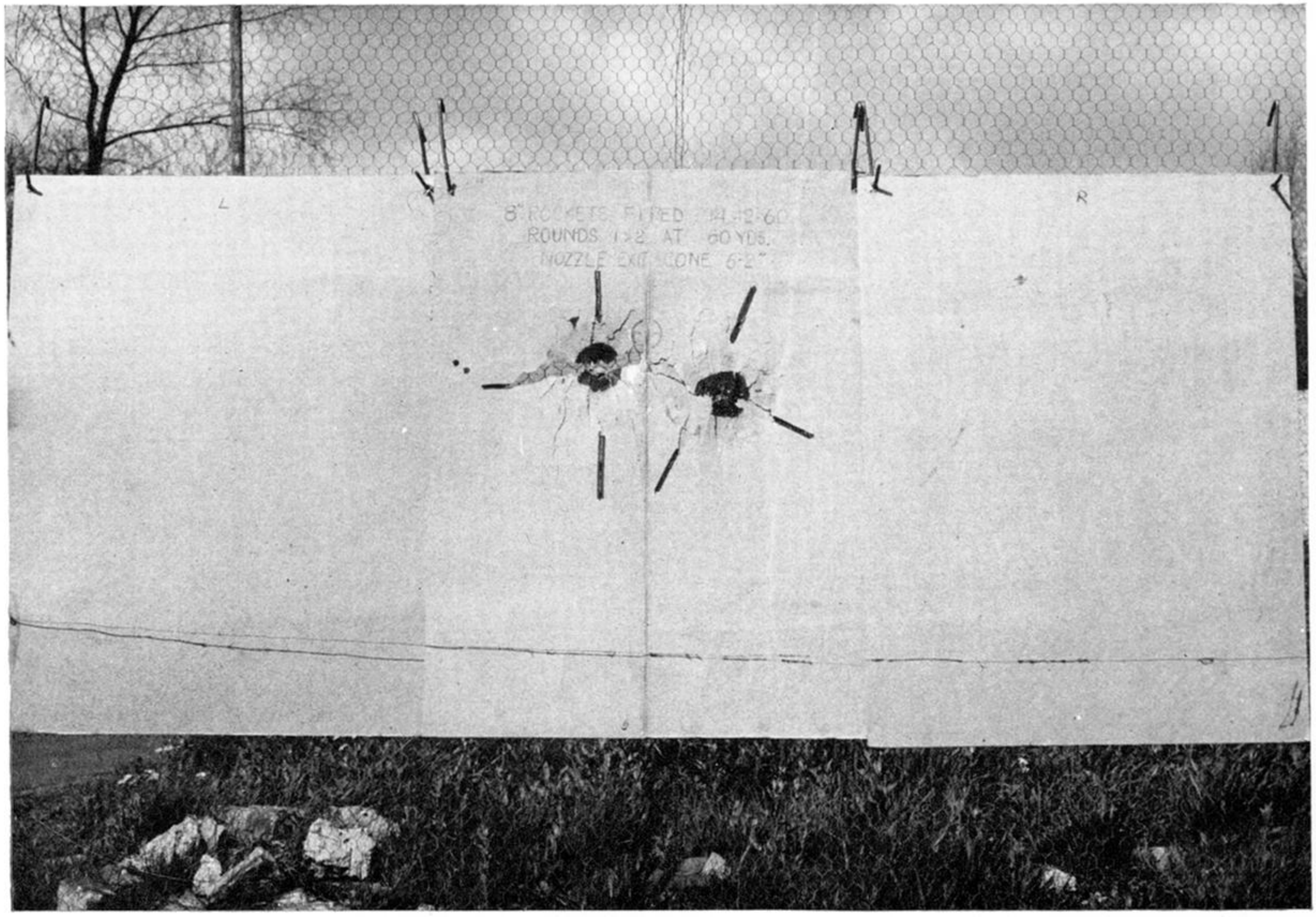

FIGURE 25. Targets showing the yaws and flight deviations of the 8 in (20 cm) test vehicle with the asymmetric entry cone and with exit cone lengths of (top) 272 mm and (bottom) 157 mm.

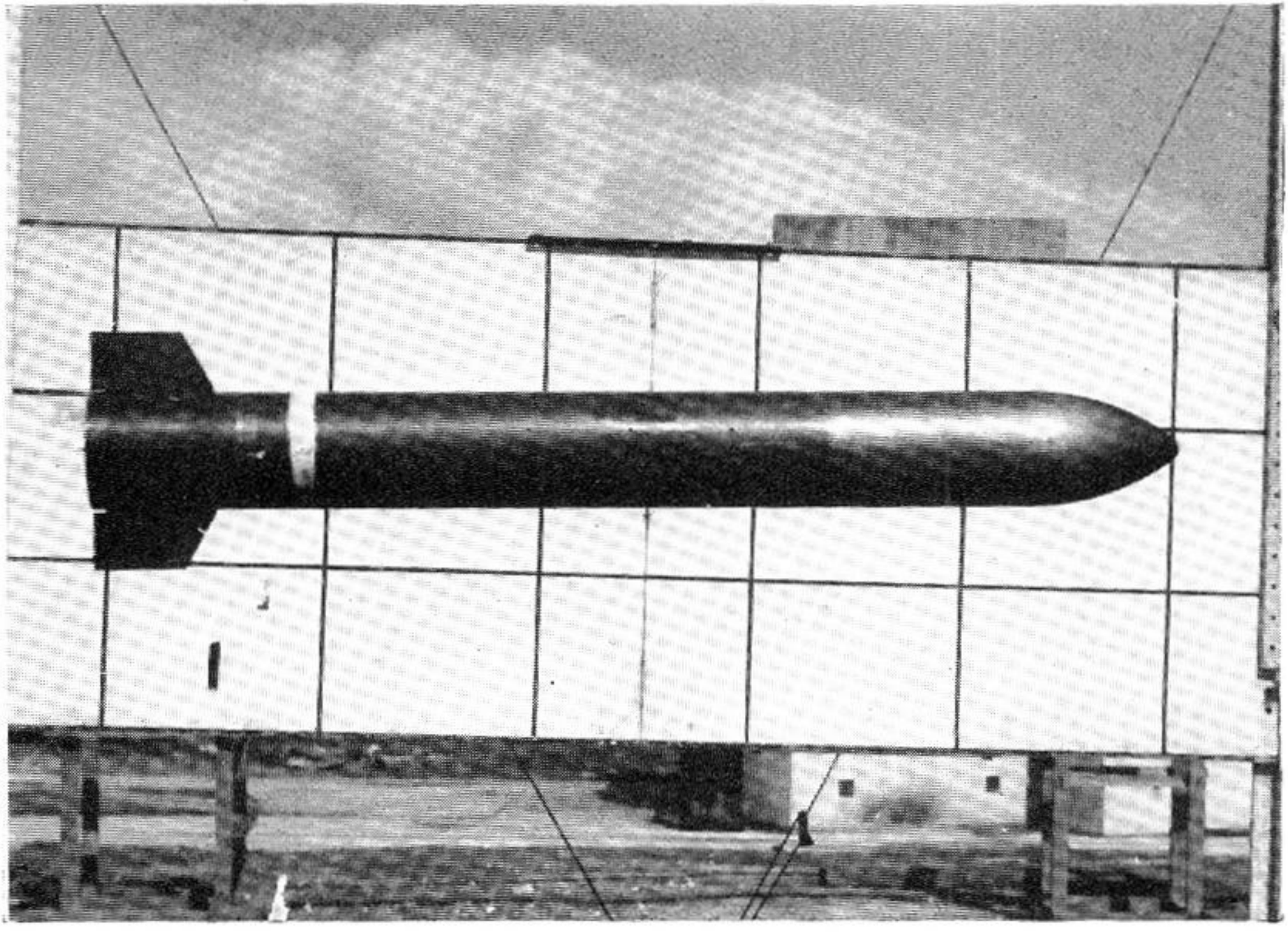

FIGURE 22. The 200 mm test vehicle.

n.e.c.l./mm

272

221

196

170

145

launch line

FIGURE 26. Composite picture of the targets showing the variation of the flight deviation with nozzle exit cone length. ◯, Orientation left; ●, orientation right.

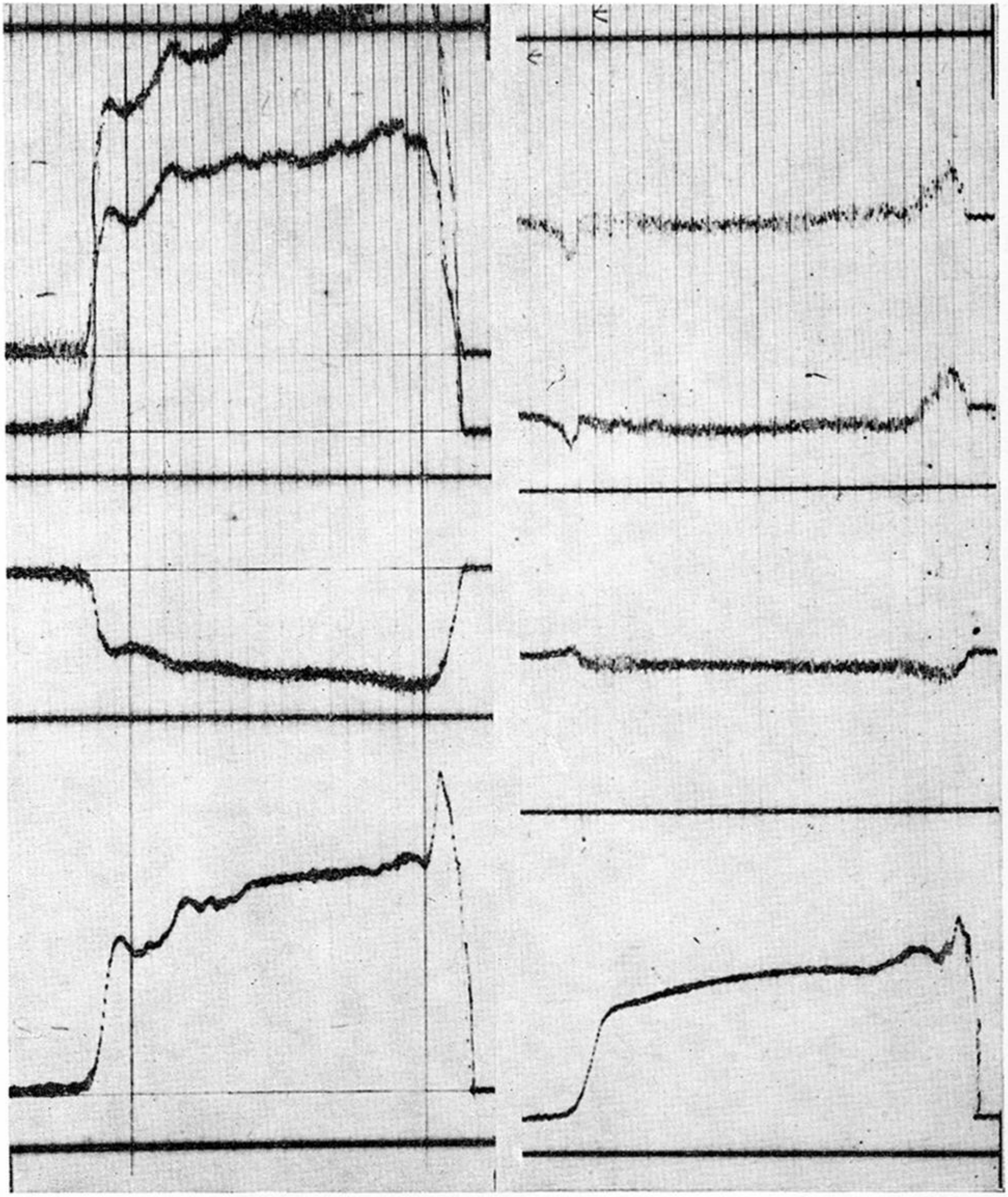

(i) (ii)

FIGURE 15. Typical dynamometer records. (i) At the maximum of the curve of figure 17; (ii) at the near-zero of the curve of figure 17. The bottom curve in each case is the axial thrust, the second being with a reduced scale to allow greater magnification of the lateral thrust.